A Thesis for the Degree of Ph.D. in Engineering

Biomechanical Study of Drilling Trabecular Bone and Lifting Maxillary Sinus Membrane in Oral Implant Surgery

March 2017

Graduate School of Science and Technology

Keio University

Mohammad Aimaduddin Atiq bin Kamisan

DISSERTATION

Submitted to the School of Science for Open and Environmental Science, Keio University, in partial fulfillment of the requirements for the degree of Doctor of Philosophy

For my parents for supporting and believing in me to achieve big,
and
for my wife, Nurul Ashikin binti Daud who made it all possible through love, support and sacrifices

Abstract

This study aims at reducing the number of serious cases occurred in the oral implant surgery through biomechanical study of mandibular trabecular bone and maxillary sinus membrane. The problem occurs when a clinician misjudges the bone quality of the trabecular bone in the lower jawbone during drilling causing perforation through the mandibular canal. Furthermore, accidents that could lead to death such as the perforation to the lingual cortical bone also might happen. In the upper jawbone the problem lies with the breakage of the maxillary sinus membrane due to perforation or dead cell caused by strain concentration that cuts the blood flow during the sinus lift up process after drilling. Therefore, to avoid the above-mentioned problems, it is important to quantify the drilling force-sensing for trabecular bone and strain distribution in lifted sinus membrane.

In relation to the quantification of drilling force-sensed, a new oral implant surgery training simulator was developed so that the users can feel the real force-sense. The apparatus was tuned through experiment using fresh cadaver and expert clinician's evaluation not only for the trabecular bone but also for cortical bone in order to simulate the accidental cases. The developed system was then evaluated by clinicians, and it was revealed that their experience was very much influential on the force-sensed by investigating the input drilling force and the output drilling speed. The developed system was then used for education of students in a problem-based learning (PBL) class at a dental college. It was quantified how correctly the students could recognize the bone quality of the trabecular bone by the drilling force-sensed. More than half of them could identify the main features of force-sensed influenced by bone quality for a bone sample. This implies that the same evaluation can be done on well experienced clinicians and they

can identify them more accurately. Hence, the developed system can also help the clinician to quantify the drilling force-sensed and the bone quality after the surgery, which can be transferred to an inexperienced student.

In regards to the strain distribution in the maxillary sinus membrane, an apparatus was designed and developed in order to measure the reaction force during the lift up process using fresh cadaver. Also with the help of nonlinear finite element analysis, the material properties of sinus membrane were calibrated using a power-law constitutive equation, and finally the strain distribution was obtained. Based on the strain values, it was concluded that the *RZ* component of the shear strain was significant to the cutting of the blood flow in the sinus membrane, where the *R* component denotes the radial direction of the membrane and *Z* denotes its thickness direction. This fundamental study on the membrane is expected to lead to the development of sinus lift up surgery training simulator with force-sensing capability.

Acknowledgements

A full praise and thanks to Allah the Almighty for making it possible for me to come at this point in life by granting me the good fortune to work on a research problem that I enjoyed in Keio University, one of the best institution in Japan and for seeing me through the ups and downs through the journey that every Ph.D bring about.

The present work would not have been possible without the help of many persons, to whom I am trully indebted. First of all, I would like to thank my advisor, Prof. Naoki Takano, for teaching me s much over the past three years and inspiring me through his experiences, knowledge, and examples of his hard work. The countless thought-provoking, lively, and very interesting discussion shaped my thought and the foundation of my present work. I am very glad to have such a generous doctoral advisor.

In addition, I want to express my deepest gratitude to the committee members, Prof. Naomichi Ogihara, Assoc. Prof. Kenjiro Takemura, and Assoc. Prof. Shogo Miyata, for their valuable critism and advice during the defense and private discussios that helped me in improving this thesis.

I would also like to thank a few person from Tokyo Dental College—

Prof. Shinichi Abe from Dept. of Anatomy, Prof. Yasutomo Yajima from Dept. of Oral and Maxillofacial Implantology, and Dr. Hideaki Kinoshita from Dept. of Material Science for their help in the drilling experiment on fresh cadaver especially in the preparation of the cadaver,

Prof. Shinichi Abe, Assoc. Prof. Satoru Matsunaga, and Dr. Kento Odaka from Dept. of Anatomy, Dr. Shinya Homma from Dept. of Oral and Maxillofacial Implantology, and Dr. Hideaki Kinoshita from Dept. of Material Science for their in the problem-based learning (PBL) class,

Prof. Shinichi Abe, Assoc. Prof. Satoru Matsunaga, and Dr. Kento Odaka from Dept. of Anatomy, and Prof. Yasutomo Yajima, and Dr. Toshiyuki Morioka from Dept. of Oral and Maxillofacial Implantology for thier help in the experiment on the sinus membrane.

All cadavers used in the experiment was approved by the Ethics Committee of Tokyo Dental College. I also wish to express my heartfelt thanks to the donors family for their generosity in the face of their tribulation. A noteworthy mention also to the Imoto Machinery Co. Ltd. for the manufacturing of the apparatus used in this study. Not to forget,

Assoc. Prof. Daisuke Tawara from Ryukoku University which help in the analysis for the database for the simulator. Also a full gratitude to former and current student of Keio University—Masahiro Nagahata, Kenichiro Yokota, Fumiya Nakamura and Sayaka Yamazaki—which gave a lot of contribution in this study.

I would also like to extend my gratitude to my advisor in Yamaguchi University, Prof. Xian Chen. He has helped me throughout my final year course of my undergraduate and master's degree by keeping a constant eye on my progress in study. His passion and interesting thought brought me to explore more in the field of bioengineering.

A great source of motivation and inspiration for me throughout my time as a Ph.D candidate has also come from my circle of friends here in Keio University—Ahmad Rosli, Erialdi, Ahmad Muzaffar, and Khairul Anuar—and also to my countless circle of friends out there—Akmal, Dr. Ahmad Athif, Ahmad Khushairy, Nik Izual, Yoshizumi Okawa, Md. Masri, Haziq, and Aidil—to name a few among others.

I would also like to thank all of my colleagues in the Mechanical Simulation Laboratory (Takano Lab), including Akimoto, Ishijima, Kamijo, Kurita, Nishikawa, Hagiwara, and many others. The atmosphere in our laboratory was very inspirational and supportive throughout these years.

I would like to reserve a very special gratitude, especially to my parents which have sacrificed so many in order to make my education possible. My wife, Nurul Ashikin binti Daud, always being very supportive through her encouragement, unconditional love and understanding, taking care of our kid eventhough she herself is doing Ph.D.This dissertation is dedicated to my parents, my wife, and my beloved daughter—thank you for seeing me through every step of the way, through ups and downs, and for praying for me during times of trouble.

From financial point of view, I would like to thank Keio Leading-edge Laboratory (KLL) for proiding my research grant every year making me able to participate in overseas and domestic conferences in order to share the idea of my research to the public. Finally, the financial support from Yayasan Pelajaran MARA (YPM) towards my scholarship for all these years is gratefully acknowledged.

Contents

List of Figures

List of Tables

Chapter 1

Introduction

1.1 Motivation

Oral implant surgery has been one of the many treatments for tooth's deficiency for more than 30 years by replacing the missing teeth and their supporting structure with artificial prostheses. The surgery mainly consists of drilling the jawbone and implanting or anchoring the artificial crown to the jawbone (Albrektsson, Sennerby, & Wennerberg, 2008). At first, the phenomenon known as osseointegration was discovered by Brånemark in 1952 and work on the development of dental implants began (Adell, Lekholm, Rockler, & Brånemark, 1981). In recent years, there has been a vast amount of scientific research and development in the oral implant surgery especially in the implant design, geometry, materials, and techniques (Coelho et al., 2009; da Silva, Pellizzer, Quinelli Mazaro, & Garcia Júnior, 2010). The objective of these research has been the same which is to improve the success of the oral implant treatment. Based on the research that had been

done, the main idea of this study is to improvise in the technique of the oral implant surgery and also tackling the problem in the education system as it is rarely done.

The survey done by Japan Academy of Maxillofacial Implants, as shown in Figure 1.1, between the year 2009 and 2011 describes that more than half of the serious accident occurred in the oral implant surgery were directly related to the mandibular canal and maxillary sinus membrane. One of the reason as suggested by Chrcanovic et al. (2014) is the doctor's own lack of knowledge and experience. Other research finding on the bone drilling and oral implant also points toward the same conclusion (Augustin et al., 2008; Kim, Yoo, Kim, & Shin, 2010; Limbert et al., 2010; Melo, Shafie, & Obeid, 2006). Moreover, regarding the education of the dental students, De Bruyn et al. (2009) and Ucer et al. (2014) stated that dental colleges and universities rarely include syllabus about dental implant in their education system especially during their undergraduate year. However, the numbers started to increase by the year by implementing various syllabus and types of classes such as the problem-based learning (PBL) classes (Donos, Mardas, & Buser, 2009; Mattheos et al., 2009; Mattheos, Wismeijer, & Shapira, 2014). As an educational tool, various initiatives had also been introduced such as the use of haptic devices and the use of detailed educational polymeric model (Kusumoto et al., 2006; Rhienmora, Haddawy, Khanal, Suebnukarn, & Dailey, 2010; Urbankova, 2010; Wierinck, Puttemans, Swinnen, & van Steenberghe, 2007). In both the usage of the haptic device and the educational polymeric model, the tactile sensation is one of the identical point that was noticed.

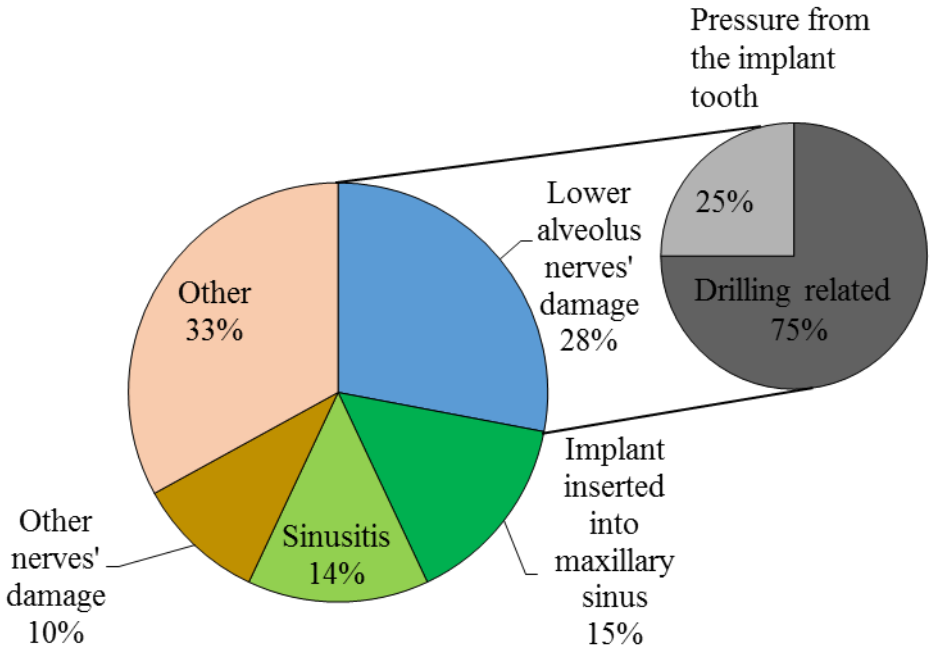

Figure 1.1 Breakdown of serious medical problem (421 cases) in 3 years between 2009 and 2011

(Source: Serious Medical Trouble Related to Implant Surgery, Japan Maxillofacial Implants Society, Academic Committee, Trouble Investigation Working Group)

Drilling force-sensed was the keyword put as the sensation of the drilling force for drilling the jawbone and it seems to be difficult to quantify the value felt by the clinician. Consequently, the force-sensed is nearly impossible to be taught to an inexperienced clinician. The drilling force itself is closely related to the apparent mechanical properties as reported especially regarding the bone stiffness, which leads to the issue of the quality of the bone. The understanding of the bone quality itself varies and many research about the bone (Donnelly, 2011; Seeman & Delmas, 2006) or its biomechanics particularly in oral implantology had been done (Bonnet, Postaire, & Lipinski, 2009; Mathieu et al., 2013, 2014; Matsunaga et al., 2010; Matsunaga, Takano, Tamatsu, Abe, & Ide, 2011; C. Misch, Qu, & Bidez, 1999; Sui, Sugita, Ishii, Harada, &

Mitsuishi, 2014; Yeniyol et al., 2013) and few suggested that a few factors that affects the bone quality includes its microstructure (Basler, Traxler, Müller, & van Lenthe, 2013; Dempster, 2000; Pothuaud et al., 2002) and bone mineralization (Sansalone et al., 2012). In relation to the bone quality, one of the way to predict the drilling force is through the image-based modeling technique and finite element analysis (FEA) that is widely used in bone stress analyses (Hannam, 2005; Jianping, Weiqi, & Wei, 2008; Limbert et al., 2010; Ohashi et al., 2010). Based on the drilling force that could be predicted, the calculated force could be the fundamental in quantifying the drilling force-sensed.

In regards to the maxillary sinus membrane, drilling being the least concern problem (Misch, 1988), the reason could be caused during the surgery or even post-surgery as a result of highly concentrated strain on one or many points that lead to the membrane breakage. The breakage of the membrane could cause other complications such as sinusitis and infection whether to the teeth or the sinus (Al-Dajani, 2014). Research had been done in relation to the sinus membrane such as the finding of the mechanical properties (Pommer, Unger, Sütö, Hack, & Watzek, 2009) and the simulation of the sinus lift using a unique lift up tool (Ching-Chieh, Li-Wen, Dong-Feng, & Yung-Chuan, 2012; Franceschetti, Minenna, Farina, & Trombelli, 2012). However, to the best of the author's knowledge, there has been no research carried out to measure the strain concentration in the sinus membrane especially during the sinus lift up process in order to make the results applicable in the oral implant surgery. The finding of the strain concentration is important in order to find out the quantitative value that lead to a membrane breakage rather than the qualitative value since a quantified result is easier to transfer to another clinician. Moreover, the same tactile sensation or force-sensed in this scenario also seems applicable for the transfer to an inexperience person.

1.2 Purposes

This study was done in order to reduce the number of serious cases occurred in oral implant surgery through the biomechanical study of drilling the mandibular trabecular bone and lifting up the maxillary sinus membrane. The final goal of this study is to develop an oral implant surgery training simulator with force sensing capability using an actuator. This is done in order to transfer the force-sensed during surgery from an experienced clinician to an inexperience dental college student. The overview of the development can be seen as shown in Figure 1.2. Both simulator of the lower and upper jawbone follows the same overall procedure in the development process.

The development starts from the measurement done on a fresh cadaver in order to identify the force and location curve during the oral implant surgery. The experiment closely follows the procedure during the surgery. The identified curve is then used in order to determine the actuator power output as a function of input force and location. The power output is lastly implemented in the force-sensing device and it is tune up by expert clinician to improve its reliability for usage by others.

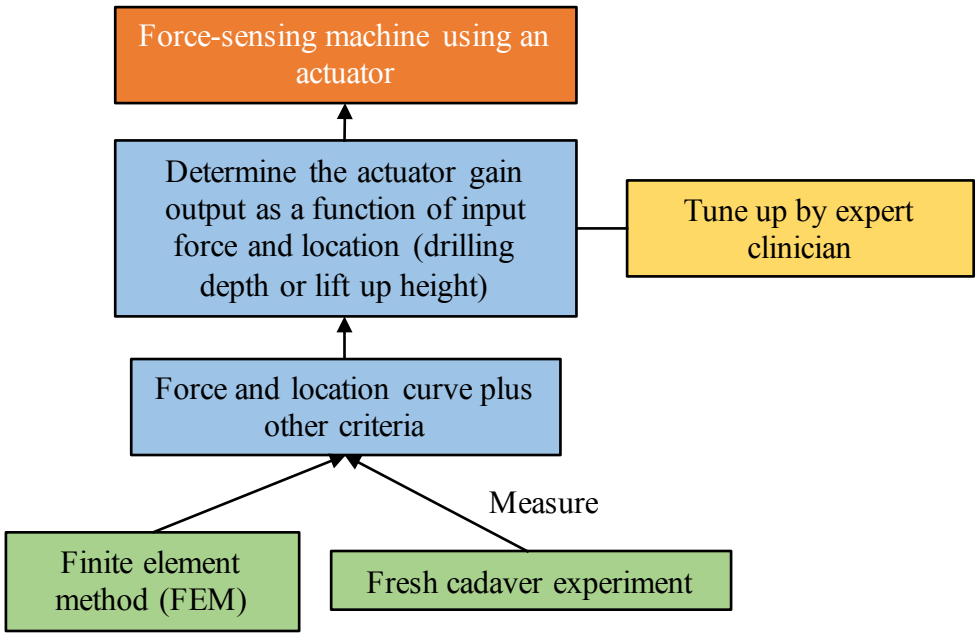

Figure 1.2 Overview of the development of oral implant surgery training device with force sensing capability

1.2.1 Lower jawbone

Despite the haptic device available today, most of them are readily equipped with surgical tools or mock tools that are not actually usable in an actual surgery. The feeling might be different than holding the real tools for surgery. In the case of the polymeric model, it only provides one type of drilling sensation (Van De Velde, Glor, & De Bruyn, 2008) eventhough four types of bone were reported based on the Lekholm description (Lekholm, 1985). Plus, the destructive technique of using the model making it quite expensive. By tackling the problem through the education system, the oral implant surgery training simulator comes as a solution to these problems as it enables the user to use a real handpiece and motor unit used in an actual surgery and repeatable drilling can be done (Curran, 2006).

As shown in Figure 1.3, the development started with the calibration done based on the trabecular bone of the lumbar (Basaruddin et al., 2013). The data was then used in the calculation of the database for the trabecular bone region in the mandible. The database was calibrated with the experiment done on fresh cadaver of a human jawbone. In this study, the database for the cortical bone region was added after that. The completed database was implemented in the force-sensing machine with the actuator power being the value given as output to the user. This value was tuned up by expert clinician and it was then evaluated by a panel of experienced clinician and students of dental college. The data was also compared with the conventional method used in teaching the drilling case for students by using a polymeric model.

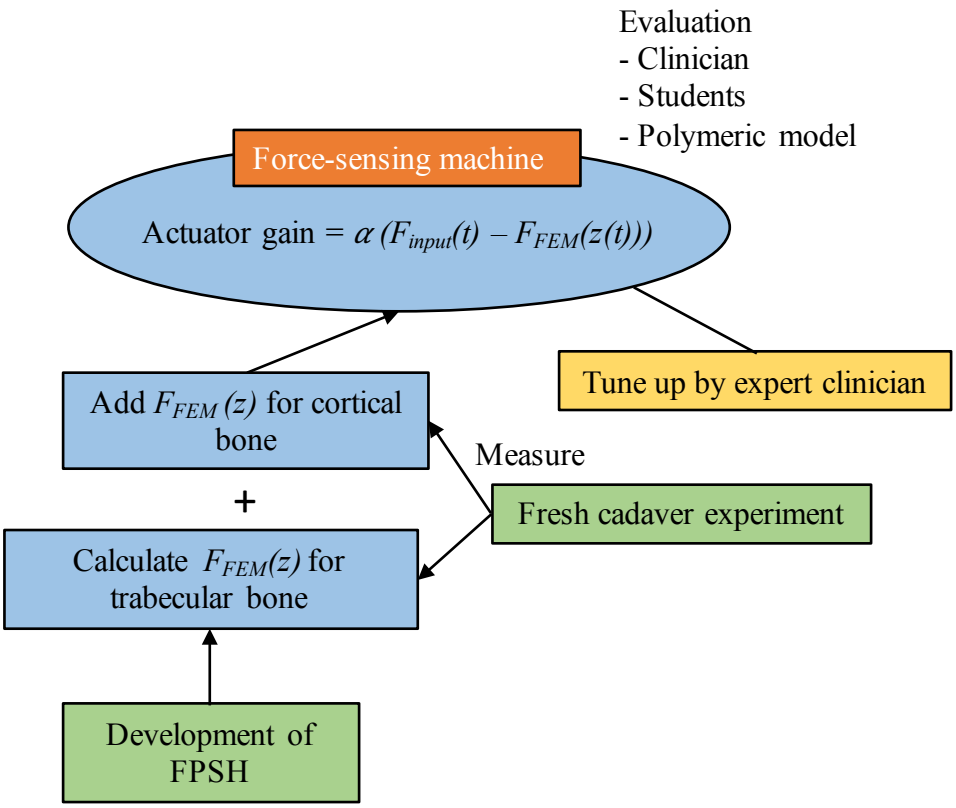

Figure 1.3 The development of oral implant surgery training simulator for drilling mandibular trabecular bone

1.2.2 Upper jawbone

Regarding the sinus membrane, in this study, the osteotome is considered based on the typical cases of sinus lift surgery rather than using a special tool (Büchter et al., 2005; Çehreli et al., 2009; Jurisic, Markovic, Radulovic, Brkovic, & Sándor, 2008; Pjetursson et al., 2009; Summers, 1994) in order to find out about the strain distribution in the maxillary sinus membrane during the sinus lift up process. A method to evaluate the strain on the membrane was proposed by doing an experiment on a fresh cadaver and making it a base to calibrate study using a numerical procedure to increase the number of condition to be applied to the membrane while doing the lift up process. This is to ensure a more reliable information to be conveyed to the clinician.

This marked the first step of development in order to calculate the critical strain value due to breakage as shown in Figure 1.4. The next step is to get the graft material properties and determine the critical strain value during the breakage of the membrane by curve-fitting the experiment with and without the graft material. This will also include the uncertainties such as the thickness of the membrane in order to establish a database for the simulator. The completed database will be used in the force-sensing machine and the actuator power will be tuned up by expert clinician in the future.

So, the investigation of the strain distribution is done for the purpose of establishing the database for the force-sensing machine in the future and to see the correlation with the cutting of the blood flow. This study focuses more on the correlation of the strain distribution with the cutting of the blood flow. Rather than the usage of a semi-spherical bar, a cylindrical bar was used in designing the testing apparatus as it seems to be much more informative to many clinicians.

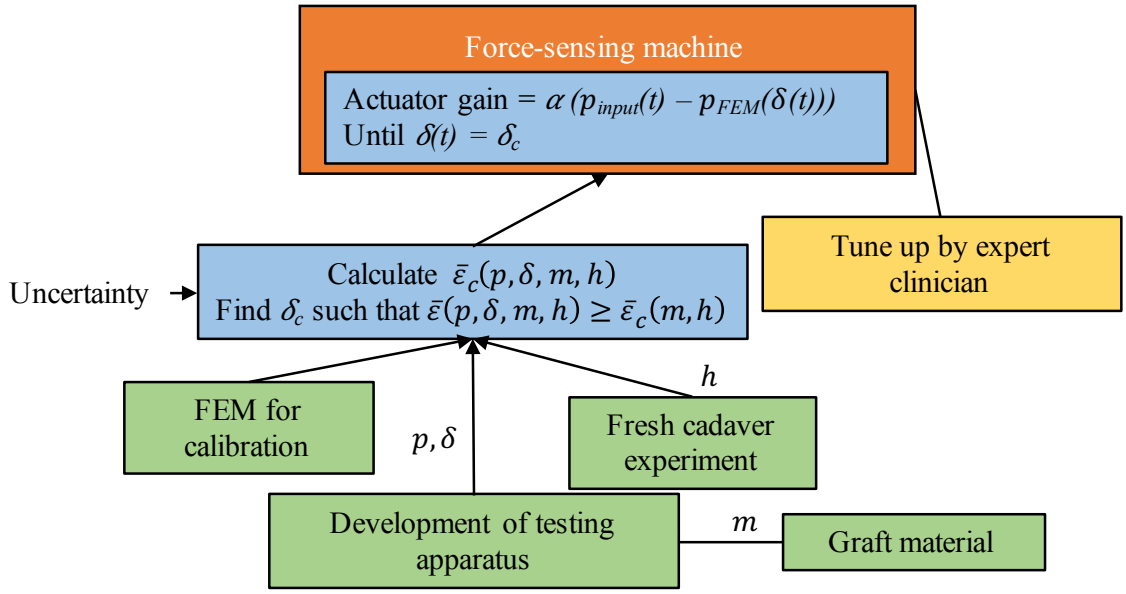

Figure 1.4 The development of oral implant surgery training simulator for lifting up maxillary sinus membrane

1.3 Organization of thesis

Chapter 3 explained the strategy of designing the oral implant surgery training simulator and its use in the clinician's evaluation in order to establish a review from a panel of expert clinicians. The evaluation was compared with the drilling on the educational polymeric model to discuss about the drilling force and speed and the adjustment of the actuator movement on the simulator. In Chapter 4, the simulator was applied in the problem-based learning (PBL) class of a dental college students to classify the drilling force and speed obtained from the clinicians' evaluation and it was discussed thoroughly in order to quantify the drilling force-sensed based on the drilling force and speed. The chapter also included the application of the simulator to quite a large number of students for their experience on drilling the jawbone. Chapter 5 described the strategy used in

designing the sinus lift up testing machine in order to experiment the sinus membrane in a similar condition during the sinus lift up process. The chapter end with a test done on a natural rubber that could easily be found in a home center in order to establish an experiment procedure. The experiment procedure was compared with a numerical procedure design in order to measure and calculate the strain concentration explained in Chapter 6. The comparison of both results was done by doing a calibration of the material model in the designed numerical procedure. Chapter 7 described the new findings, limitations, and future works related to the study. Finally, the list of publications related to the present study is in Appendix A.

Chapter 2

Background and literature review

2.1 Cortical bone and trabecular bone

Figure 2.1 shows a model of the jawbone made by Nissin Dental Products to explain about the oral implant surgery procedure to a patient. Mainly, the human body parts are described as anterior posterior, mediodistal and buccolingual direction (Clarke, 2008). Regarding the human bone, although produced and maintained by the same type of cell, a human skeleton consists of two different types of bone which differs in structure and distribution, the cortical and trabecular bone (Goodyear, Gibson, Skakle, Wells, & Aspden, 2009; Rho, Kuhn-Spearing, & Zioupos, 1998). Figure 2.2 shows the bone structure which consists of the cortical bone and the trabecular bone in a human femur.

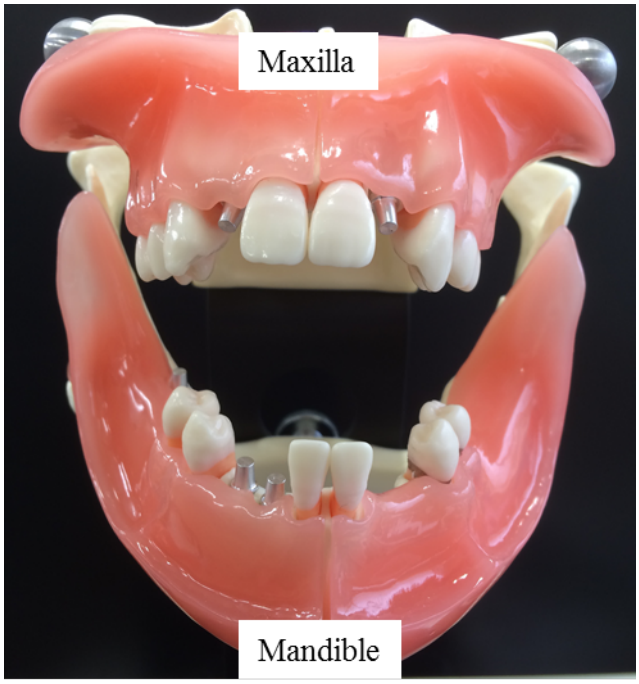

Figure 2.1 Model of the jawbone made by Nissin Dental Products Inc.

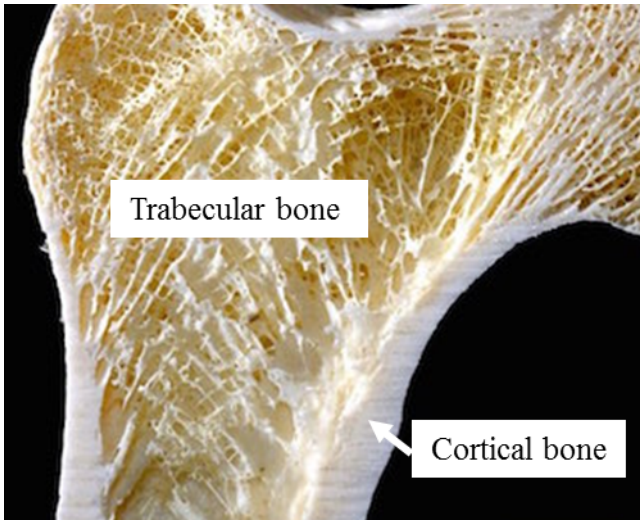

Figure 2.2 The bone structure of a human femur

The cortical bone is also known as compact bone or lamellar bone. It can be found mainly in the shafts of long bones and it make up for roughly 80% of the human weight (Cowin & Telega, 2003; Martin & Burr, 1989; Weiner, Traub, & Wagner, 1999). This bone forms the outer part of most bones and is much denser than trabecular bone making it much harder, stronger and stiffer (Augat & Schorlemmer, 2006).

Trabecular bone can also be called as cancellous bone or spongy bone (Keaveny, Morgan, Niebur, & Yeh, 2001; Oftadeh, Perez-Viloria, Villa-Camacho, Vaziri, & Nazarian, 2015). It is found in the vertebrae and at the ends of long bones, proximal to joints. In contrast with the cortical bone, this type of bone is a porous foam-like structure with voids filled with bone marrow. It spans a higher surface area but less dense making it softer weaker and less stiff.

At a macroscopic scale, both bone types appear largely different with the cortical bone comprising cylindrical structure and the trabecular bone forming a lattice of plates and rods. However, at a microscopic scale, both types appear to be similar being composed of mineralized collagen fibrils set with a preferred orientation in lamellae.

The distribution of both bone has evolved to provide ultimate bone strength, flexibility, or stiffness where it is needed the most (Hadjidakis & Androulakis, 2006). In addition, both types of bone are required in order to maintain the successful rate of a dental implant. Despite that, in relation to the boundaries of the cortical bone and the trabecular bone, there is no definitive border between the two and in the jawbone, the border depends on individual thus in order to perform a dental implant, the classification was done based on radiographic assessment and sensation of resistance experienced by

the clinician when preparing the implant placement. Lekholm (Lekholm & Zarb, 1985) found and distinguished four types of bone accordingly as follows (Figure 2.3):

Type I: Entirely homogeneous cortical bone

Type II: A thick layer of compact bone surrounding a core of dense trabecular bone

Type III: A thin layer of cortical bone surrounding a core of dense trabecular bone

Type IV: A thin layer of cortical bone surrounding a core of low-density trabecular bone

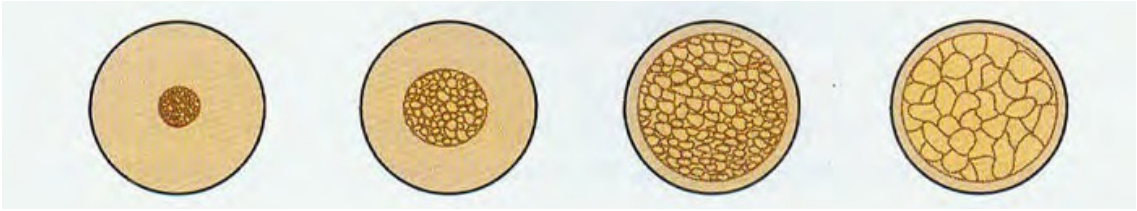

I II III IV

Figure 2.3 Type of the bone quality as describe by Lekholm

The distributed types can be known usually from the clinical CT images taken from a patient but it can be rather doubtful based on clinical CT images alone. Consequently, three years later, Misch (1988) defined four types of bone density groups based on the macroscopic characteristic of the cortical and trabecular bone as follows:

D1: Dense cortical bone

D2: Thick dense to porous cortical bone on crest and coarse trabecular bone within

D3: Thin porous cortical bone on crest and fine trabecular bone within

D4: Fine trabecular bone

and it was further expanded to divide the human jawbone into four regions as listed in Table 2.1

Table 2.1 The classification based on the divided region of the jawbone (% occurrence)

Bone type	Anterior maxilla	Posterior maxilla	Anterior mandible	Posterior mandible
D1	0	0	6	3
D2	25	10	66	50
D3	65	50	25	46
D4	10	40	3	1

The characteristic of the bone actually defined a part of the bone quality which was actually agreed by the National Institute of Health in a consensus in the year 2001. According to the consensus, the bone quality is related to various aspect of the bone including its macro- and microarchitecture, turnover, resorption, and mineralization. Radiological imaging techniques such as using a micro-CT can be used to visualize and quantify the bone macro- and microarchitecture however it is impossible to be done on a living patient as it required a very high exposure to the radiation dose.

2.2 Sinus membrane

Concerning the topics to oral implant, most research mainly focused in the aspects of the bone but not many were done on the sinus membrane or rather largely known as the maxillary sinus membrane. Figure 2.4 shows the anatomy of the maxilla or also referred to as the upper jawbone. The maxillary sinus is the largest pneumatic space in the human body (Woo & Le, 2004). It is located in the maxilla and opens in the middle nasal of the nasal cavity with one or many openings.

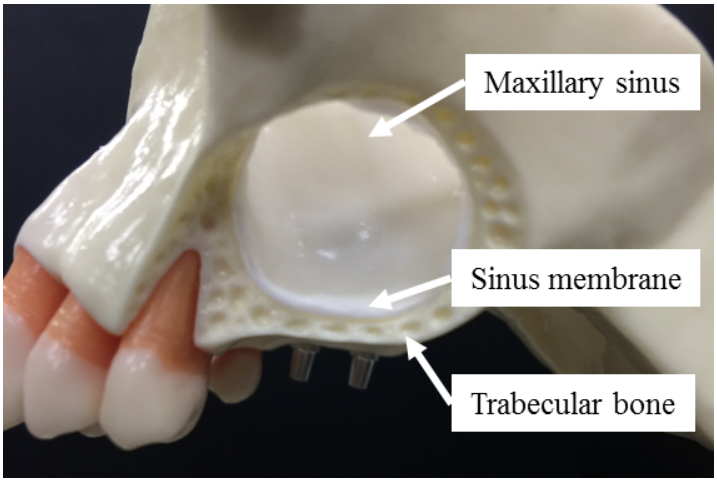

Figure 2.4 Side view of the anatomy of the maxilla

The sinus varies in size, shape, and position even in the same individual. It is a pyramid-shaped cavity with the base adjacent to the nasal wall and the apex pointing towards the zygomatic process of the maxilla (van den Bergh, ten Bruggenkate, Disch, & Tuinzing, 2000). There are also four walls with the anterior wall is actually the facial surface of the maxilla, the posterior wall taking the infratemporal surface of the maxilla, the roof being the floor of the orbit and its floor is the alveolar process of the maxilla. The sinus may have septa that divide itself partially into intercommunicating compartments.

In relation to the oral healthcare, the bone forming the floor of the sinus can also be the bone surrounding the apex of a tooth thus an infection of the teeth can spread to the maxillary sinus and vice versa (Yan, Zhang, Chi, Ai, & Wu, 2015). The nerves that supply to the maxillary teeth are also those that supply the maxillary sinus allowing dental pain of a healthy teeth coming from maxillary sinusitis which is an infection of the sinus (Janner et al., 2011).

2.3 Oral implant surgery

Oral implant surgery or widely known as dental implant surgery is one of the many aspects of dental implantology (Misch et al., 2008). It has become one of the main field in dentistry. Dental implantology is the field which concerned with the replacement of missing teeth and their supporting structures with artificial prostheses implanted into the jawbone. Replacing lost teeth with implant is not a new concept as it dated back during the Mayan origin in the 600AD as archeologist found a fragment of mandible bone which had three tooth-shaped pieces of shell placed into the sockets of three missing teeth (Derrick, 1986). Not only a tooth loss causes functional problems, but it can also lead to psychological problems which could affect the quality of one's life.

In the modern oral implantology, the missing tooth is replaced with implant which consist of three main components as shown in Figure 2.5. The root implant is input into the implant site and the abutment was put next after the process of osseointegration. Lastly, the crown is put based on the patient's condition.

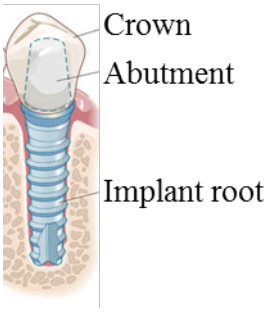

Figure 2.5 Component of oral implant

The dental implant surgery is actually a restorative guided discipline with a significant in oral surgery component. Since the implant surgery is often a nonobligatory procedure, it should be planned and executed well to ensure a high probability of success at both the functional and aesthetical level of the implant. It is also best to ensure minimum patient discomfort and minimum risk damage especially to vital places. The oral implant surgery procedure can be simplified as shown in Figure 2.6.

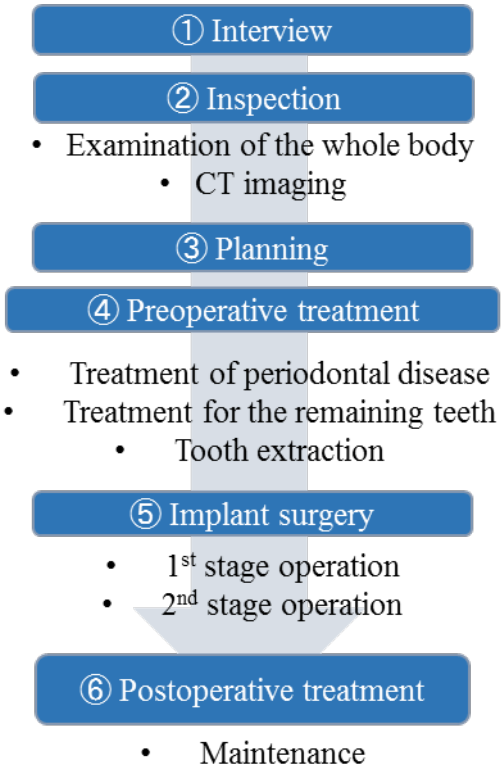

Figure 2.6 Flow of the oral implant surgery procedure

A normal implant surgery consists of three main components which should be mastered by the dentist. Firstly, it is the surgical planning which takes into account the possibility of the surgical procedure while concerning the patient's suitability such as his

or her age, bone condition, and also other diseases. Secondly, the preoperative preparation which include getting the patient ready for the surgery, both physically and mentally such as making sure that the patient is plaque-free and also no infection present at the time of surgery. Thirdly, it is the basic training that should be received in order to do the implant procedure such as the surgical technique, knowledge of surgical anatomy and vital structure, and also the post-operative management and treatment.

In all of the dental implant cases, drilling is required in order to put the base for the implant. For that reason, drilling is one of the basic training that should be receive and known prior to an oral implant surgery. The training should include knowledge about the bone and also practical implementation of drilling a real jawbone (Abouzgia & James, 1995; Bachus, Rondina, & Hutchinson, 2000; Karaca & Aksakal, 2013; Reingewirtz, Szmukler-Moncler, & Senger, 1997). However, due to its riskiness, practical training of drilling in an oral implant surgery is nearly impossible and this made the usage of simulator or other method such as the use of polymeric model or haptic device become much popular (Kusumoto et al., 2006; Razavi, Talebi, Zareinejad, & Dehghan, 2015; Sohmura et al., 2009; Xiaojun et al., 2010; Zheng et al., 2012).

The drilling of the jawbone is a part of the 2-stage operation in the procedure of the oral implant surgery in order to prepare the implant site. Figure 2.7 shows the 2-stage operation of the implant surgery. Figure 2.8 shows the drilling process in the 1st stage operation of the oral implant surgery. The round bur or guide drill is used to drilled and mark the top part of the cortical bone. Then, a twist drill or also known as pilot drill is used to drill through the trabecular bone. For the lower jawbone, it is drilled at a set depth or above the mandibular canal located in the trabecular bone region. During this procedure, drill with a diameter of about 2 mm is used. Lastly, the implant site made by

the pilot drill is broaden with a set of different twist drill with bigger diameter. The diameter of the implant site is usually broadened until 6.6 mm.

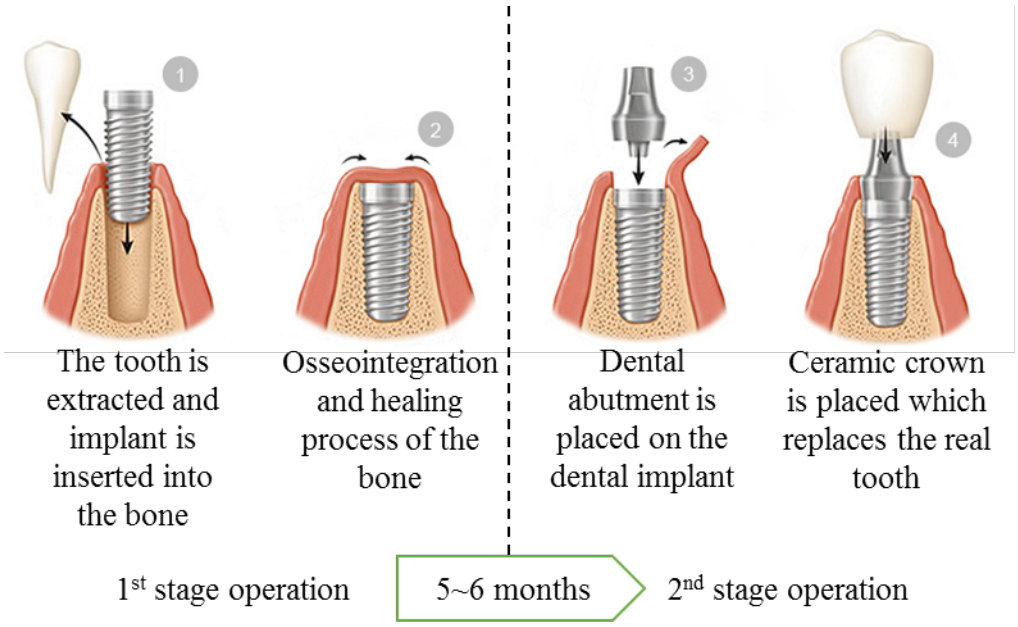

Figure 2.7 Two stage operation of the implant surgery

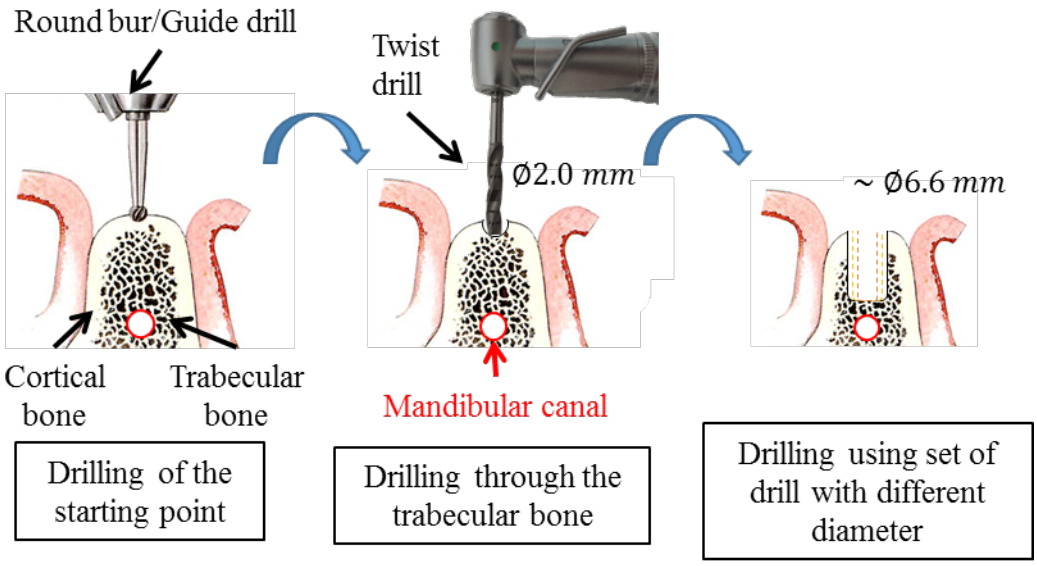

Figure 2.8 Drilling process during the oral implant surgery

Another technique that is focused in this thesis is the sinus augmentation. Sinus augmentation, osteotome or closed sinus lift technique, also referred to as Summer's technique (Summers, 1994) is the elevation of the sinus membrane through a vertical osteotomy within the implant site and placement of a particulate graft to increase bone volume for placement of implants (Agamy & Niedermeier, 2010; Franceschetti et al., 2012; Inglam, Suebnukarn, Tharanon, Apatananon, & Sitthiseripratip, 2010; Pjetursson et al., 2009; Tilotta, Lazaroo, & Gaudy, 2008; Yan et al., 2014). It can be carried out concurrently or as a separate procedure prior to implant placement. It is actually an advance technique that is not usually done by fresh graduate or inexperienced clinician due to its risk and the treatment for the surgical after-care or any complications if it occurs. Figure 2.9 shows the procedure of the process mentioned. Before the sinus is lift up, the same drilling process mentioned above were used to prepare the implant site.

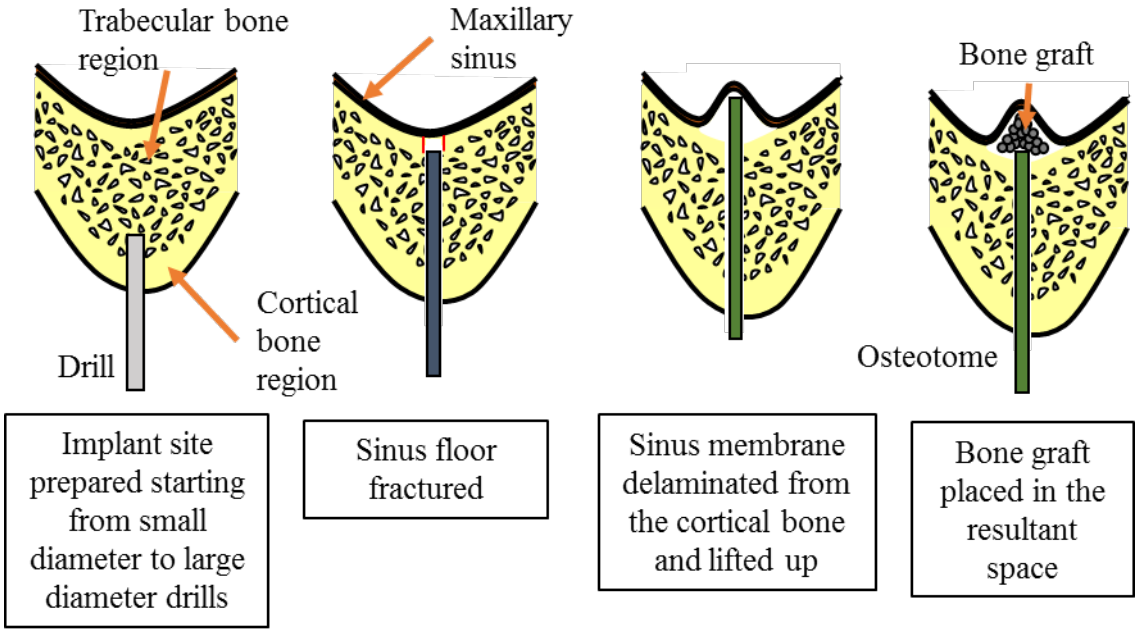

Figure 2.9 Sinus lift up process

Figure 2.10 shows the part of the mandible and maxilla after the oral implant surgery. Notice that in the mandible, the implant is above the mandibular canal which is marked by a yellow line and the sinus membrane had been lift up in the maxilla in comparison with Figure 2.4. The white part is the graft material used in replacement of a real bone in order to promote osseointegration (Holmgren, Seckinger, Kilgren, & Mante, 1998).

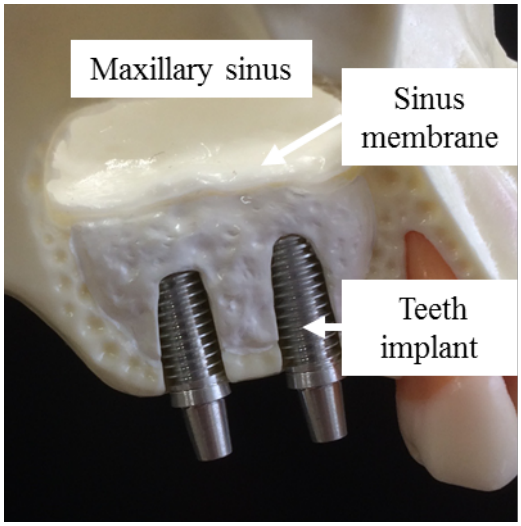

(a) Maxilla

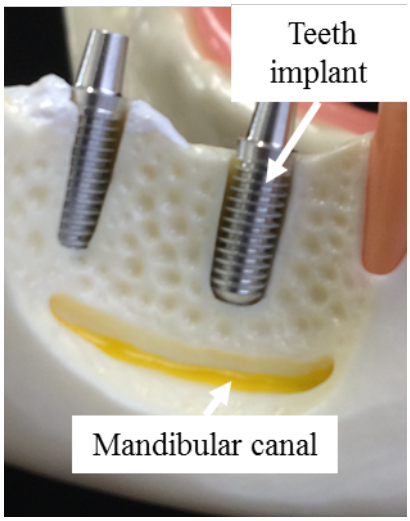

(b) Mandible

Figure 2.10 The jawbone after the oral implant surgery

2.4 Multiscale finite element method

Gibson and Ashby, (1997) described the trabecular bone structure as a heterogeneous cellular medium making it harder to analyze the mechanical properties of the jawbone. Hence, the homogenization method of the multiscale theory in the finite element method was considered. However, this theory was firstly introduced to solve the periodic microstructure problem not related to the bone (Guedes & Kikuchi, 1990; Sanchez-Palencia, 1980). Regardless, Takano et al. (2003) proved that it is quite accurate even for material with random microstructures. One of the initial study using the theory on trabecular bone was done by Basaruddin et al. (2013) with the work expanded into stochastic homogenization theory which will be described in the next section. In order to understand the theory, a macroscopic structure Ω that has a heterogeneous microscopic property is considered. A microscopic unit cell structure of Y is defined to represent the global heterogeneity and the macroscopic properties can be defined as the average volume of the microscopic properties in the unit cell. The heterogeneous material can be exchanged with a homogenized model by assuming that the unit cell repeated periodically. By defining the microscopic scale as y and the macroscopic scale as x, a scale ratio λ with a very small positive number is also defined and the relationship of can be written as follows:

$$y = \frac{x}{\lambda} \tag{2.1}$$

The displacement $\boldsymbol{u}$ is expressed to be asymptotic with respect to parameter lambda as in the following

$$\boldsymbol{u} = u_i(x,y) = u_i^0(x) + \lambda u_i^1(x,y) \tag{2.2}$$

where u_i^0 is a macroscopic displacement and u_i^1 is a perturbed term as a result of the microscopic heterogeneity. By supposing a traction t_i is applied on the boundary Γ_t while neglecting the body force, the equilibrium equation can be written as follows

$$\int_\Omega D_{ijkl}^\lambda \frac{\partial u_k^\lambda}{\partial x_l}\frac{\partial v_i^0}{\partial x_j} d\Omega = \int_\Gamma t_i v_i^\lambda d\Gamma \tag{2.3}$$

where v_i is the virtual displacement and the elasticity tensor is denoted by D_{ijkl}. By taking the limit of $\lambda \to 0$, the integral in equation 2.3 can be decoupled into microscopic and macroscopic equations as follows, respectively by neglecting the traction force in the microscopic level:

$$\int_\Omega \frac{1}{|Y|}\int_Y D_{ijkl}\left(\frac{\partial u_k^0}{\partial x_l} + \frac{\partial u_k^1}{\partial y_l}\right)\frac{\partial v_i^1}{\partial y_j} dY d\Omega = 0 \tag{2.4}$$

$$\int_\Omega \frac{1}{|Y|}\int_Y D_{ijkl}\left(\frac{\partial u_k^0}{\partial x_l} + \frac{\partial u_k^1}{\partial y_l}\right)\frac{\partial v_i^0}{\partial x_j} dY d\Omega = \int_\Gamma t_i v_i^0 d\Gamma \tag{2.5}$$

Since the microscopic displacement relates to the macroscopic boundary conditions and deformation, the solution for the microscopic can be assumed as follows:

$$u_i^1 = -\chi_i^{kl}(y)\frac{\partial u_k^0(x)}{\partial x_l} \tag{2.6}$$

Where χ_i^{kl} is the characteristic displacement that is a periodic function of y. Consequently, the microscopic and macroscopic equation in 2.4 and 2.5 becomes as follows:

$$\int_{\Omega} \frac{1}{|Y|}\left\{\int_{Y} \left(D_{ijkl} - D_{ijmn}\frac{\partial \chi_m^{kl}}{\partial y_n}\right)\frac{\partial v_i^1}{\partial y_j} dY\right\}\frac{\partial u_k^0}{\partial y_l} d\Omega = 0 \tag{2.7}$$

$$\int_{\Omega} \frac{1}{|Y|}\int_{Y} \left(D_{ijkl} - D_{ijmn}\frac{\partial \chi_m^{kl}}{\partial y_n}\right) dY \frac{\partial u_k^0}{\partial x_l}\frac{\partial v_i^0}{\partial x_j} d\Omega = \int_{\Gamma} t_i v_i^0 d\Gamma \tag{2.8}$$

From the above macroscopic equation, it can represent the macroscopic problem and the homogenized elastic tensor can be expressed as follow

$$D_{ijkl}^H \equiv \frac{1}{|Y|}\int_{Y} \left(D_{ijkl} - D_{ijmn}\frac{\partial \chi_m^{kl}}{\partial y_n}\right) dY \tag{2.9}$$

2.5 Stochastic multiscale analysis of trabecular bone

Considering the large scattering of mechanical properties of trabecular bone due to individual differences, stochastic homogenization analysis method was introduced. The homogenized elastic tensor $\boldsymbol{D}^H$ is written by the following equation.

$$\boldsymbol{D}^H = \boldsymbol{D}^H(\boldsymbol{X}, \boldsymbol{D}(\alpha), \beta) \tag{2.10}$$

where $\boldsymbol{X}$ is the geometrical information. $\boldsymbol{D}$ is the elastic tensor of bone tissue with a function of random parameter α whose expected valued is zero. β is a scalar correction factor due to unknown miscellaneous uncertainties, which was calibrated by many published measured values for human vertebral trabecular bone. Basaruddin et al. (2013) predicted the value of $\beta = 8$. In this analysis of human mandibular bone, it was assumed that the same large scattering happens and the same value of β was used. The intra-individual difference by image-based modeling is considered as $\boldsymbol{X}$ and the parameter, α

and β are considered as the inter-individual differences calibrated by the human vertebra. The elastic tensor $\boldsymbol{D}$ is assumed to be in a normal distribution and for small fluctuation α the homogenized elastic tensor was approximated in an expansion form as follows

$$\boldsymbol{D}^H = \sum_{j=1}^{n} Pr(\boldsymbol{Y}_j)\, \boldsymbol{D}^H_{\boldsymbol{Y}_j}(\alpha, \beta)$$

$$\approx \sum_{j=1}^{n} Pr(\boldsymbol{Y}_j)\left\{\left(\boldsymbol{D}^H_{\boldsymbol{Y}_j}\right)^0 + \beta\left(\boldsymbol{D}^H_{\boldsymbol{Y}_j}\right)^1 \alpha\right\}$$

$$= (\boldsymbol{D}^H)^0 + (\boldsymbol{D}^H)^1\alpha \tag{2.11}$$

The superscript '0' indicates the deterministic term, while '1' represents the first-order differential of stochastic variable, α at $\alpha = 0$. There are two cases that consider one (3) and two (4) α respectively as shown in the next equations. For example, equation (4) considers the fluctuation in the Young's modulus, *E* and the shear modulus, *G* [2]. In this study, Eq. (3) using only one α is employed

$$\boldsymbol{D}(\alpha) = \boldsymbol{D}^0 + \boldsymbol{D}^1\alpha \tag{2.12}$$

$$\boldsymbol{D}(\alpha_1, \alpha_2) = \boldsymbol{D}^0 + \boldsymbol{D}^1_1\big(E(\alpha_1)\big) + \boldsymbol{D}^1_2\big(G(\alpha_2)\big) \tag{2.13}$$

Next, the expected value and variance of the homogenized elastic tensor $\boldsymbol{D}^H$ can be defined as follows:

$$Exp[\boldsymbol{D}^H] = (\boldsymbol{D}^H)^0 \tag{2.14}$$

$$Var[\boldsymbol{D}^H] = (\boldsymbol{D}^H)^1(\boldsymbol{D}^H)^1 cov[\alpha, \alpha] \tag{2.15}$$

The zeroth and first order terms in the above equations can be obtained according to the conventional deterministic homogenization theory by solving the following equations;

$$\left(\boldsymbol{D}_{\boldsymbol{Y}_j}^H\right)^0 = \frac{1}{|\boldsymbol{Y}_j|}\int_{\boldsymbol{Y}_j} \boldsymbol{D}^0\, d\boldsymbol{Y}_j - \frac{1}{|\boldsymbol{Y}_j|}\int_{\boldsymbol{Y}_j} \boldsymbol{D}^0\boldsymbol{B}\boldsymbol{\chi}^{\boldsymbol{0}}\, d\boldsymbol{Y}_j \tag{2.16}$$

$$\widehat{\boldsymbol{\chi}}^{\boldsymbol{0}} = \left[\int_{\boldsymbol{Y}_j} \boldsymbol{B}^T\boldsymbol{D}^0\boldsymbol{B}d\boldsymbol{Y}_j\right]^{-1}\left\{\boldsymbol{B}^T\widehat{\boldsymbol{D}}^0 d\boldsymbol{Y}_j\right\} \tag{2.17}$$

$$\left(\boldsymbol{D}_{\boldsymbol{Y}_j}^H\right)^1 = \frac{1}{|\boldsymbol{Y}_j|}\int_{\boldsymbol{Y}_j} \boldsymbol{D}^1\, d\boldsymbol{Y}_j - \frac{1}{|\boldsymbol{Y}_j|}\int_{\boldsymbol{Y}_j} (\boldsymbol{D}^0\boldsymbol{B}\boldsymbol{\chi}^{\boldsymbol{1}} + \boldsymbol{D}^1\boldsymbol{B}\boldsymbol{\chi}^{\boldsymbol{0}})\, d\boldsymbol{Y}_j \tag{2.18}$$

$$\widehat{\boldsymbol{\chi}}^{\boldsymbol{1}} = \left[\int_{\boldsymbol{Y}_j} \boldsymbol{B}^T\boldsymbol{D}^1\boldsymbol{B}d\boldsymbol{Y}_j\right]^{-1}\left\{\boldsymbol{B}^T\widehat{\boldsymbol{D}}^1 d\boldsymbol{Y}_j\right\} \tag{2.19}$$

where $\boldsymbol{\chi}$ is the collection of six modes of characteristic displacements $\widehat{\boldsymbol{\chi}}$ and the superscript denote the order terms. $\widehat{\boldsymbol{D}}$ is the corresponding column of $\boldsymbol{D}$. $\boldsymbol{Y}_j$ denotes the region of representative volume element (RVE) and $|\boldsymbol{Y}_j|$ its volume.

2.6 Stochastic finite element analysis of drilling force calibrated by measured data using fresh cadaver

The finite element analysis (FEA) of the drilling force in the oral implant surgery is very difficult to measure due to the drill behavior such as its dynamic motions, the interaction between the muscle joints and the jawbone, the effects of the debris from drilling the jawbone, the contact condition between the drill and the jawbone, and the destruction of the jawbone. In this case a nonlinear analysis is most preferable. In spite of that, with many unknown parameters, Tawara et al. (2015) proposed a simplified sequential linear analysis to calculate the drilling force in oral implant surgery.

Figure 2.11 shows the schematic view of the cross section of the computational model. The model consists of the jawbone constructed based on micro-CT images of a cadaver, the drill which was simplified by a 2.0 mm cylinder with the length of 20 mm and a rigid stand attached to the bottom of the jawbone. For the contact condition between the drill and the jawbone, it was simplified with a soft material as shown in Figure 2.12. The direction of the mesiodistal, buccolingual, and drilling of the jawbone was defined as x, y and z respectively. For the mechanical properties, every element was assumed as isotropic material and the drill and the bone Young's modulus were defined as E_{stain} and E_{bone} respectively.

The soft material surrounding the drill as shown in Figure 2.12 was set with a lower material property than the bone. The starting point of the drilling was set as $z = 0.6$ mm and at the location at which the drill enters the trabecular bone area. The analysis was carried out at the intervals of 0.5 mm until the depth of 13 mm. In the case that the

mandibular canal was not fully perforated, the drilling continued until the drill passed through the canal. For the boundary conditions, the constraint condition was set with the jawbone secured to a rigid stand and a normalized prescribed displacement of 0.01 mm was set at the nodes of the front edge of the drill to imitate the drill's movement of entering the jawbone. The reaction force was then calculated at the underside of the drill and only the drilling force for the trabecular bone region was calculated. The whole analysis was done using VOXELCON (Quint Corporation, Tokyo, Japan).

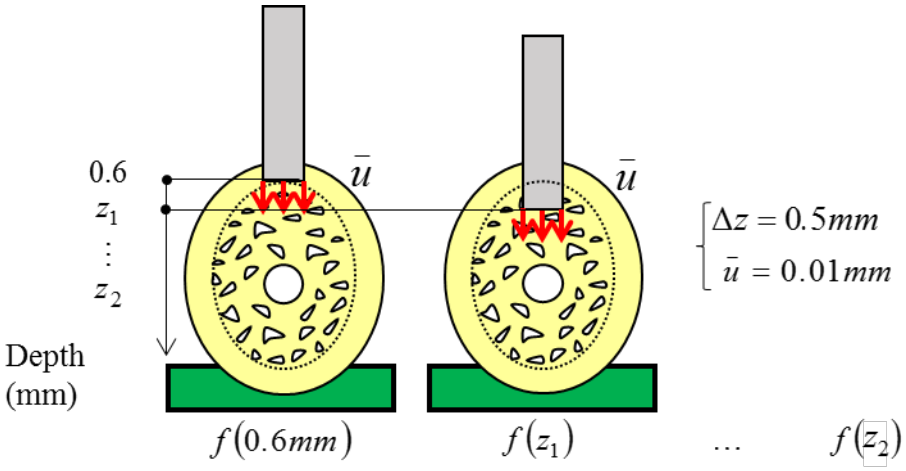

(a) Normal case

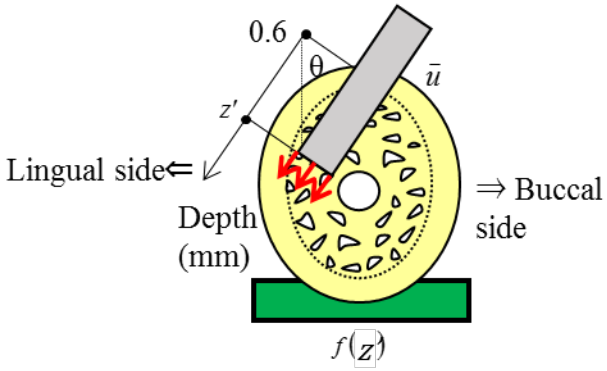

(b) Perforation case

Figure 2.11 Schematic view of the cross section of the computational model

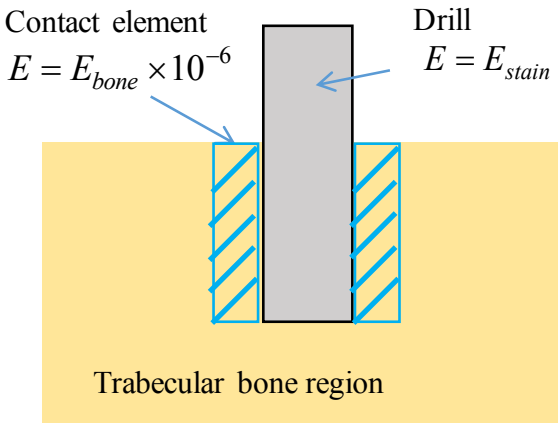

Figure 2.12 Set up of the contact condition between the drill and the jawbone

Regarding the material property of the bone, as reported by Tawara et al. (2015), two types of analysis was done considering the variability of the calculated homogenized elastic moduli in the drilling direction as which was described in the previous section. The expected value and variance of the homogenized property of Young's modulus was used and the material properties was calculated as follows

$$\boldsymbol{E}_{bone} = \boldsymbol{E}^0 \tag{2.20}$$

$$\boldsymbol{E}_{bone} = \boldsymbol{E}^0 \left(1 - \frac{\sqrt{Var[\boldsymbol{E}_z^H(\theta)]}}{Exp[\boldsymbol{E}_z^H(\theta)]}\right) \tag{2.21}$$

The calculated reaction forces were then defined as μ and $\mu - \sigma$. Based on findings by Miyabe et al. (2007), the orientation of the biological crystalline apatite in the trabecular bone had a normal distribution so the distribution of the force would relate closely and the individual differences could be described as a probabilistic distribution.

As a result, the 50% and 90% probability was shown as the individual differences and implemented as the drilling force database.

In order to improve confidence and reliability, the calculated drilling force was calibrated by an experiment done on a fresh cadaver. Three cases of drilling the cadaver were tested including normal drilling, the perforation of the mandibular canal and the perforation of the lingual cortical bone. In all the cases, the fresh cadaver was fixed completely to a stand. Figure 2.13 shows the cadaver during the calibration process done by an expert clinician. The cadaver was placed on top of an electronic balance in order to measure the force impressed on the cadaver. The results on the experiment were between 10 N and 12 N for the cortical bone and between 5 N and 6 N for the trabecular bone region.

Figure 2.13 Calibration done based on experiment on fresh human cadaver by expert clinician

(Tokyo Dental College Ethics Committee approval number: 00356)

The calibration method followed the description by Tawara et al. (2015), as an imaginary cortical bone was inserted at the location of $z = 0.6$ mm by assuming there is a thin layer of cortical bone left after drilling the upper layer of the cortical bone with

a round bur. The reaction force was assumed to be 10 N as obtained from the experiment and calibrated as follows

$$F(z) = \frac{10}{f(0.6)} f(z)[N] \tag{2.22}$$

The calibration was adapted for all types of jawbone regardless of the depth of the upper cortical bone.

On the subject of the perforation case considered for the drilling force database, a z' axis was defined as the new drilling direction by rotating the angle of drilling by theta. The same condition was considered and analyzed. For the material properties, a new axis was defined and recalculated as follows. The same method was the used for the implementation of the database. The whole calculation can be summarized as follows

$$\text{Normal case} \begin{cases} \text{Exp}\left[\boldsymbol{D}^{H}\right] \\ \text{Var}\left[\boldsymbol{D}^{H}\right] \end{cases} \rightarrow \begin{cases} \text{Exp}\left[E_z^H\right] \\ \text{Var}\left[E_z^H\right] \end{cases} \tag{2.23}$$

$$\downarrow \text{Rotation by } \Theta$$

$$\text{Perforation case} \begin{cases} \text{Exp}\left[\boldsymbol{D}^{H'}\right] \\ \text{Var}\left[\boldsymbol{D}^{H'}\right] \end{cases} \rightarrow \begin{cases} \text{Exp}\left[E_{z'}^H\right] \\ \text{Var}\left[E_{z'}^H\right] \end{cases} \tag{2.24}$$

Where the homogenized elastic moduli of the z' axis were calculated as the rotation of the z axis at θ-degree.

The results of the calculation are as shown in Figure 2.14. Note that the calculation is only done on the trabecular bone region for both cases and it was assumed the starting point is $z = 0.6$ mm as mentioned previously. The reaction force obtained was calibrated based on Equation 2.22.

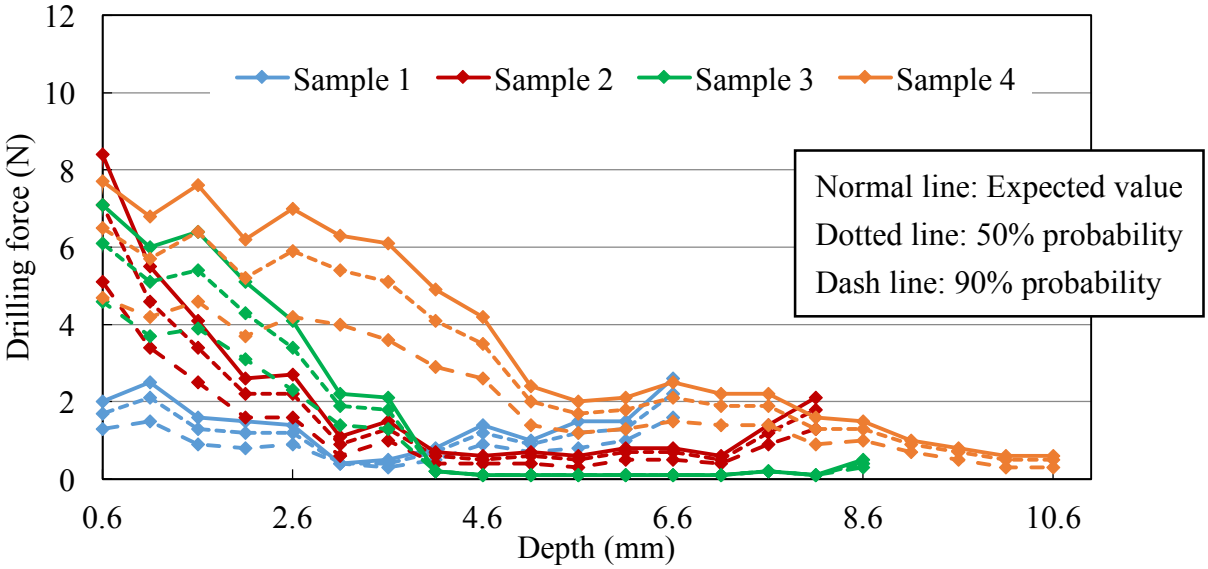

(a) Normal case

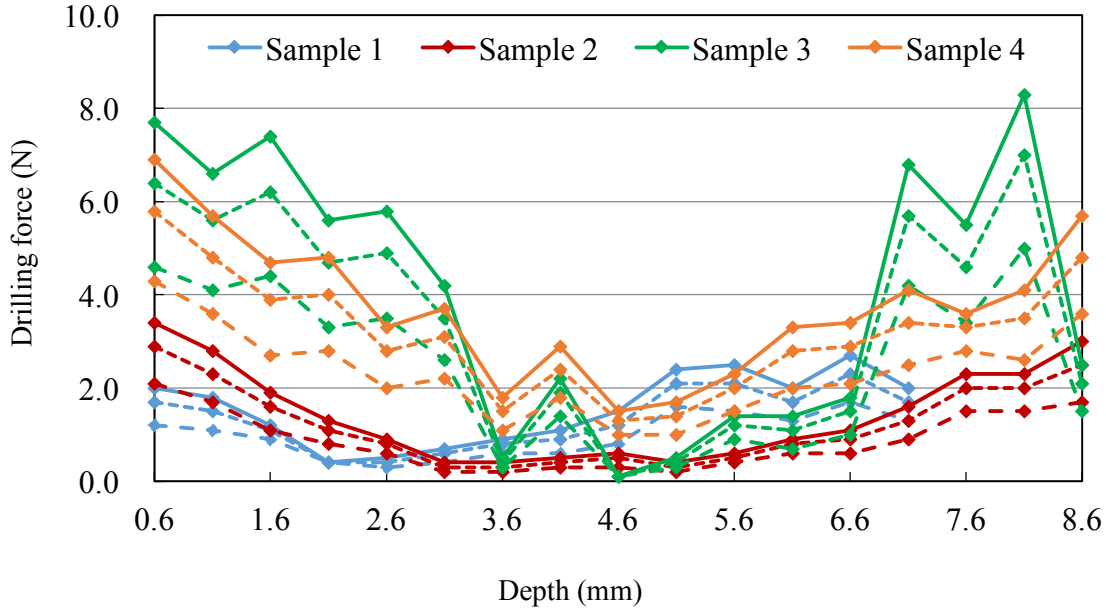

(b) Perforation case

Figure 2.14 Calculated drilling force in the trabecular bone region

Chapter 3

Development of the oral implant surgery training simulator

3.1 Machine design

Research suggested that one of the reasons of oral implant failures is the dentist's own lack of knowledge and experience (Chrcanovic et al., 2014; Paquette, Brodala, & Williams, 2006). This was also pointed out in a few studies on bone drilling and oral implant (Limbert et al., 2010; Melo et al., 2006). Furthermore, dental colleges and universities rarely amend their education system to include the syllabus about oral implant (Aljohani & AlGhamdi, 2009; De Bruyn et al., 2009; Koole, Vandeweghe, Mattheos, & De Bruyn, 2014). However, various initiatives had been done in order to overcome this problem such as the introduction of haptic device (Zheng et al., 2012).

Despite of the haptic device available as of today, most of them are readily

equipped with surgical tools that are not actually usable in an actual surgery. As the solution, an oral implant surgery training simulator was designed and developed targeting the students of dental colleges, universities and also the owner of a town clinic.

The design of the machine is based on a few studies that were done earlier and it was implemented into the simulator. Figure 3.1 shows the overview of the development of the oral implant surgery training simulator. The development started from the prototype machine which includes a drilling force input device, a user interface, the drilling force database.

The machine was then evaluated by clinician and compared with educational polymeric model which was used by students of dental colleges to tune up the control device. During the tuning up process, the design was further improved and the final version of the machine was readied to be used in class which will be further explained in the next chapter. An overview of the newest version of the machine is shown in Figure 3.2**.**

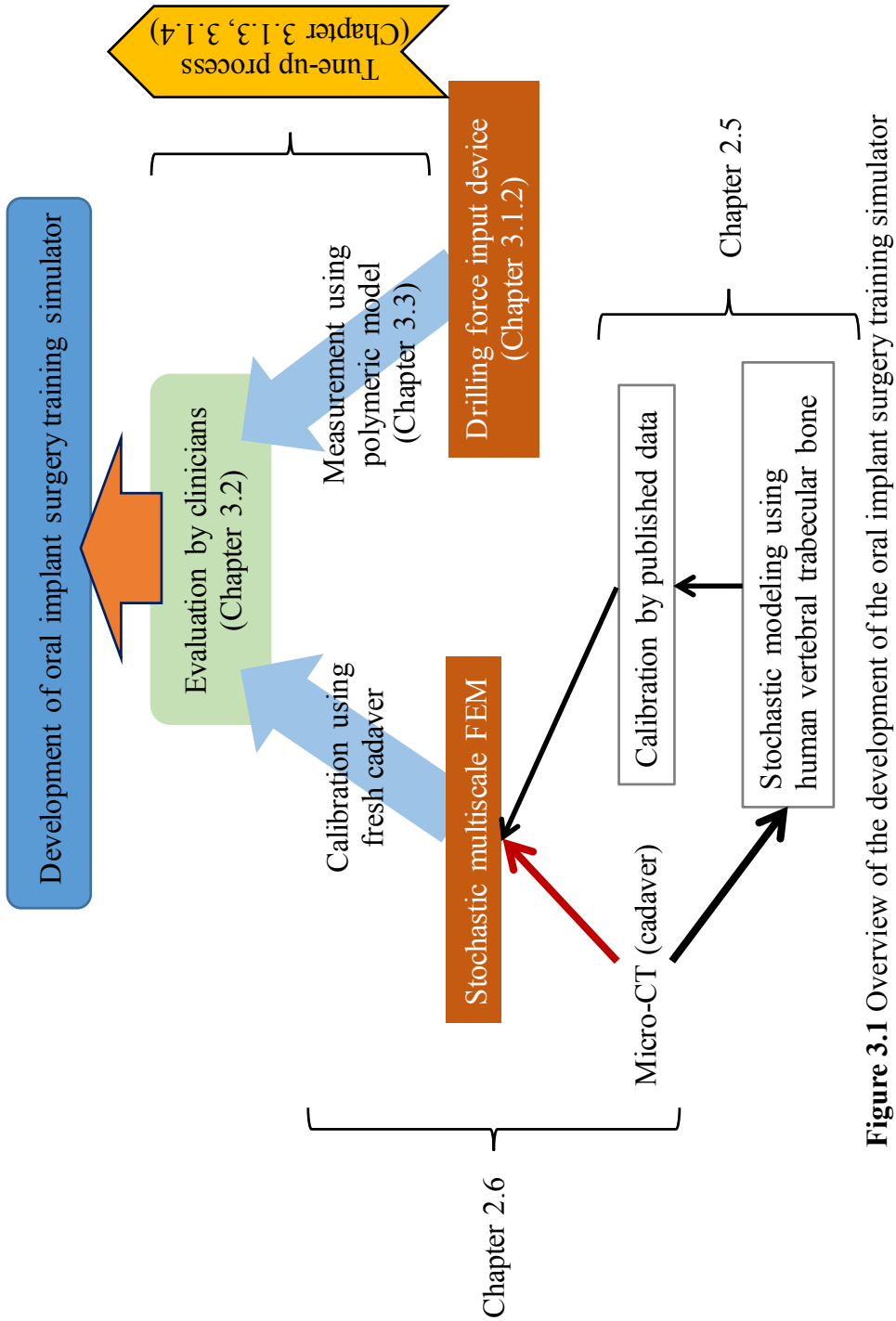

Figure 3.1 Overview of the development of the oral implant surgery training simulator

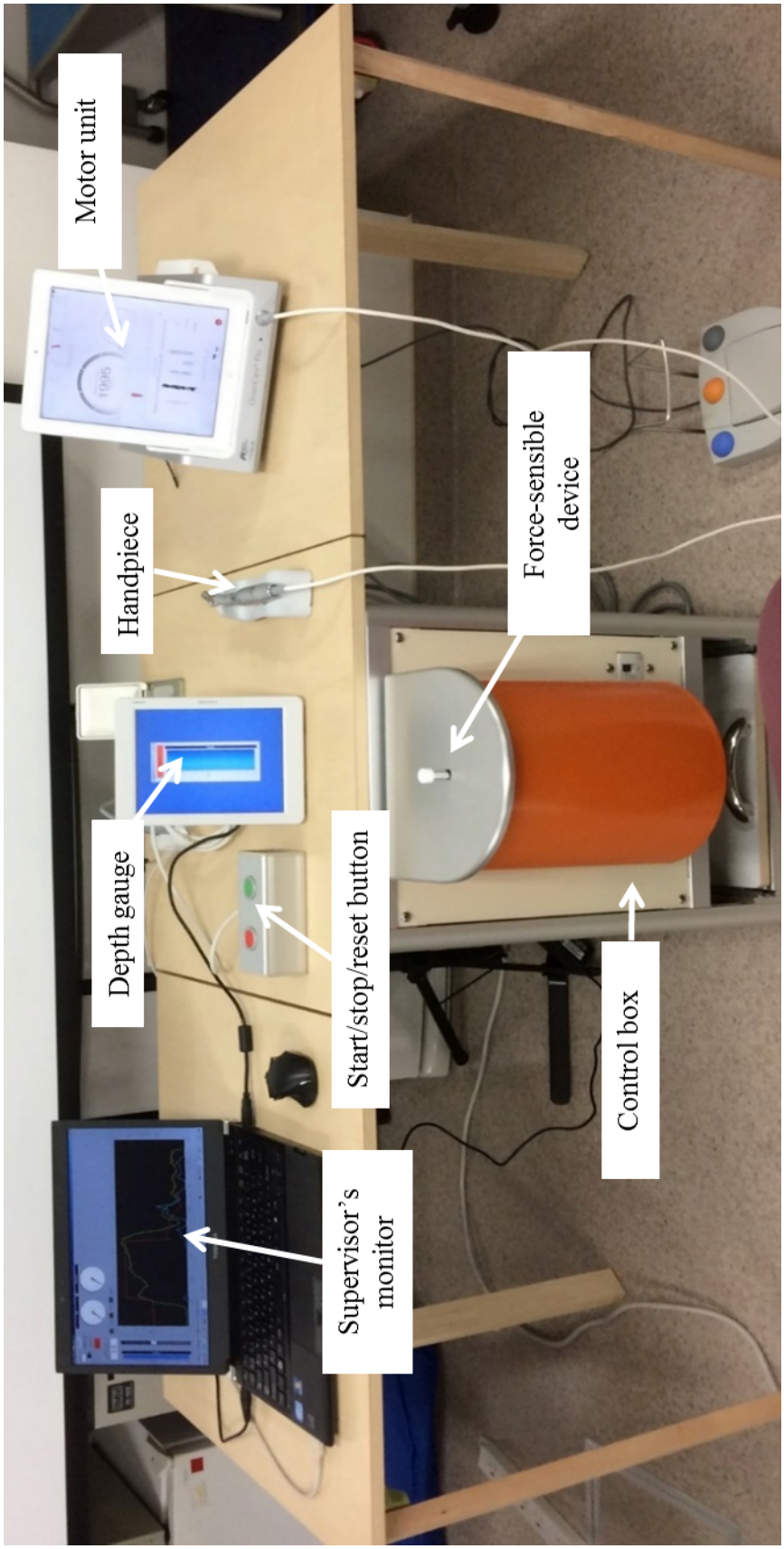

Figure 3.2 Overview of the oral implant surgery training simulator

3.1.1 Requirements and design strategy

The base design of the machine is the drilling process in an oral implant surgery right after the cutting of the cortical bone in the upper part of the jawbone using a bur. The main focus of this simulator is the situation of drilling a thin layer of cortical bone left due to the cutting and drilling the trabecular bone region of the posterior mandible. An overview of the simulator database which controls the simulator movement can be seen in Figure 3.3. This is actually the pilot drilling part in the drilling process as shown in Figure 2.6.

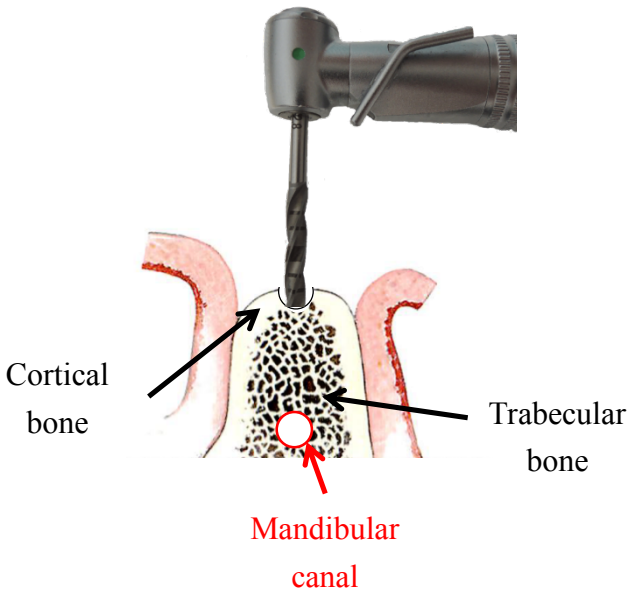

Figure 3.3 An overview of the simulator database

In a real surgery, the drill is used by attaching it to the handpiece. The motor unit is attached to the handpiece as shown in Figure 3.2. This motor unit controls the rotational

movement of the drill. The movement follows a setup of rotational speed and also the direction of rotation; clockwise or counter-clockwise. The rotational speed is usually defined by rotation per minute (RPM) which is the rotational speed of the drill during the whole drilling process. The rotational speed of the drill can be adjusted using the foot pedal which is attached to the motor unit. There is also a motor unit that sets the rotational speed first and the user had to stop the drilling if they wanted to change the rotational speed.

The drilling speed is defined as the downward movement speed of the drill as the drilling is done with respect to depths. This value is one of important calculation in this study. The rotational speed is different based on the guideline of the universities when using the pilot drill and they changed the rotational speed according to the drill that they used. So, the rotational speed was neglected in this study from the variational parameter because of the different guideline of universities.

Following closely the movement of the drilling process. An actuator (DRS42SA2G-04MK, Oriental Motor Co. Ltd., Tokyo, Japan) which uses a stepping motor was programmed to move a drilling force input device according to the input force given by the user as measured by a load cell (LMB-A-50N, Kyowa Electronics Instrument Co. Ltd., Tokyo, Japan). The programmed movement is actually based on the database that was created by applying the finite element analysis (FEA) of drilling force that was calibrated by measuring the data using fresh cadaver as explained in the previous chapter.

In order to understand more about the design strategy, the machine can be divided into three main components. Firstly, the drilling force input device. Secondly, the actuator control system and thirdly, the user interface. The actuator control system will

be described and explained in the later section as it was tuned up after the evaluation done on expert clinicians.

The whole system was finally added with feature that increase the usability of the machine that can be seen in the newest design as shown in Figure 3.2. One of them is the mobility of the apparatus as it can be transform to a compact mode (Figure 3.4(a)) and equipped with a caster underneath the machine, which is suitable for portability, easier transportation and also stored easily. Moreover, under the control box there is a compartment to store the laptop and motor unit used with the machine (Figure 3.4(b)) making storage a lot easier.

The control box can also be adjusted according to the user height making it a universal and robust design (Figure 3.4(c)). The height adjustment can be made within the range of 30 cm based on the preferences of a clinician treating the patient. The height from the floor to the patient's mouth is about 60 to 90 cm thus the determined range. This number changes based on the bed used by the clinicians and their own preferences which is one of inter-individual differences.

To sum up, the simulator measures the user's input load by a load cell and the elapsed time of the drilling. The actuator calculates the distance it traveled that is equivalent to the depth of the drilling. These values are used together with an implemented database to determine the actuator gain output. By calculating the depth increment divided by interval time of 0.2 seconds, the simulator output the drilling speed.

(a) The compact version of the simulator. The legs of the table can be attached and detached to fold the table for mobility.

(b) The lower part of the simulator has a compartment to store the laptop and motor unit

(c) View of the simulator after it is set up. The force-sensible device (orange part of the machine) can be adjusted according to the user height

Figure 3.4 The added feature of the oral implant surgery training simulator

3.1.2 Drilling force input device

This device consists of a decentering jig, a receiver plate attached to a center pole, and a load cell (LMB-A-50N, Kyowa Electronics Instrument Co. Ltd., Tokyo, Japan) that sense the input force given by the user. The load cell is then attached to an actuator that control the movement of the center pole as it drops down according to the force given through the receiver plate. The schematic view of this device can be seen in Figure 3.5. The whole device is connected to the control box which controls the whole system.

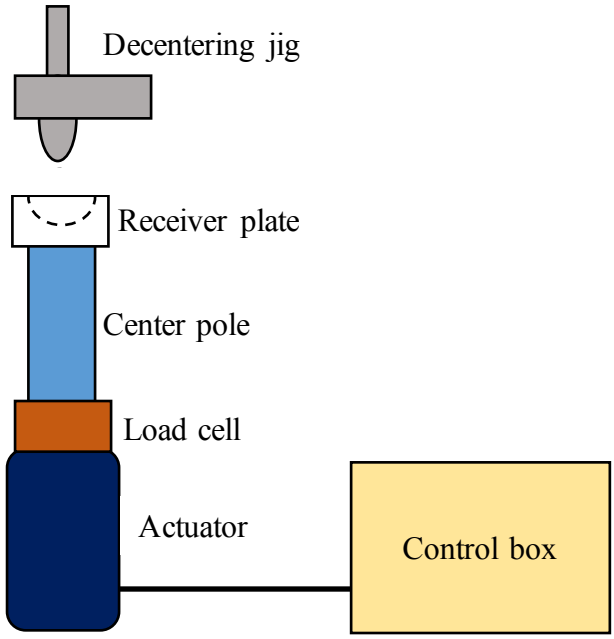

Figure 3.5 Schematic view of the drilling force input device

Figure 3.6 shows the actual figure of the drilling force input device. Most of the device is hidden in the final product. It is located in the orange curve section of the simulator shown in Figure 3.2.

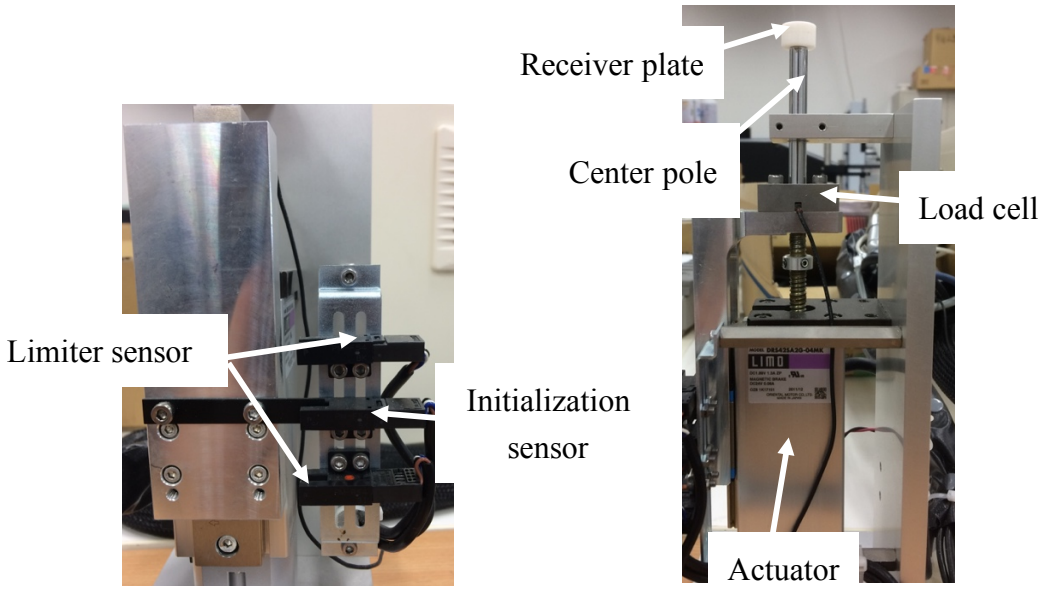

(a) Side view (b) Main view

Figure 3.6 The drilling force input device hidden in the simulator

The decentering jig was designed to give the feeling of the drill vibrating sideways in a real drilling process while using the simulator. The jig was firstly designed using wood as its material and made with the cutting process. Next, it was made using a polymeric material. To show the depth, a depth mark was devised making the part that touch the receiver plate to be quite lengthy. The material for the jig was then changed to aluminum to reduce the cost. Figure 3.7 shows the polymeric jig and the aluminum jig during the early stage of design. While drilling, the depth mark seems hard to be seen and deem unusable, thus making the part that touches the receiver plate much shorter as shown in Figure 3.8. This is the jig that is used as of today as one of the drilling input force device.

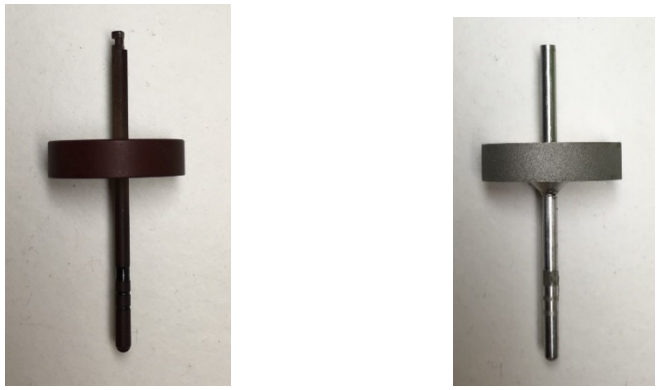

Figure 3.7 Decentering jig in the early development, polymeric jig (left) and aluminium jig (right)

Figure 3.8 Decentering jig

During the early stage of design, a screw was used at the place of the receiver plate. This leads to the jig being easily wear and become unusable due to the friction of the jig with the top of the screw. To reduce the cost of making the jig in a large quantity, the receiver plate was devised as its solution. The plate is made from a polymer that could give the sense of the reaction force to the user without wearing the jig. There are 3 types of receiver plate that was designed with different radius of the plate valley; 7.5 mm, 12.5 mm and 15 mm. One plate which is 12.5 mm, was then chosen with the preferences of an expert clinician. Figure 3.9 shows the receiver plate while unattached to the pole.

(a) Top (left) and side (right) view of the receiver plate

(b) The receiver plate

Figure 3.9 Receiver plate from different angle of view

Working as an intermediate attachment between the user and the load cell, the pole is designed to accommodate the full length of the drilling sensation. The length of the pole is 66 mm and it is enough to let the user feel drilling through a whole cadaver while being not too long so that the force feedback from the load cell and actuator is not wrongly sent.

Load cell works as a sensor as it measures the user input force and sending it to the control box to be calculated. The calculated force will then be sent back to the actuator to control the movement of the pole attached to the actuator. This way, the user can feel the drop of depth as they were drilling an actual mandible.

There are also limiter sensors (FPMF54, MISUMI Corporation, Tokyo, Japan) attached to the device, as shown in Figure 3.6, in order to limit the movement of the device and an initialization sensor to move the sensor to the initial location after resetting the device. The sensors are also used to verify the calculated depth during the initial setup of the device. The movement of the actuator is checked starting from the location of initialization sensor to the location of the lower limiter. The movement according to that control signal was checked visually and verified.

3.1.3 Actuator control system

The control of the simulator mainly lies in the load cell and the actuator which is part of the force sensing device. It measures the force given by the user and moves the actuator according to the drilling force database which is a part of the software for the simulator. The control system is an open loop system and the control algorithm of the simulator, which is implemented in the control box, is shown in Figure 3.10.

When the user starts the system, the sampling time, t, starts. At time, t, the current location is sent from the actuator. As mentioned previously, the actuator uses a stepping motor which calculates the current location based on the signal pulse obtained from each step of the motor's movement sent from the control box. The force and gain output from the database at the identified location are retrieved and compared with the user input force which is measured by the load cell. If the input force is higher than the force from the database based on the margin as referred in Equation 3.1, the actuator moves accordingly based on the setting of the gain. The system repeats itself until the user stops or the

location, z, is at the maximum point. The sampling time for this simulator is 0.2 seconds. For every sampling time, the value of input drilling force and output drilling speed is recorded.

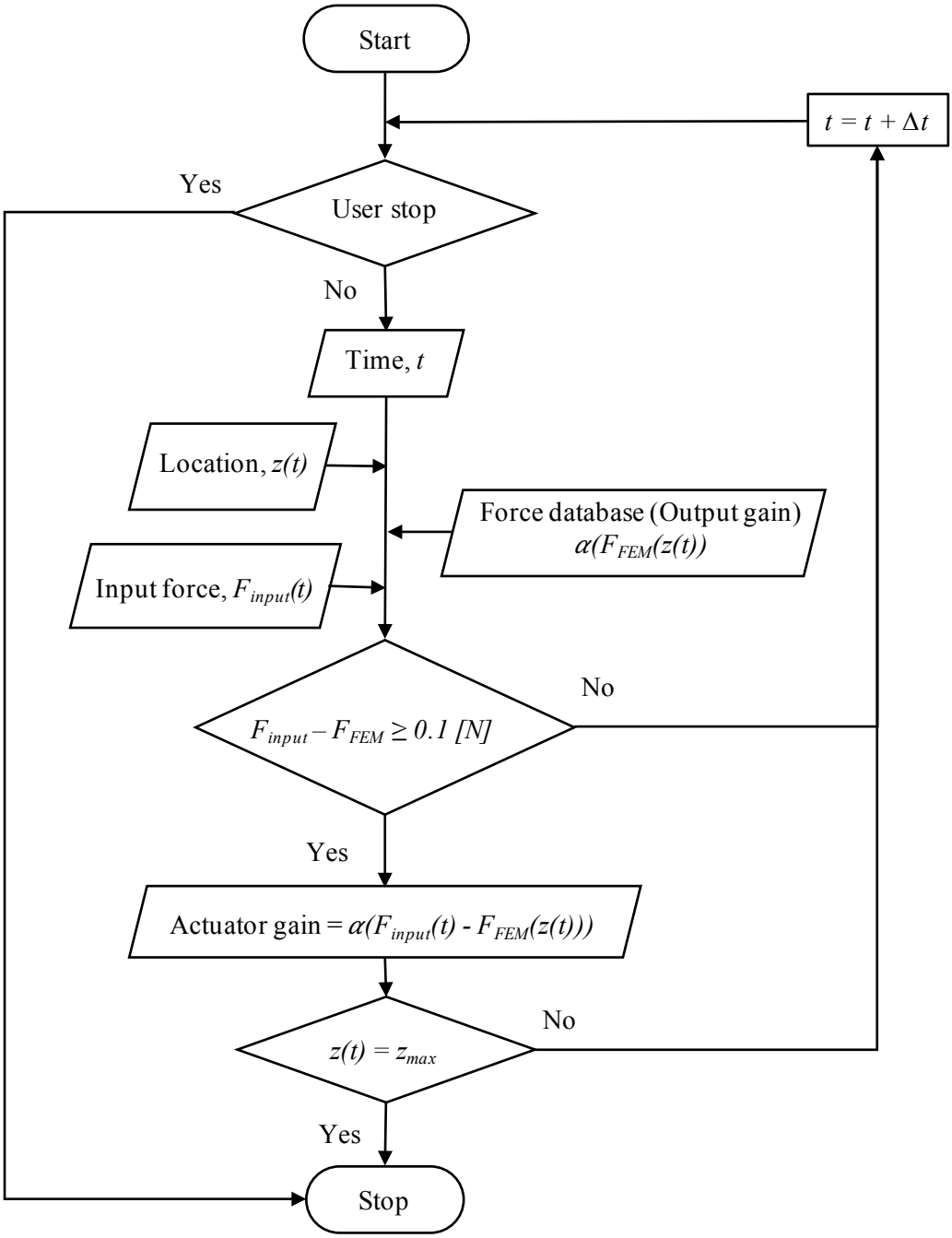

Figure 3.10 Flowchart of the actuator control system

The user input force and the drilling force database determines the speed of the force-sensing device based on these equation:

$$V = \begin{cases} 0, & F_{input} < F_{FEM} + 0.1\ \text{N} \\ U_0 + \alpha\left(F_{input}(t) - F_{FEM}(z(t))\right), & F_{input} \geq F_{FEM} + 0.1\ \text{N} \end{cases} \quad (3.1)$$

For input force, F_{input} higher than the database, F_{FEM} the drilling speed is $U_0 + \alpha\left(F_{input}(t) - F_{FEM}(z(t))\right)$ and it follows the algorithm as shown in Figure 3.11. A margin of 0.1 N was considered to assure that the input force is surely larger than the required force. Based on the clinicians' evaluation, an expert clinician was able to feel and identify the difference of 1 N of force change. Then, about 10 percent of the value which concludes to 0.1 N was taken as the margin which is impossible to be sensed even by an expert clinician.

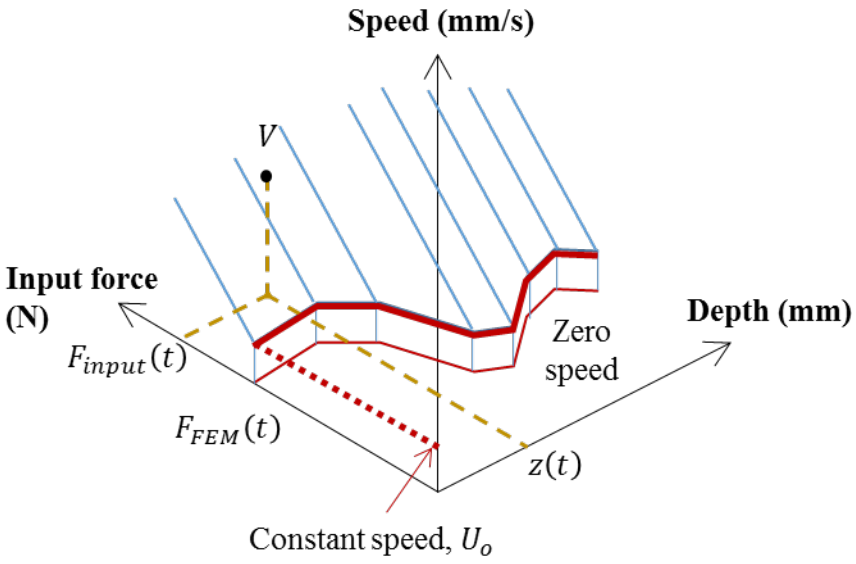

Figure 3.11 Algorithm for the speed of the force-sensible device

In the drilling force database, as represented in Figure 3.12, when the drill enters the trabecular bone region just after drilling the top part of the cortical bone, a small gap might happen between the real and output location. The gap happens as a result of different force value at a singular point in the stated location. However, if a feedback system is used, it makes a wrong movement if the location returns back. In that case, if the correct location is detected and used then the system misread the database. The location is also used to calculate the speed for each sampling time. The information about the drilling force database will be explained later in the next section.

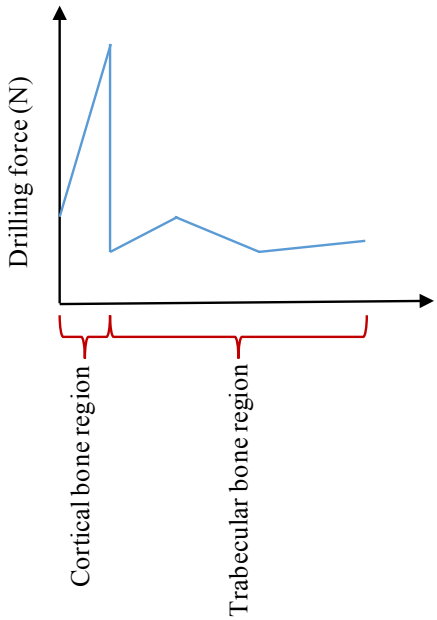

Figure 3.12 The curve representation of the drilling force database

Regarding the depth, it is calculated based on the signal pulse sent from the control box. The calculated depth is verified using sensors that act as the limiter as shown in Figure 3.6. The movement of the actuator is checked starting from the location of the initialization sensor to the location of the lower limiter. The movement according to that control signal was checked visually and verified. This verification was done with a level

of actuator power usually used in the trabecular bone region. On the contrary, at the singular point when the drill enters the trabecular bone region just after drilling the top part of the cortical bone, 25 times larger actuator power command is used compared to the trabecular bone region.

The system outputs the drilling speed which is calculated by the derivative of the actuator. In Chapter 3, the depth was derived from the output drilling speed by integrating it. In a newer version of the simulator, which is shown in Chapter 4, the system could output the location of the actuator to a CSV file thus making the recorded output much easier to be retrieved and analyzed.

The simulator output gain was tuned up by an expert clinician, Clinician A, which have a very extensive experience in oral implant surgery (Table 3.1). The clinician used Sample 1 and 2 for the tune up process as shown in the table. The information about the samples will be explained in the next section. Then, the program is slightly adjusted according to the clinician's comment and his feeling of drilling in comparison with a real case drilling.

Table 3.1 Information of Clinician A

Clinician	Clinicians' information		Sample tested	
	Cases handled	Years after graduation	Sample 1	Sample 2
A	Over 100	33	○	○

3.1.4 Calibration and tune up of drilling force database

The software part of the simulator is actually a drilling force database that was calculated using sequential linear static three-dimensional finite element analysis (FEA) on micro-CT images taken from different samples of cadaver (Tawara et al., 2015). The cross section of the model extracted from micro-CT images for the calculation process can be seen in Figure 3.13. There is a total of four samples obtained from different individuals used as the database as of today. Each of the samples has two cases in which a normal drilling and an accident of lingual perforation was done. Appending the calculation done in Section 2.9, this study adds the cortical bone region for the database as shown in Figure 3.12. This is done in order to provide a more realistic feeling of doing an oral implant surgery when using the simulator. For the perforation case, the cortical bone region is added once more at the bottom part after the trabecular bone region. Figure 3.14 shows the drilling force database of the normal drilling and the perforation case. The top part of the drilling force value for both cases and the bottom part of the perforation case was added to the drilling force calculated in Section 2.9.

After drilling the top part of the cortical bone with a round bur, the database puts a cortical bone region with 0.6 mm of thickness at the top part. The force value was calibrated based on the experiment done on a fresh cadaver as shown in Figure 2.13. As shown in Figure 3.13, notice the yellow region which represents the top part of the cortical bone. In some sample as it can be seen, the top part of the cortical bone was too thick and there are also samples that have too thin cortical bone. So, this value of 0.6 mm of thickness was determined to be the same for every sample of the database. The thickness of the cortical bone is added just before the calculated trabecular bone region. For the

perforation case, the thickness of the cortical bone is also adjusted to be similar for every sample. The thickness is set at 0.5 mm of thickness.

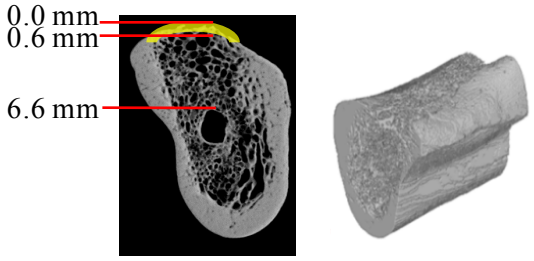

(a) Sample 1

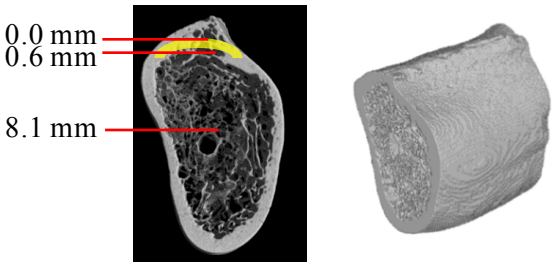

(b) Sample 2

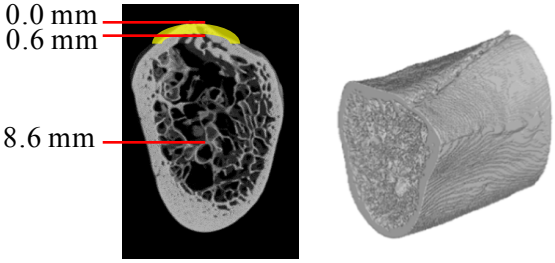

(c) Sample 3

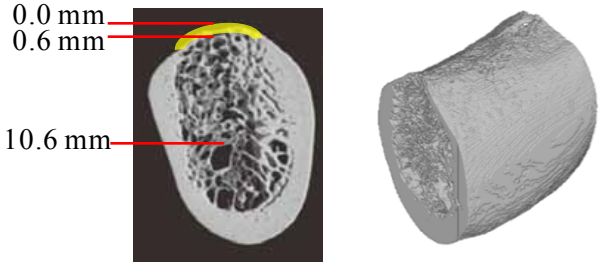

(d) Sample 4

Figure 3.13 Micro-CT images of the samples used for the database

The experiment consists of drilling the top part of the cortical bone, the normal drilling through the trabecular bone region and the perforation of the lingual cortical bone. The recorded value for drilling the cortical bone region was around 10 to 12 N. So, the value of 10 N was used for the top part cortical bone region and the value for the perforation of lingual cortical bone was calibrated to 12 N. These values can be seen in Figure 3.14. Notice the peak value at the top part of the drilling force database and also the value at the bottom part for the perforation case.

As mentioned in the previous section, these databases were tuned up by an expert clinician, Clinician A, which have many experiences of handling real surgery. The value of the output gain was selected based on the clinician preference. The clinician selected the best output gain that describe the feeling of the drill entering the trabecular bone region and the perforation of lingual cortical bone. Thus, the value of 25 times larger output than the trabecular bone region was chosen. The clinician also said the thickness set for the cortical bone is just nice and felt realistic for both cases.

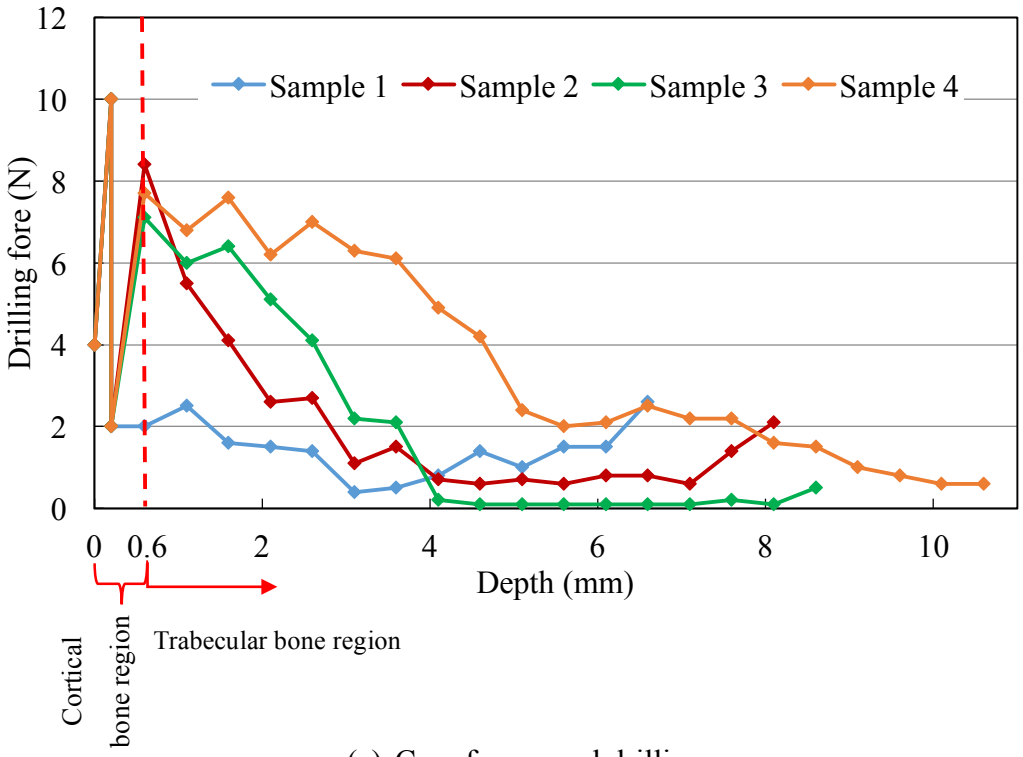

(a) Case for normal drilling

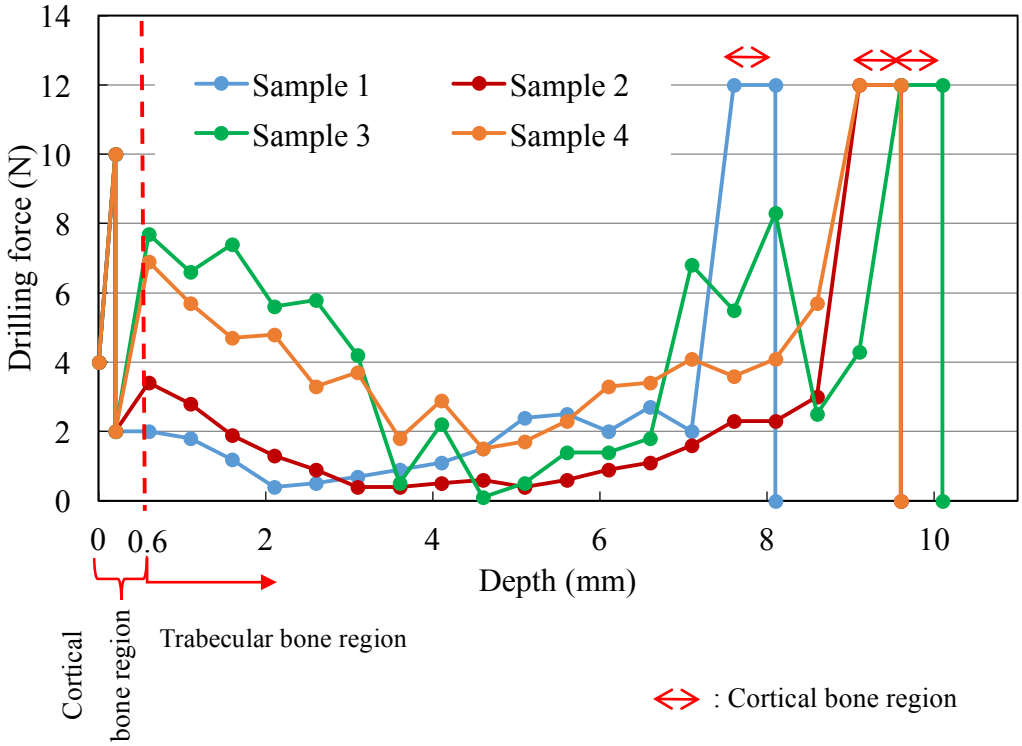

(b) Perforation case

Figure 3.14 The oral implant surgery simulator database

3.1.5 User interface and usage of the simulator

The user interface of the machine was designed and made to give information to the user about the drilling process. There are two interface designed which is the output software as shown in Figure 3.15 and the depth gauge as shown in Figure 3.16.

The output software was designed to give information to the user of their input force, drilling speed and also showing the drilling force database. This way, the user can learn from experience and an experienced clinician could also give advice based on the information provided.

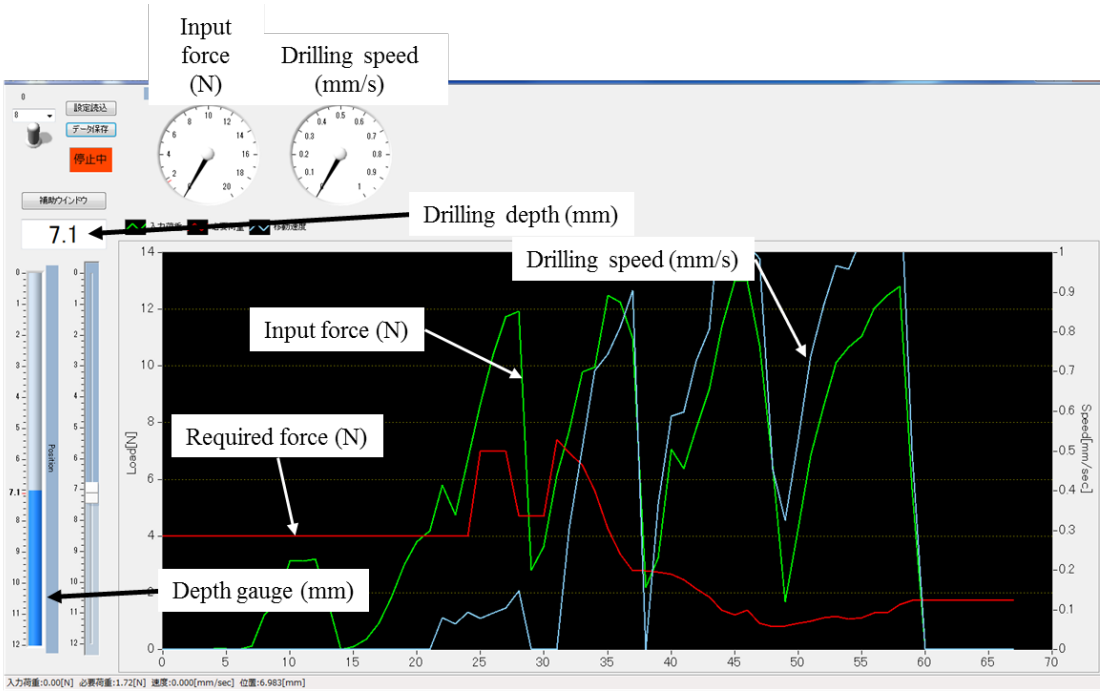

Figure 3.15 User interface of the output software

The depth gauge can be move and shown in a different monitor showing the user the drilling depth and also the target depth of drilling. The target depth shown on the depth gauge is actually set up to be 1 mm above the mandibular canal of the cadaver in the drilling force database. The gauge is thought to be the best way of showing the depth drilled by the user as the usage of a depth mark on the jig cannot be clearly seen while drilling.

The location is actually excluded from the output file as shown in Figure 3.15, so to output the file it has to be converted from the raw data. The depth is calculated based on the signal pulse sent from the control box. The verification of depth is as mentioned in section 3.1.2. This verification was done with a level of actuator power usually used in the trabecular bone region. On the contrary, at the singular point when the drill enters the trabecular bone region just after drilling the top part of the cortical bone, 25 times larger actuator gain command is used compared to the trabecular bone region.

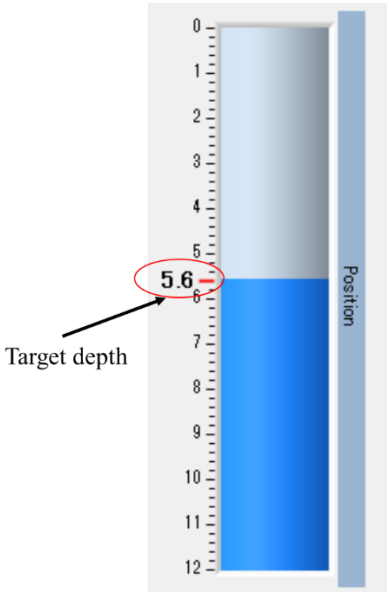

Figure 3.16 The depth gauge that can be shown in a different monitor

Figure 3.17 shows the flowchart of the usage of the simulator. Firstly, the user chooses a database of drilling force available. The database of the simulator is described in the previous section. The database consists of a few cadavers with different characteristic. Each cadaver has a few selectable scenarios including the perforation case.

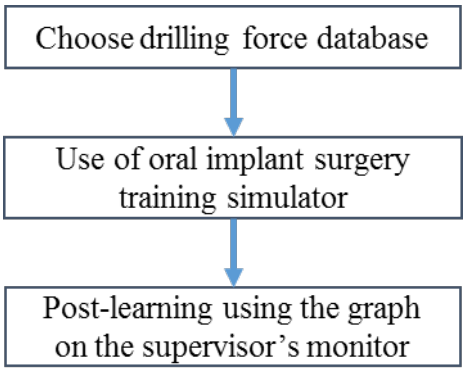

Figure 3.17 Flowchart of the usage of the simulator

The selected database is then sent to the control box in order to program the actuator movement according to the database. The user now can start the simulation by moving the handpiece that was attached with a decentering jig.

The usage of the training simulator requires the user to use their own handpiece and motor unit that is used in an actual surgery. This way, the user could sense the reaction force, sound and vibration of a real handpiece making it feels closer to a real surgery. However, instead of using a real drill, the simulator requires the usage of decentering jig as shown in Figure 3.18. The jig is able to imitate the slight vibration during drilling.

Next, the decentering jig is put on top of the receiver plate and the user can start

giving force to the pole. The pole will then move accordingly based on the selected database. Figure 3.19 shows an experienced clinician using the simulator.

When using the simulator, the user's input force is recorded together with the time and depth. The recorded data can be used to do a post-learning. One of the thing that the user may be able to learn is understanding whether his or her own input force performs just as they are expected or not. Stress acting on the jawbone is an important factor to ensure the safety of the surgery and if the actual load value and the user input value differs greatly, there is a possibility of an accident happening when surgery takes place.

Another lesson that can be done is the understanding how the input force of the user complies with the changes of drilling force based on depth and individual differences because even if the user's input force is as expected, the sparse structure of the trabecular bone would accidentally have made the input force to be much higher and the drilling speed faster causing the user to drill deeper than expected.

Figure 3.18 Decentering jig used to replace the actual drill when using the simulator

Figure 3.19 Experienced clinician using the oral implant surgery training simulator

3.2 Evaluation by clinicians

3.2.1 Evaluation method

The overview flow of the method is as shown in Figure 3.20. During this evaluation, only 3 samples were available, which is Sample 1, 2, and 3. Firstly, they were given a detailed explanation of the system of the training simulator and its database. They were shown the micro-CT images of the samples and the target depth that need to be drilled, which was located 1 mm above the depth of the mandibular canal. Next, the drilling simulation was done using the developed oral implant surgery training simulator. During the entire simulation, the information on the supervisor's monitor was hidden from the clinicians' view. In addition, during the drilling process, they were asked to give comments of the feeling that they sensed. However, the depth gauge as shown on Figure 3.16 was shown. The information of the required drilling force based on the numerical procedure explain earlier, and their input force and speed was only revealed after the simulation was done.

Then they are asked to mark the stiffness felt of the samples tested on a stiffness scale based on their experiences of handling actual surgical procedure as shown in Figure 3.21. Furthermore, the clinicians were asked to give their overall impression of the developed oral implant surgery training simulator.

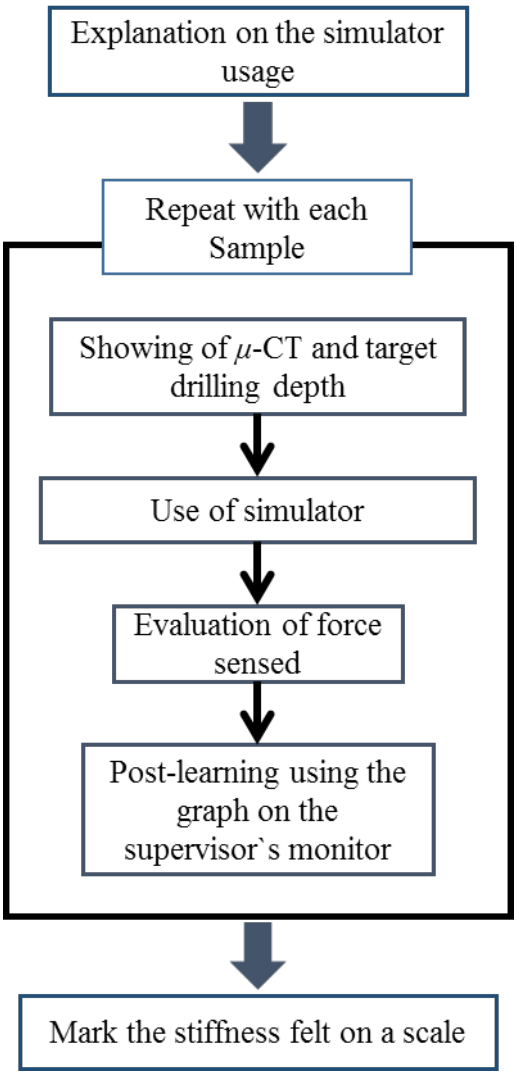

Figure 3.20 Flowchart of the evaluation method

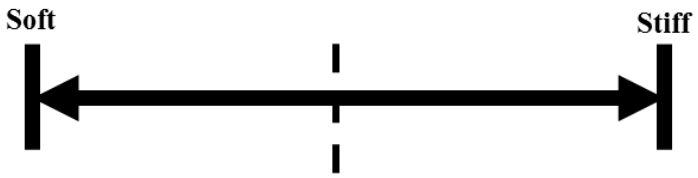

Figure 3.21 Stiffness scale made for the clinicians' evaluation

As shown in Table 3.2, a total of 7 clinicians that have experience on oral implant surgical procedures tested and evaluated the samples from the drilling force database. Only Clinician B and C tested all available samples and for the other clinicians, they tested only Sample 1 and 2. It is important to note that all clinicians have experience performing an actual surgery of oral implant.

Table 3.2 The clinicians' information that tested and evaluated the samples

Clinician	Clinicians' information		Sample tested		
	Cases handled	Years after graduation	Sample 1	Sample 2	Sample 3
B	Over 100	14	○	○	○
C	30	5	○	○	○
D	20	6	○	○	-
E	15	3	○	○	-
F	5	6	○	○	-
G	3	5	○	○	-
H	1	2	○	○	-

3.2.2 Results of evaluation

During the evaluation, as it can be seen in Table 3.2, most of the clinicians only tested two samples, which is Sample 1 and 2. Interestingly, they also showed different handpiece holding style as shown in Figure 3.22, mirroring their personal drilling style. As informed by the clinicians, the one hand handling as if holding a pen is the general handling style when doing a cavity treatment as the wrist could move really well when in that handling style. The handling style with accompanying left hand is to prevent mistake in the drilling direction. For the reverse hand style, it is done to remove the freedom of the hand and directly drill in one direction while removing the vibration.

Figure 3.22 Some of the clinicians' way of handling the handpiece

Another point of interest as shown in Figure 3.22 is the head mount display (HMD) that the clinicians wear. The HMD actually shows a video of a drilling process in an oral implant surgery in order to make the exercise more realistic. However, no further study was done in regards to the HMD because of the lack of time in order for it to be used as a part of the simulator. This part was actually omitted in the final design of the oral implant surgery training simulator.

All of the clinicians could differentiate the stiffness for each sample and accordingly marked them in the stiffness scale. For all of them, the stiffness felt marked in the scale were mostly in the lower region of the trabecular bone as they felt that Sample 1 is much stiffer than Sample 2 as shown in Figure 3.23. For comparison purposes, only some of the clinicians' result were selected. These clinicians showed the best representation of the typical type of drilling done by the other clinicians.

Figure 3.24 shows some of the individual results of the clinicians that done the evaluation with some comments added at the point of their drilling process. Two clinician's results were handpicked among all of the other clinicians as they best described the situation during the drilling by explaining the samples that they felt while drilling. Both clinicians also best described the comparison between an expert; as shown by Clinician C, and a beginner; as shown by Clinician F based on their different experience of handling real cases.

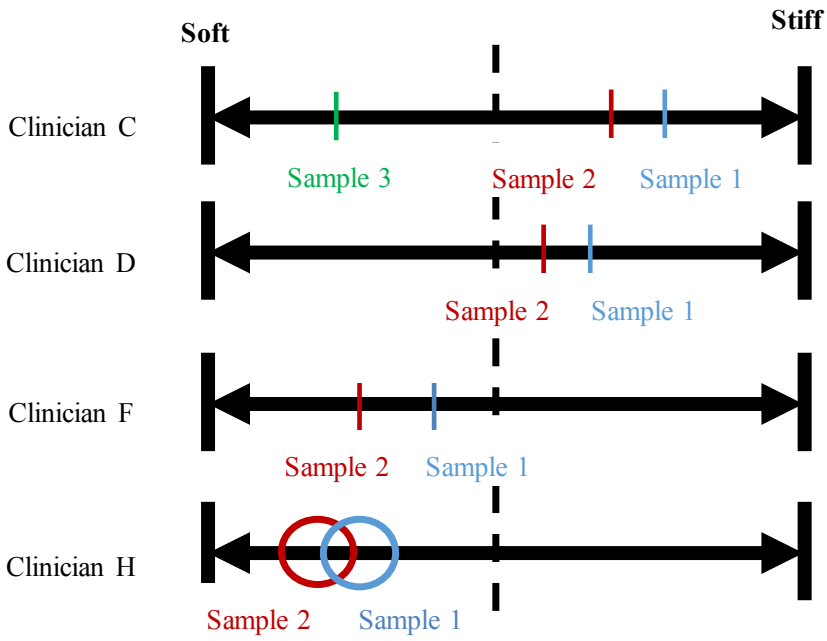

Figure 3.23 Results of some of the clinicians' evaluation

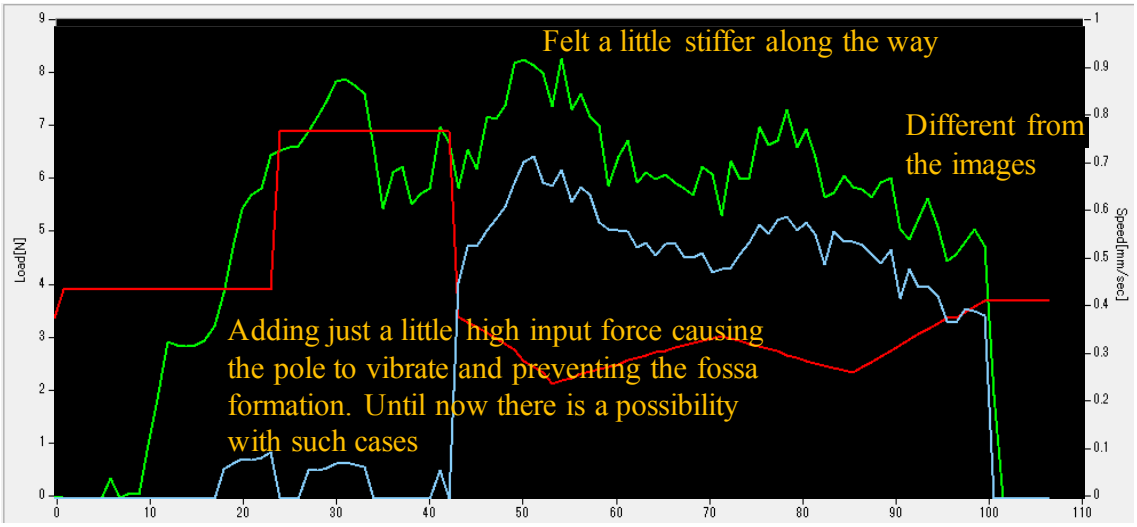

(a) Clinician C on Sample 1

(b) Clinician C on Sample 3

Figure 3.24 Individual results of the clinicians based on the output software with their comments

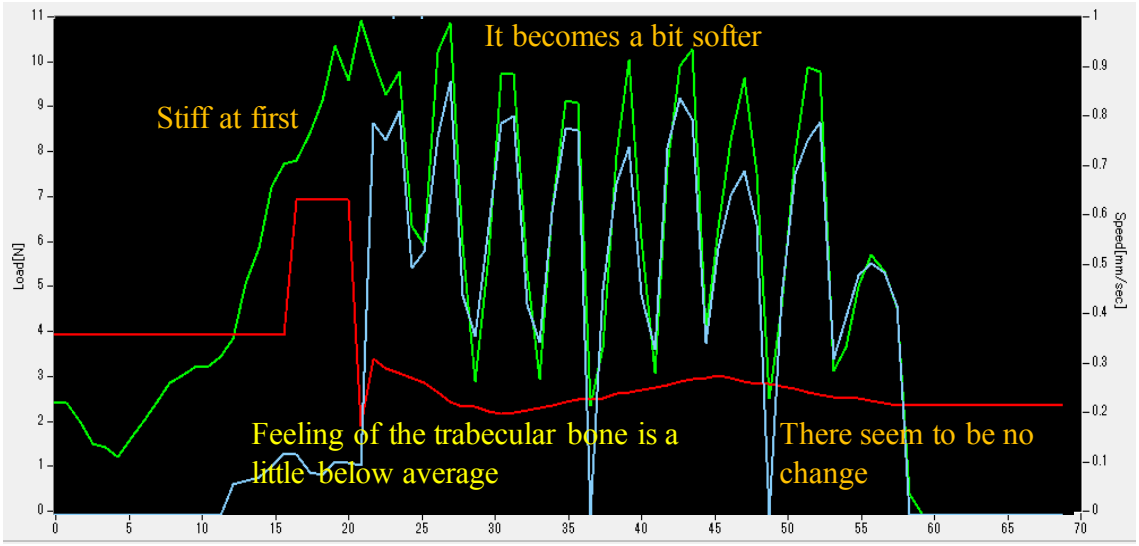

(c) Clinician F on Sample 1

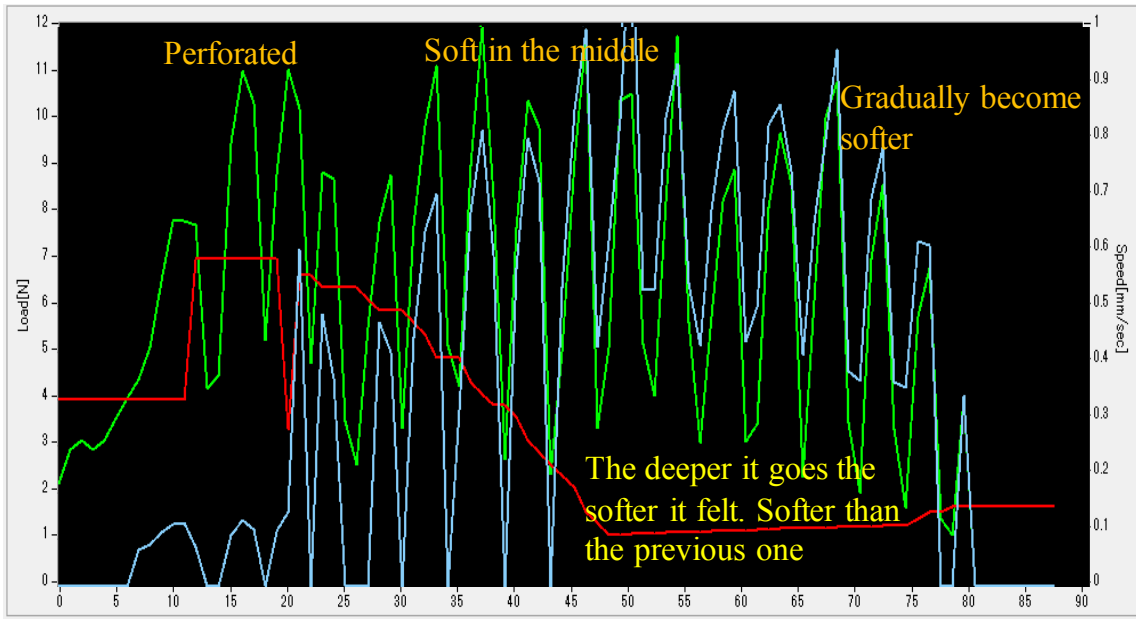

(d) Clinician F on Sample 2

Figure 3.24 Individual results of the clinicians based on the output software with their comments (continued)

By comparing the result with the drilling force database, it can be seen that the feeling of stiffness of the mandibular bone describe by the clinician is the lower part of the bone which is the depth of more than about 4 mm. Based on Table 3.2 and Figure 3.23, what is interesting in this data is that the feeling of stiffness for the samples shifted according to their experiences accumulated while doing an actual surgery. The more experienced clinician felt that the database's sample is stiffer than his average force felt while drilling in an actual surgery.

The comparison of results was further done by comparing the clinician's drilling speed. By comparing Figure 3.23 and Figure 3.25, focusing on the deeper region which is larger than 2.6 mm, the result seems to be interesting. This is because the feeling shown and the quantitative value obtained seems to be not correlated to each other. Taking a look at the peak value, although Clinician F could feel that the bone is softer than Clinician H, the drilling speed value in Figure 3.25(a) shows otherwise. The drilling speed value of Clinician F is slightly faster than Clinician H and even much faster than Clinician D. In Figure 3.25(b), by comparing Clinician F drilling different samples, the drilling speed considerably corresponds properly with the stiffness felt but it only showed near the end part just as the drilling was about to finished. This showed that the Clinician F describe the different feeling of stiffness based on the end part of the drilling.

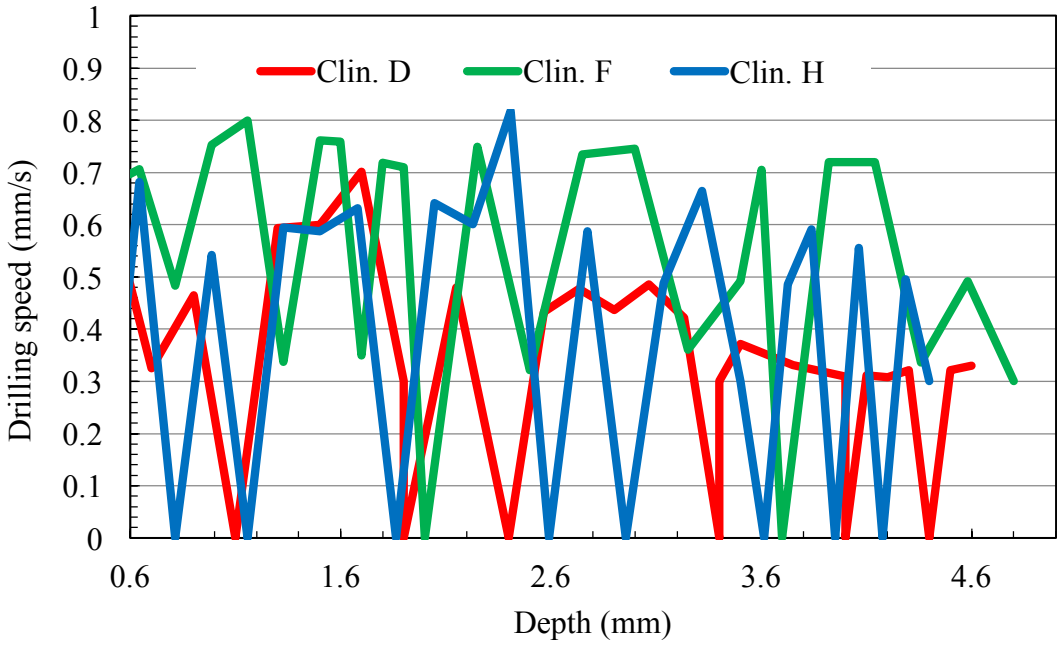

(a) Comparison of Clinician D, F, and H drilling Sample 1

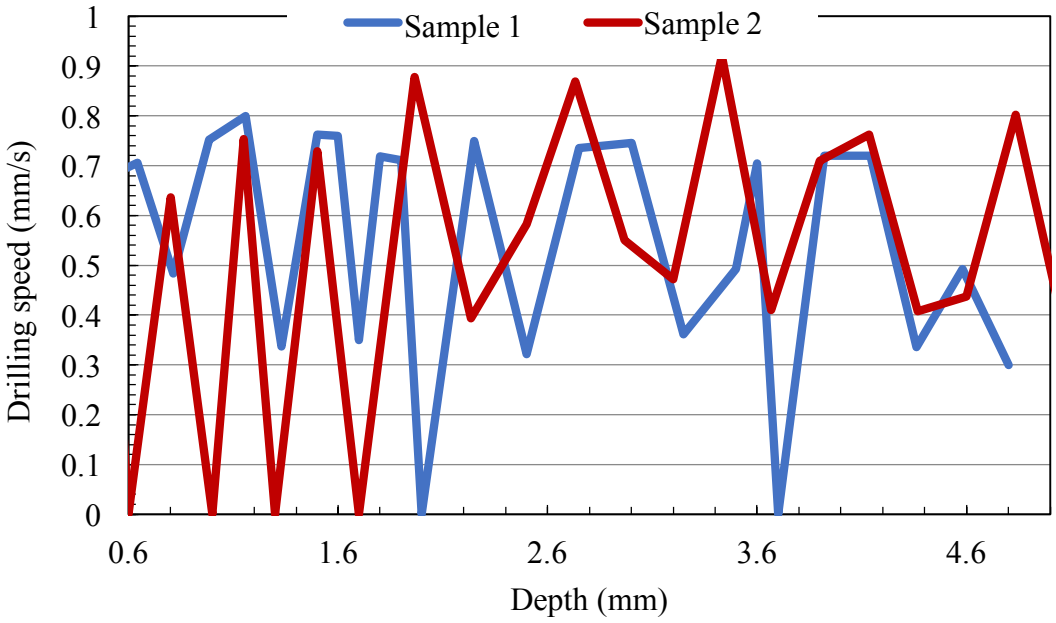

(b) Comparison of Sample 1 and 2 drilled by Clinician F

Figure 3.25 Drilling speed obtained from the evaluation done on the clinicians in the trabecular bone region

However, the slight difference of drilling speed of Clinician F and H seems to be arguable, so a detailed observation was done on both the combination of drilling force and speed of each clinician. Figure 3.26 shows the drilling force and speed of each clinician from drilling Sample 1. Based on the result of Clinician D as shown in Figure 3.26(a), the clinician being an experienced person, input the force accordingly as the required force from the database. Clinician D adjusted the input force as he enters deeper into the trabecular bone region. In contrast, Clinician H and F being a beginner on the oral implant surgery adopt the pumping style of the drilling as shown in Figure 3.26(b) and (c). This show that the style adopted by the clinician seems to affect the force-sensed by the clinician during drilling.

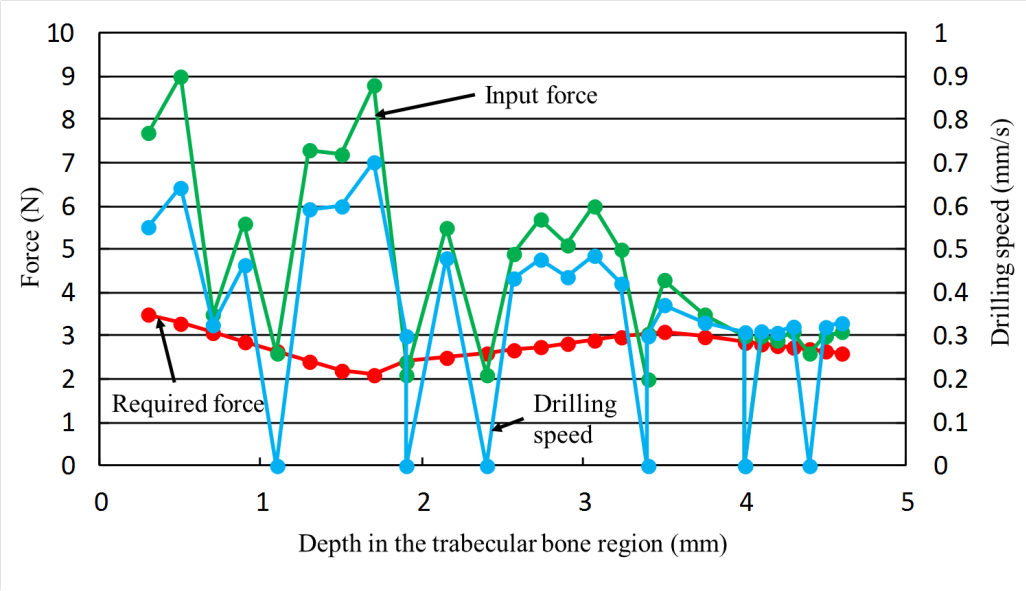

(a) Clinician D

Figure 3.26 Drilling force and speed obtained from the evaluation on each clinician drilling Sample 1

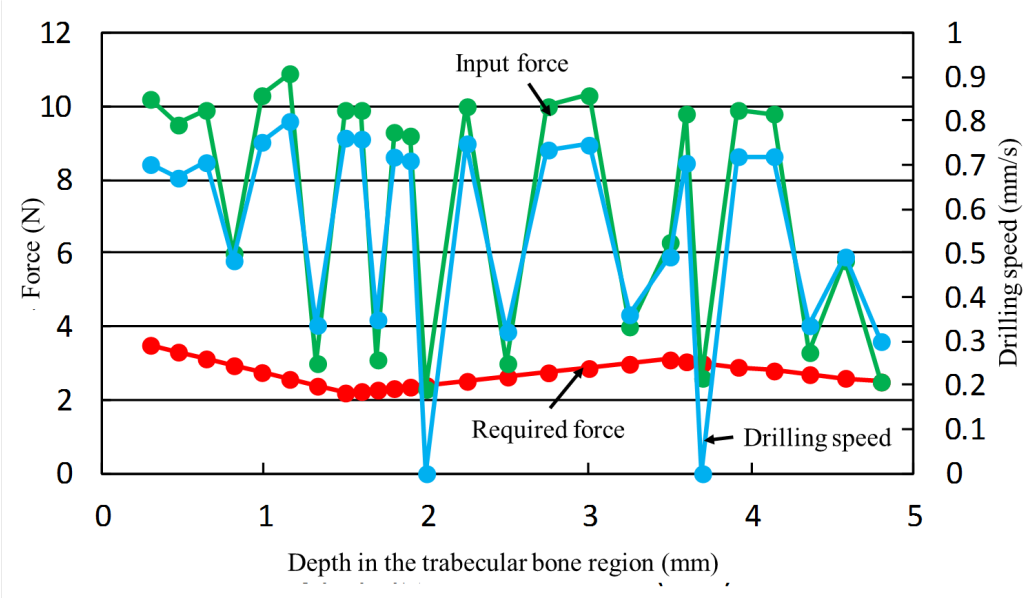

(b) Clinician F

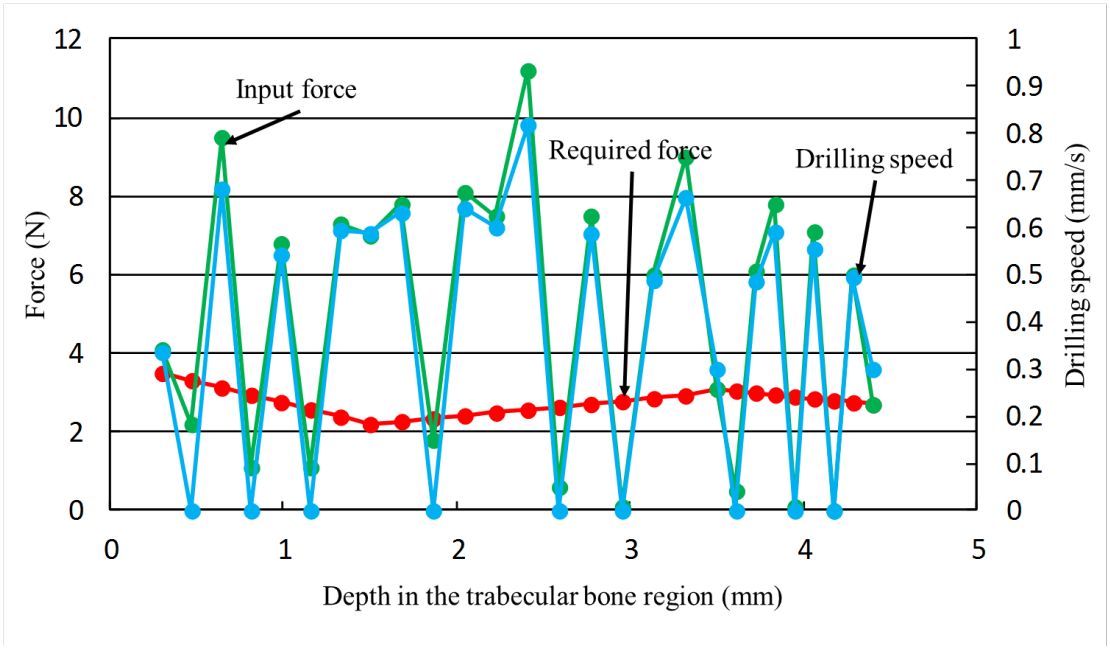

(c) Clinician H

Figure 3.26 Drilling force and speed obtained from the evaluation on each clinician drilling Sample 1 (continued)

By comparing Clinician F and H, it can be seen that both of them gave almost the same input force during drilling thus it can be concluded that only the drilling force value itself does not fully describe the drilling force-sensed. So, the two values that seems to correlate to each other and could be obtained from the clinicians' evaluation; the drilling force and speed is the key to define the drilling force-sensed. Besides that, Clinician D having more experience could determine the adjustment of the input force while also having a realistic feeling of drilling by using the simulator shows that the experience of the clinician could also affect the drilling force-sensed.

Conclusively, the combination of drilling force and speed seem to be one of the methods to define the drilling force sensed based on the positive comments received from the experienced clinicians using the training simulator. During the evaluation, there seems to be other unknown factors that also affects the drilling force-sensed. Nonetheless, two of them were able to be identified. Firstly, it was the way of handling the handpiece as the clinicians used different way of handling and also adopts different style of drilling such as the drilling accordingly to the tactile sensation and also a pumping style which load and unload the input force at an interval. Secondly, it was the experience of the clinician as each of the clinician had different experience of handling a real surgery but all of them gave a positive comment and approve the realistic value of the simulator.

As mentioned earlier, an important note to be taken from the clinician's evaluation and the comparison done is that the experience is very influential in the force-sensed. They could remember their past surgery very well and could even compare them with the database of the simulator as in the stiffness scale in Figure 3.23. All of them could recognize even a slight change of force at about 1 N.

The realistic feeling describes by the clinicians suggest that the output information of drilling force and speed is highly reliable and valid for further discussion on quantifying the drilling force sensed. The experienced gained from doing an actual surgery and comparing it with the training simulator and its database provides evidence of the system validity.

3.3 Comparison of drilling speed with educational polymeric model

Focusing on the realistic feeling of the clinicians and the results of the evaluation, experimental work on educational polymeric models (Nissin Dental Products Inc., Kyoto, Japan) were done. This is because, the models are used in class to teach about the drilling processed and most of the dental college students are exposed to it. So, an experiment to investigate on the force-sensed of the polymeric model was done by giving a constant input load on the models. The experiment was done on three types of models as shown in Figure 3.27. The models imitate the mandibular part of the jawbone and made from polymeric foam material resembling the trabecular bone, surrounded by a thick dense polymer for the cortical bone. The model P9-IMP.6 is an exception, since it exclusively contains a wire surrounded by thick solid polymeric material that is used to show the mandibular canal inside the jawbone. This model was devised by the Japanese Oral of Implantology Society. According to its maker, based on the Lekholm and Zarb's bone classification (Lekholm, 1985), all the models are of Type III with the exception of model P9-IMP.6 being in between Type II and III.

(a) P9-X1141

(b) P9-X1140

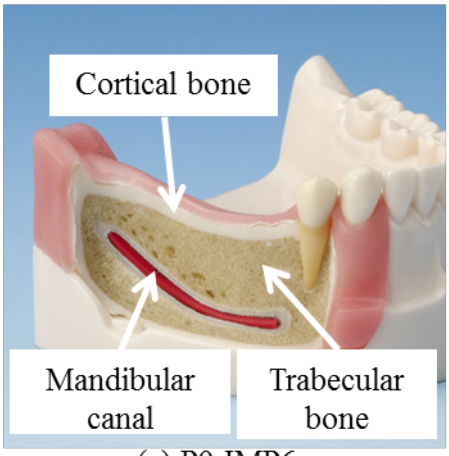

(c) P9-IMP6

※ Nissin Dental Products

Figure 3.27 Educational polymeric model manufactured by Nissin Dental Products

3.3.1 Method

There are two types of drill used in the experiment as shown in Figure 3.28 which is a round bur and a twist drill. Using the drills (Drill kit 7-15mm, Nobel Biocare, Zurich, Switzerland), the polymeric model was drilled until the desired depth. The model was drilled until the depth of 15 mm except for model P9-IMP.6, whose depth was set until the drill touches the mandibular canal. The depth of the mandibular canal is different for each part of the drilling.

Figure 3.28 Round bur (left) and drill (right) that was used in the experiment

Using the same motor unit and handpiece used during the clinicians' evaluation, the rotation speed was set at 800 rpm. Next, the polymeric model was loaded on a precision balance (UW4200H, Shimadzu, Kyoto, Japan) connected to a computer. The precision balance was used to measure the input force given during the drilling and it was recorded in the computer. A measuring scale was put parallel to the handpiece in order to measure the depth and calculate the drilling speed. In order to measure the scale during the drilling a video camera is used to record the movement of the drill as it moves parallel to the scale. The setup of the experiment is as shown in Figure 3.29.

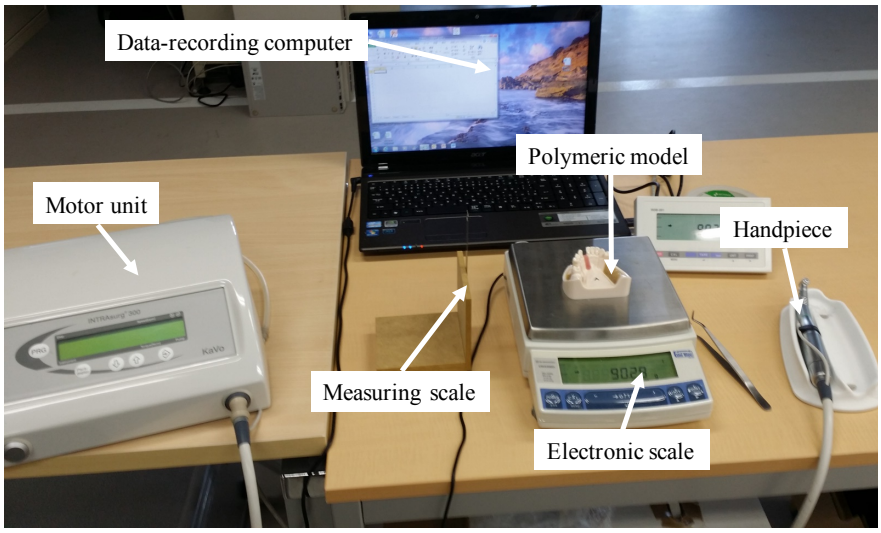

Figure 3.29 The experiment setup for drilling the polymeric experiment

Figure 3.30 View taken from the camera to measure the drilling speed

3 sets of models were used for each type and each of the model was drilled 3 to 4 times. Each type and set of model was marked and drilled with a supposed constant input force of 1.5 N, 2.2 N and 3 N. So, a total of 9 models were drilled in this experiment. The polymeric models were divided into two regions based on the drilled depth. The shallow region for depth lower than 7.5 mm and the deep region for depth beyond 7.5 mm. The average drilling speed of each region was taken and recorded because of the fluctuation that occurs during the experiment. The results were then compared with the clinicians' evaluation.

The results of the clinician's evaluation were taken at each point of the recorded drilling force and speed as shown in Figure 3.26. Figure 3.31 shows the flowchart of action done in order to take the clinicians' result for comparison. Initially, the output of the simulator only shows the graph of input force and drilling speed against time as shown in Figure 3.24. There was no output location recorded in the prototype machine used in

this chapter. So, it was integrated by calculating it from the drilling speed obtained. Only the values in the trabecular bone region is taken for comparison and the point that is less than the required value were omitted because of the zero point that do not have any meaning.

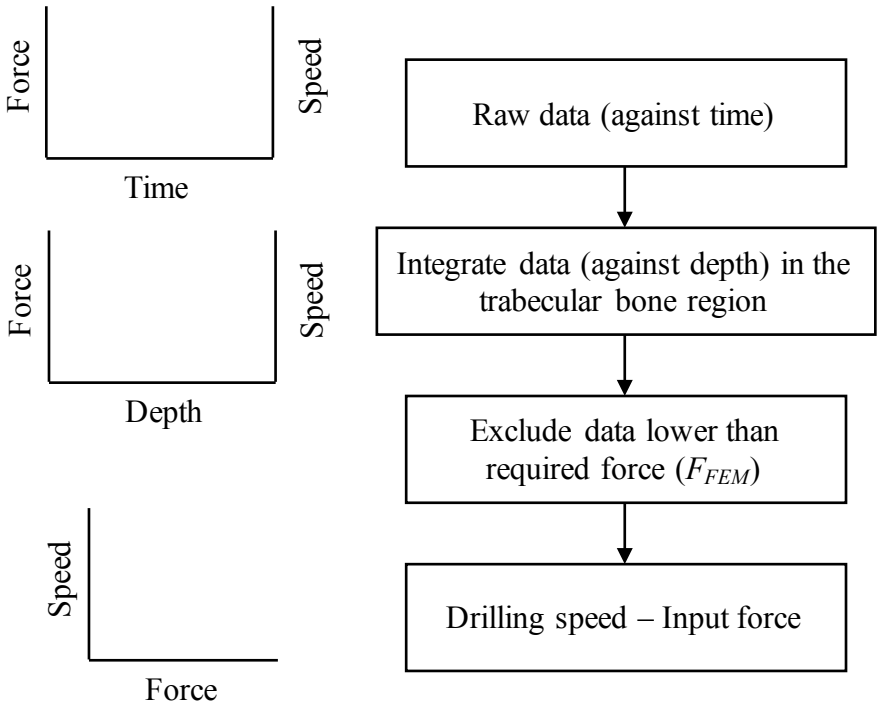

Figure 3.31 Flowchart of the prototype machine output integration done for the clinicians' evaluation

In order to compare the relation of speed against load with the polymeric model, the consideration of integrating the raw data of drilling speed and input load to be against depth is done because the time among the clinician differs and very different number of

plot points was obtained. This is cause by different action or operation of the clinician. Using the same interval with respect to depth, the raw data is integrated to be against depth to similarize the data points in order to evaluate the results of the clinicians evenly. In the conversion, the number of plotted data is almost the same among clinicians. All the 8 clinicians' data was taken for Sample 1 and 2 but only 2 clinicians data was obtained for Sample 3 as can be seen in Table 3.1 and Table 3.2.

3.3.2 Results

The result of the comparison is as shown in Figure 3.32. The graph of speed against load was done because of the supposed constant input load used during the experiment on the polymeric model. As it can be seen, there are unclear differences between each sample and each polymeric model, although they show differences in terms of microstructure and bone type classification (Lekholm, 1985).

In general, the comparisons of the polymeric models show a much higher drilling speed in the deep region than in the shallow region. By comparing the drilling speed from both the proposed approach, the drilling speed of the clinicians ranged from 0.3 mm/s to 0.9 mm/s but the drilling speed based on the experimental work on the polymeric model ranged as high as 1.5 mm/s. The higher drilling speed was obtained from drilling the polymeric model although it was done with an input force of 3 N, lower than the force used for clinicians' evaluation. Even with a higher input force of 9 N, the drilling speed is much lower than that of the polymeric models. Looking at the obtained data, the curve of the clinicians' evaluation seems to show a lower slope than the curves recorded using

the polymeric model thus showing the polymeric model to be much softer than the calculated data from a real jawbone.

Based on this finding, the tune up of the variable, α to be in a linear condition seems agreeable as the experiment done on the polymeric model was also seen to be linear. However, the polymeric model has a steeper slope as it seems that the model is made softer than the real bone in order to teach students to be careful while drilling.

The scattering of the clinician seems to follow the algorithm of the movement speed as shown in Equation 3.1 and Figure 3.11. The scattering occurred because of the different action or operation done by the clinician. There are clinicians that do a normal drilling with constant input force while adjusting to the database and there are also clinicians that did a pumping movement as shown by some of the clinician in Figure 3.26. The high input force in comparison with the database cause a higher drilling speed calculated.

Comparing the value of drilling speed and force of the polymeric model and that of the database from the simulator, a higher input force would produce a very fast and large drilling speed when using the polymeric model. In this case, it can cause misunderstanding to teach the force-sensed using the polymeric model.

Conclusively, the purpose of this figure was to compare the bone quality or force-sensed between the polymeric model and that of a real surgery. It is clear that the drilling speed is much higher that the clinicians' operation.

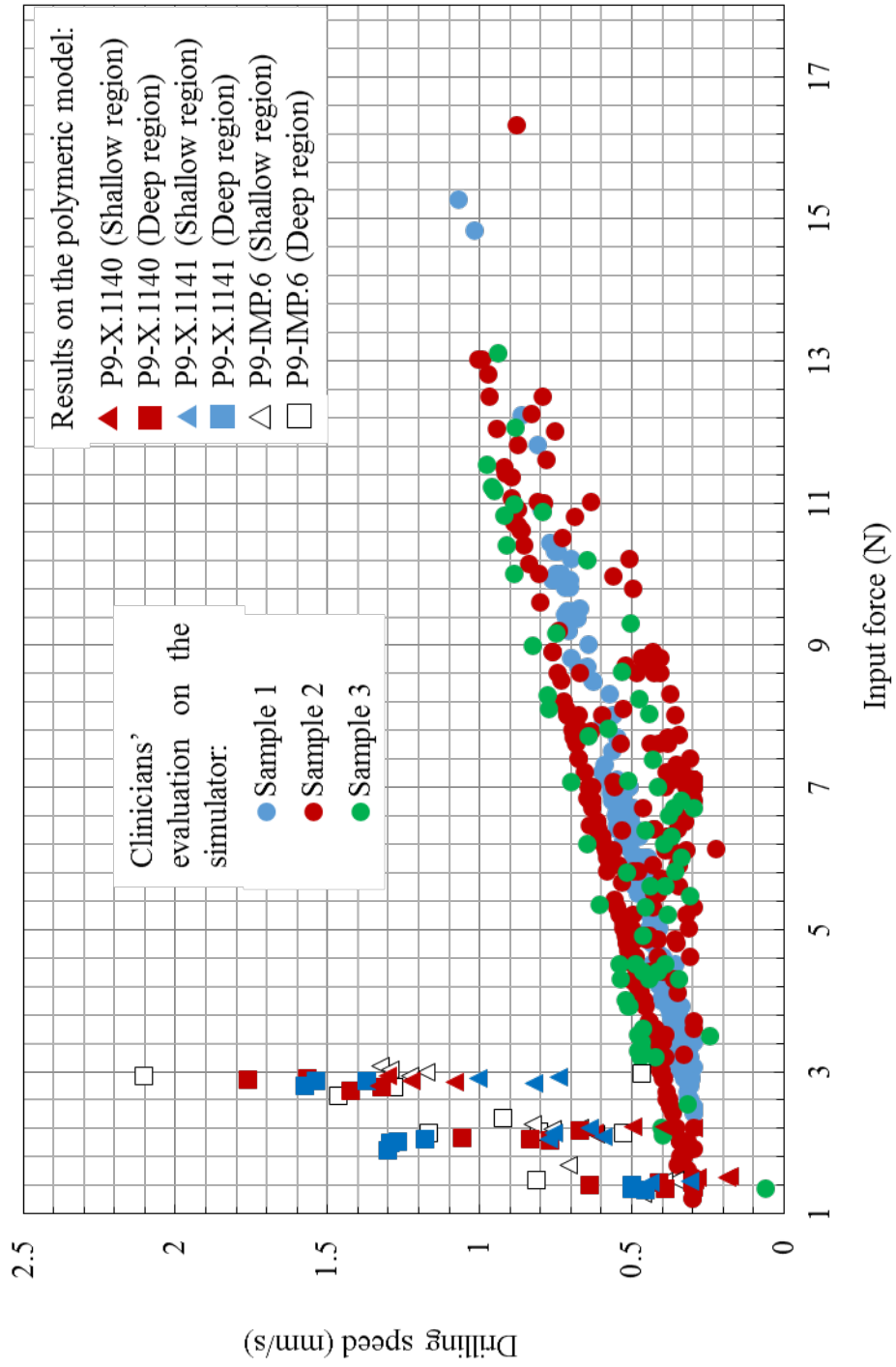

Figure 3.32 Comparison of the drilling speed and force of the clinicians' evaluation on the training simulator and the experiment done on the educational polymeric model

3.4 Discussion and summary

As mentioned in the comparison of the clinicians' evaluation, the change of speed in the trabecular bone area, Δs, is proportional to the load increment, $\Delta f = f_2 - f_1$. But the force-sensed is influenced not only by Δs and Δf but also by f_1. So, the combination of Δs, Δf, and f_1 is important.

By using the simulator, the users can learn the appropriate input force. Thus, in the clinicians' evaluation, the input force was strongly influenced by the clinicians' experience. Under this condition, the discussion focused on if the drilling speed could explain the difference in force-sensed. The comparison of Clinician D, F, and H in Figure 3.25(a) showed that only the speed itself cannot explain about the drilling force-sensed. Moreover, just a little difference of speed was shown by Clinician F in Figure 3.25(b). He only had a different drilling speed at the final push that lead to his conclusion of the different of stiffness felt. This implies that the speed can explain partially about the drilling-force sensed but it is not perfect.

Detailed comparison of each clinician drilling speed and force is done in order to study about the drilling force-sensed. The source of drilling force-sensed is the force value and the speed felt by the clinician during the drilling plus other added factor and experience is known to be one of the main factor. By looking at the experience of all the clinician, and taking a detailed look at both the value of drilling force and speed of all clinician, the experience was identified to be the main factor since surprisingly, they all could remember the feeling of drilling in their past surgery. By comparing it with the samples drilled, the samples move accordingly with their experience accumulated. Taking

a look at Clinician D also revealed that he adjusted the drilling force accordingly with the sample of the database hence giving the low input force thus leading to a low drilling speed.

Although the drilling speed could only explain the force-sensed partially and the experience is an important factor, the comparison in Figure 3.32 showed that the experienced clinician could adjust the input force by feeling the bone quality and the load is adjusted in the polymeric model by giving constant input load. In the clinicians' evaluation, the drilling speed of an expert clinician did not exceed 0.7 mm/s as can be seen in Figure 3.24(a) and (b). Here, Clinician C is an expert clinician. So, a higher drilling speed than 0.7 mm/s only appeared in a beginner clinician's operation as shown in Figure3.24(c) and (d). However, the lower speed than 0.5 mm/s can be neglected because it happens due to the pomping operation by the clinician.

Very large scattering can be seen in the region of the input force from 6 to 9 N and also a linear line following the algorithm in Equation 3.1. But, in the expert clinician operation, his drilling speed was not on the linear line but lower than that because he adjusted the input force. Note that the linear line is proportional to the difference between the input force minus the calculated force. So, this value is an equal index but it is implicitly plotted in Figure 3.32. So, the plot in the linear line appear mainly in the operation by a beginner clinician.

In the comparison of drilling force and speed between the two approaches as shown in Figure 3.32, the scattering of the clinicians' evaluation's data is denser than in the polymeric models. Regardless, similar scattering was measured and recorded while studying the relationship between the cutting force and bone mineral content (Sugaya,

1990). The author's study aimed at finding out more about the bone quality for dental implant by taking into account mineralization parameter of the bone quality. The ranges of bone mineral content increases as the cutting force increase, thus showing the same similarity with the present study by changing the parameter of the bone mineral content with the drilling speed. This shows that the relation of the drilling force and speed could be one of the parameters in studying and quantifying the bone quality. It could also be a way to evaluate and quantify the tactile sensation while drilling the jawbone.

The purpose of the comparison as shown in Figure 3.32 is done in order to compare the bone quality or force-sensed between polymeric model and real surgery. It is clear that the drilling speed is much higher than the clinician's operation. Thus, although the drilling speed is not perfect parameter but in this comparison the speed could explain the difference between the polymeric model and the clinician's evaluation. According to the evaluation done and the positive reviews obtained, the developed simulator can be considered as a valid tool. This shows that the polymeric model seems to be exaggerated based on the high drilling speed recorded even in low input force. Nevertheless, the structure of the polymeric model could potentially be helpful for students when they start learning the oral implant surgery since the high drilling speed could let the students be very careful while drilling, especially near the mandibular canal.

Moreover, the key to identify the source of drilling force-sensed does not only lies at the force value or speed individually but it requires both value and other factors which in this case to be identified as the experience of the clinician. The different experience of the clinician made their threshold in identifying the stiffness felt being different individually.

During the evaluation and the comparison done, the results was integrated to be plotted against the depth. The integration to define the input force and drilling speed against depth was done in order for easier comparison among individual. The graph against time is not focused because a quick surgical procedure is not always best. The graph against depth is also better in order to compare with the bone volume fraction as we can investigate the bone volume fraction along the depth. So, the depth or location was output in CSV file in the newer version of the simulator which is shown in Chapter 4.

Chapter 4

Problem-based learning class using the drilling force-sensing device

4.1 Overview of the class

Problem-based learning (PBL) was introduced as early as in the 1970s as an alternative to traditional learning system in health sciences education (Neufeld & Barrows, 1974). It is defined as an approach in which a problem serves as the center of an active learning (Fincham & Shuler, 2001). In this system students are divided into small groups and work together with the faculty facilitators to engage in many activities that promote lifelong learning and better preparation for their professional careers. However, it is important to understand that different with the medical education, the skills that needed to be acquired by dental students are not always the same. For example, the skills that are required in general dentistry mainly involve mechanical hand activities that rely on developing the psychomotor skills. Accordingly, in the dental education field, this type of learning

system was firstly introduced in 1990 (Rohlin, Peterson, & Svensater, 1998) and gradually increasing until today.

In collaboration with Tokyo Dental College, the oral implant surgery training simulator introduced in the previous chapter is used in their PBL classes for fifth grade students. The syllabus of their classes includes learning about general knowledge on implant, planning a treatment, practice session, and also a visit to the dentist to see implant treatment on an outpatient. During the practice session, the students were given the chance to use the simulator and tried many different cases included in the simulator.

The usage of the simulator follows closely the evaluation done on the clinician in order to teach the drilling force-sense. Since the students do not have any experience prior to the usage of the simulator, 2 or 3 samples were firstly introduced and drilled before an evaluated or unknown sample is asked to be drilled. This is done because as previously explained in the previous chapter, the experience highly affects the drilling force-sense during this study.

The simulator was firstly introduced to only four groups of six students which is only a part of all the students in the same grade. This is part of a trial of the simulator usage with the students as it was monitored by students from Keio University to check for any machine error. During these classes, an evaluation was also done on students as an expansion of study on the quantification of drilling force sensed based on the evaluation done on clinicians explained in the previous chapter. This will be described later in the next section.

On the next year, the simulator was finally able to be fully implemented in the

PBL classes as a lot more students are able to use the machine. It is also quite a success as there seems to be no need of a monitoring done on the machine error as it functions properly without any error reported as of today. This PBL classes will be explained later in section 4.1.2

4.1.1 Quantification of drilling force sensed

One of the objective of this class was to quantify the drilling force sensed among the students and give an overview of different samples and on-hand experience of drilling different types of sample. This was done as an elaboration of the evaluation done on the expert clinicians as mentioned in the previous chapter.

The students' evaluation was done during their PBL class for fifth grade students, which is a class set up to teach students to learn more about the surgical procedure in oral treatment especially the oral implant surgery. A total of 24 students took part in the evaluation and tested the samples from the drilling force database. During the session before using the simulator, the class teaches the student about the anatomy of the jawbone while giving some input from the mechanical point of view. Figure 4.1 shows one of the group of students attending the class.

Figure 4.1 One of the group of students attending the PBL class

The understanding of intra and inter-individual differences of the bone especially the trabecular bone region was also clearly given. Then, the students performed the drilling process using the educational polymeric model which was mentioned in the previous chapter. This is done as an introduction to the system of the training simulator. Lastly, the usage of the simulator was clearly explained to the participating student.

During this class, only Sample 1, 2 and 4 were used. Just before handling the simulator, the students were firstly given an in-depth explanation of the trabecular bone region of the jawbone in regards with the system of the training simulator. They were also shown the micro-CT images of the samples, their required drilling force and the target depth that needs to be drilled. Then they were asked to drill the two samples, Sample 1 and 2 respectively. Similar with the clinicians' evaluation, the drilling simulation was done using the training simulator and the same information was hidden from the students' view. After each drilling simulation, the students were asked the feeling of stiffness for each sample and try to compare it with one another. Next, the students were shown a different third sample, namely Sample 4.

Differs from Sample 1 and 2, only the micro-CT images of the sample and the target depth were shown to the students. Figure 4.2 shows a student during the drilling simulation. After the simulation, the students were asked about Sample 4 stiffness in comparison with Sample 1 and 2. They were then required to sketch the drilling force curve on a PC using developed software by comparing it with the previous two samples as shown in Figure 4.3. The drawn sketch was finally converted into a Microsoft Excel file. The results of the evaluation of their sketch is described and derived based on characteristics of Sample 4. Moreover, they were also asked to give their overall impression of the developed training simulator.

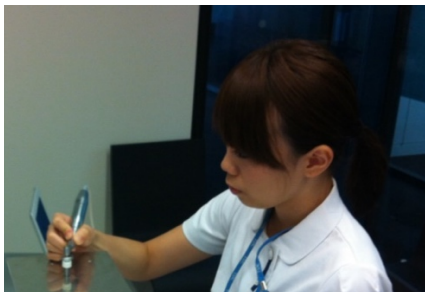

Figure 4.2 One of the students during the drilling simulation

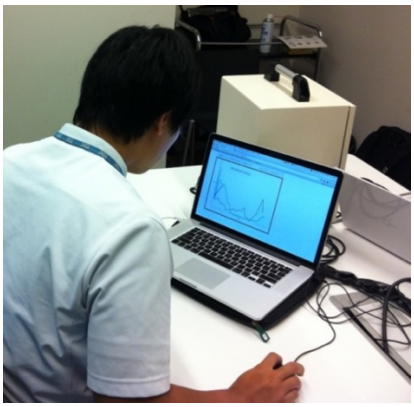

Figure 4.3 One of the students describing the stiffness of Sample 4 by drawing a sketch in comparison with Sample 1 and 2

As a result, in this class, the students are asked to sketch the drilling force versus the depth curve of Sample 4 by comparing it with the other samples. Based on Sample 4, a total of 9 point of interest were taken and evaluated for each of the students' sketch. The students sketch varies between individual and most of them move along Sample 4 curve line from the upper left to the lower right as shown in Figure 4.4(a). As shown in Table 4.1, all students (100.0%) could recognize the feeling of perforation when the drill enters the trabecular bone region and almost all of the students (91.7%) could recognize the force difference between the upper and lower region and most of them, which is about 79.2%, could identify the difference of high drilling force required, which is about 5 N. By comparing it with Sample 2, most of them (83.3%) could recognize that the drilling force in the upper region of Sample 4 is actually much higher. Interestingly, a few students, which is about 37.5% of them, could feel the zigzag curve in the upper region although its force difference is very slight, which is only around 1 N. Figure 4.4(b) and Figure 4.4(c) shows the examples of the few students that compared well with the original Sample 4.

Legend O - Able to recognize Δ- Somewhat able to recognize

Remarks

*1 Perforation of cortical bone at the upper region right before entering the trabecular bone region
*2 The difference of force between the upper region and the lower region
*3 Difference of force for the upper and lower region is about 5 N
*4 Sudden drop of required drilling force in about 2 mm of depth
*5 Required force for the upper region is higher than Sample 2
*6 Required force for the lower region is smaller than Sample 1
*7 Slight force change in the upper region
*8 The slight force change value is around 7 N with a difference of ±1 N
*9 A slight rise of required force after the big drop

Table 4.1 Results of the students' evaluation

Student	Perforation*[1]	Force difference*[2]	Difference of 5 N*[3]	Big drop*[4]	Comparison with Sample 2*[5]	Comparison with Sample 1*[6]	Zigzag*[7]	Zigzag value around 7N*[8]	Slight rise*[9]
1	O	O	O		O				
2	O	O			O		O		
3	O	O	O		O		O	O	
4	O	O	O		O		O	O	
5	O	O	O	O	O				
6	O	O	O	O	O		O	O	
7	O	O	O	O	O	O	△		O
8	O	O	O	O	O		O	O	O
9	O	O	O	O	O	O			
10	O	O	O	O	O	O			
11	O	△				O			O
12	O	O	O	O	O	O	△	O	
13	O	O							
14	O	O	O	O	O	O	O	O	
15	O	O	O		O	O			O
16	O	O	O	O	O	O			O
17	O	O	O	O	O	O	△		O
18	O	O	O	O	O	O			O
19	O	O	O	O	O				
20	O	O	O		O		O		
21	O	O	O	O	O	O			
22	O						O		O
23	O	O					O		
24	O	O	O		O				
(%)	**100.0**	**91.7**	79.2	**54.2**	83.3	45.8	37.5	25.0	33.3

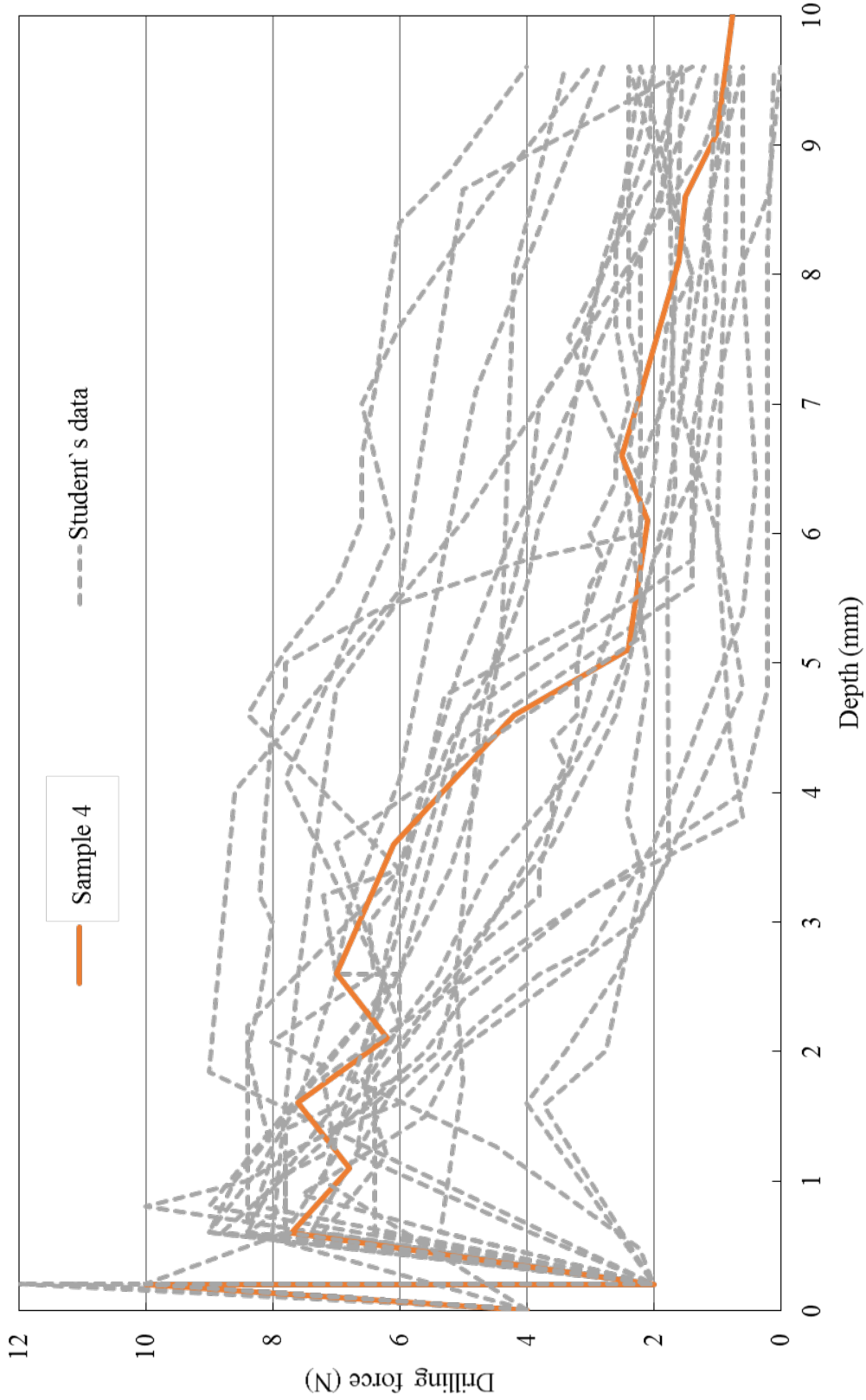

(a) Comparison of all the students' sketch with Sample 4

Figure 4.4 Comparison of the students' sketch data with Sample 4

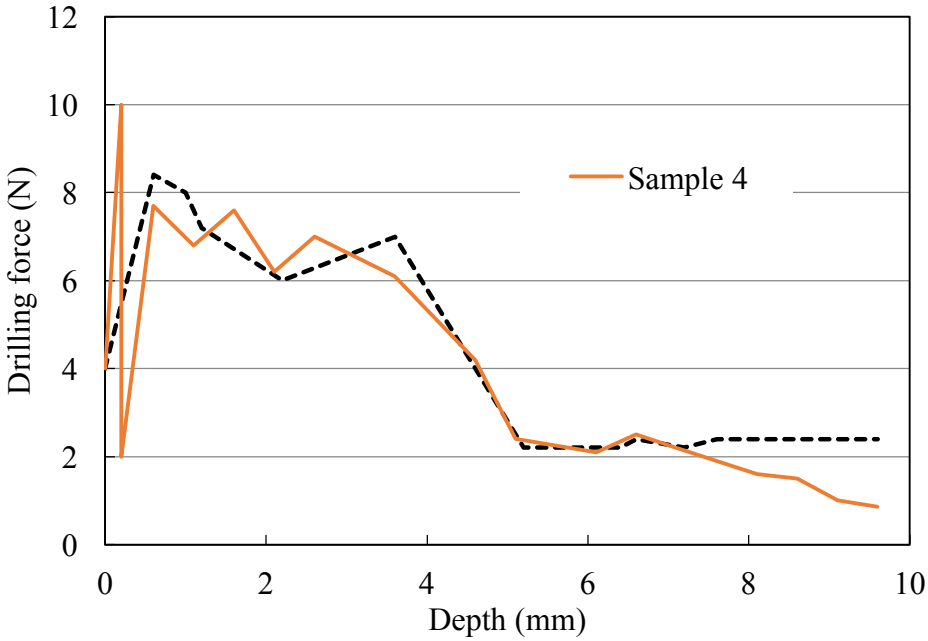

(c) Comparison of Student 8's sketch data with Sample 4

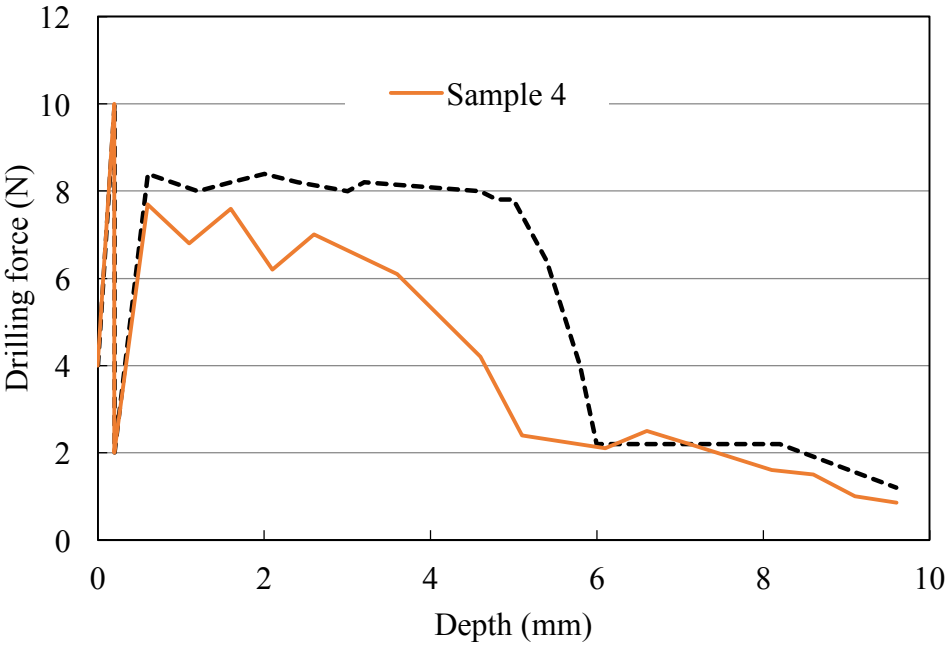

(c) Comparison of Student 14's sketch data with Sample 4

Figure 4.4 Comparison of the students' sketch data with Sample 4 (continued)

4.1.2 Perforation of the lingual side of the bone

The perforation to the lingual cortical side of the bone is the next accident that prone to happen during an oral implant surgery after the perforation through a mandibular canal. Different with the perforation through the mandibular canal, this accident is more dangerous as it can directly pull the muscles of the jawbone right after the perforation thus leading to death.

Fortunately, the feeling of drilling through each part is very much different. The user almost could not feel any force difference when they drilled through the mandibular canal especially for a fresh graduate because there is no noticeable feature in the wall of the mandibular canal. However, the cortical bone has a pretty much distinct feature in comparison with the trabecular bone hence giving a feeling of large force difference when drilling through the cortical bone.

Taking advantage of this noticeable feature, the simulator was able to utilize its potential to give the user the feeling of perforation through the lingual cortical side of the bone. This was added as one of the simulator database as mentioned in the previous chapter. All the Samples of the database was used as a fully functional simulator for the fifth-grade students of Tokyo Dental College.

The syllabus of the class is similar with the class that was mentioned in the previous chapter. The only difference is they were able to fully use the training simulator with all the database including the perforation case. So, in this class, an evaluation on the students' experience of perforating the lingual cortical side of the bone was done.

This time, a total of about 102 students was able to take part in the usage and the

evaluation process. Apart from the usual normal cases, the students were introduced about the perforation case before the drilling. Right before the perforation, the students were told to input extra strength since the cortical bone is actually very hard to perforate. This result in a feeling of sudden drop as in the real perforation case. Most of the students could feel the difference as they shown a shocked and surprised reaction when the drill pass through the cortical bone.

Figure 4.5 A student doing a simulation on the oral implant surgery training simulator supervised by an expert clinician

Figure 4.6 One of the student doing the perforation case during the evaluation

Based on the simulation and evaluation done during the class, the same results during the previous class were obtained as most of the students could recognize the feeling of perforation through the cortical bone in the upper region just before the trabecular bone layer. When asked to describe about the drilling experience, some could not expect the drilling was done at a mistaken angle that could cause the perforation of the lingual cortical bone. Overall, the feeling of hitting the cortical bone after drilling the trabecular bone part is recognized by everyone thus making one of this class objective of giving the different sensation of drilling the trabecular and cortical bone region quite a success.

4.2 Discussion and summary

Based on the previous chapter of the clinicians' evaluation and comparison with the educational polymeric model, more insight was obtained during the evaluation done on the students.

In Table 4.1 which showed the important data for the conclusion revealed that more than half of the students could feel the main qualitative value of Sample 4 which is the perforation on the upper cortical bone, the force difference of the upper and lower region, and the big drop. Interestingly, Figure 4.4 showed a very surprising finding of the study that the students which had no experience in the oral implant surgery can draw quite similar graph with the database just eventually.

However, this implies that the same evaluation on the expert clinician which have experience in the oral implant surgery can be done. The same evaluation done on expert clinician could get us a higher percentage of the qualitative value felt and the graph obtained from the clinician would be more accurate and it could be directly used in class.

This opens up a new door to the possibility of adding the database with the clinician's experience being the key factor. Based on the evaluation on the clinician, the clinician could remember well their feeling of handling past surgeries. If the clinician could use the simulator before the surgery and compare it with the database. Accurate force curve could be obtained from the surgery. This could be used as the database without the need of FEM calculation. In this case, a clinician could transfer the drilling force-sensed to an inexperience person easily.

Chapter 5

Development of mechanical testing apparatus for maxillary sinus membrane in sinus lift up process

5.1 Machine design

Dental implant placement in the maxillary area especially the posterior maxilla is a very challenging process (Al-Dajani, 2014; Tiwana, Kushner, & Haug, 2006). In the case of insufficient residual bone height, sinus lift procedure is required. This is done in order to increase the height of the posterior maxilla by repositioning its sinus floor in an upward direction thus forming an appropriate bone height that can contain a functional dental implants (Călin, Petre, & Drafta, 2014; Del Fabbro, Corbella, Weinstein, Ceresoli, & Taschieri, 2012; Esposito et al., 2010).

During the sinus lift procedure, the sinus membrane is prone to breakage thus

leading to the case of membrane perforation causing a much more complicated scenario (Al-Dajani, 2014). About 70 percent of the failed procedure were followed by perforation of sinus membrane and this will increase the risk of sinusitis or infection (Nolan, Freeman, & Kraut, 2014). To the best of the author's knowledge, the sinus lift procedure is mostly done by the clinician's intuition and sense of touch without any prior knowledge of any quantified or visible value when lifting the sinus membrane. There is also scarce information regarding the sinus membrane especially from the mechanical point of view.

Thus, a machine was design and a method was proposed in order to measure and observe the sinus membrane in a more quantified value, in the author's case the strain distribution on the sinus membrane during the sinus lift up procedure. In this chapter, the design of the machine and usage of the machine will be explained and the method of finding and observing the strain distribution will be described in the next chapter.

5.1.1 Requirements and design strategy

Similar with the sinus lift process, the act of pushing the membrane upwards was the base in designing the testing apparatus. The main part was designed by taking the idea of the dentist using an apparatus or equipment to push the membrane upwards. This act is done after the breakage of the sinus floor exposing the membrane to a direct touch with the equipment used for lifting the sinus. An indirect sinus lift with the crestal approach is considered when designing the machine in order to make the experiment by using the machine as similar as possible with the sinus lift procedure done by dentist. The schematic idea of the design is as shown in Figure 5.1.

Figure 5.2 shows the overall picture of the machine which consist of the membrane holder as the main part, a load cell attached to an actuator, and the data recording computer. The main part of the machine will be explained more in the next section. A steel bar was designed to represent the dentist's equipment during the lifting up of the sinus membrane. It is connected to the load cell (LMB-A-50N, Kyowa Electronics Instrument Co. Ltd., Tokyo, Japan) that measures the reaction force obtained from the contact of the steel bar with the membrane when moving upwards. The movement is controlled by an actuator (DRS42SA2G-04MK, Oriental Motor Co. Ltd., Tokyo, Japan) that can be programmed to move at a designated speed and height destination via the touch panel (GOT1000, Mitsubishi, Japan) on the control box. The reaction force is then recorded to the computer at an interval 0.2 seconds and can be saved and exported as a Microsoft Excel file through a user interface program that was designed with the machine. The user interface of the software is shown in Figure 5.3.

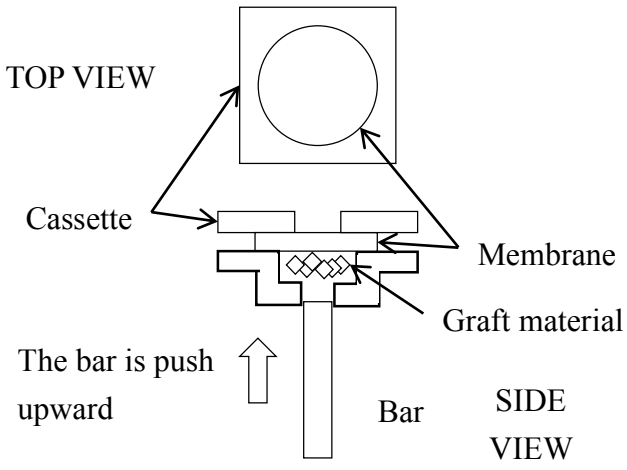

Figure 5.1 Schematic view of the machine design

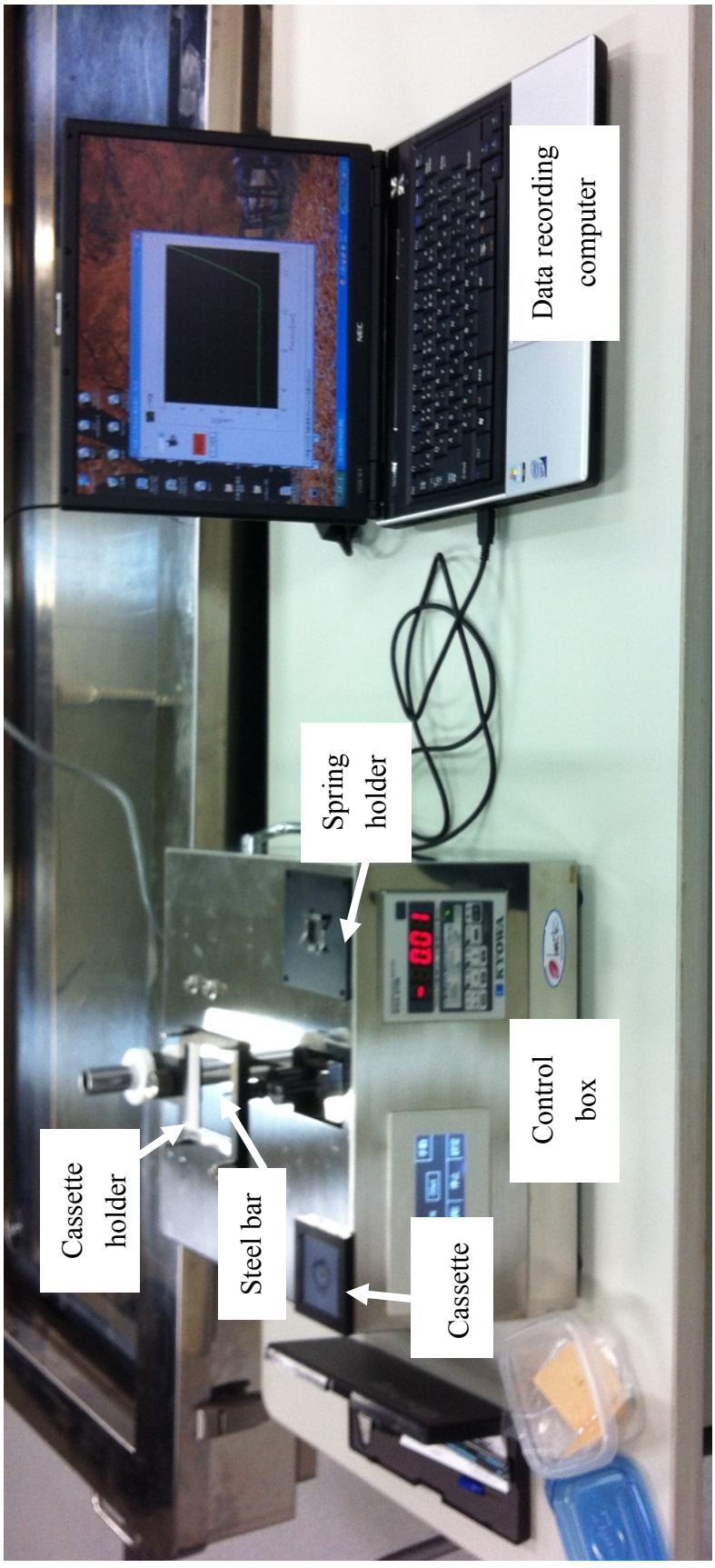

Figure 5.2 Overall picture of the mechanical testing apparatus connected to a computer for data recording

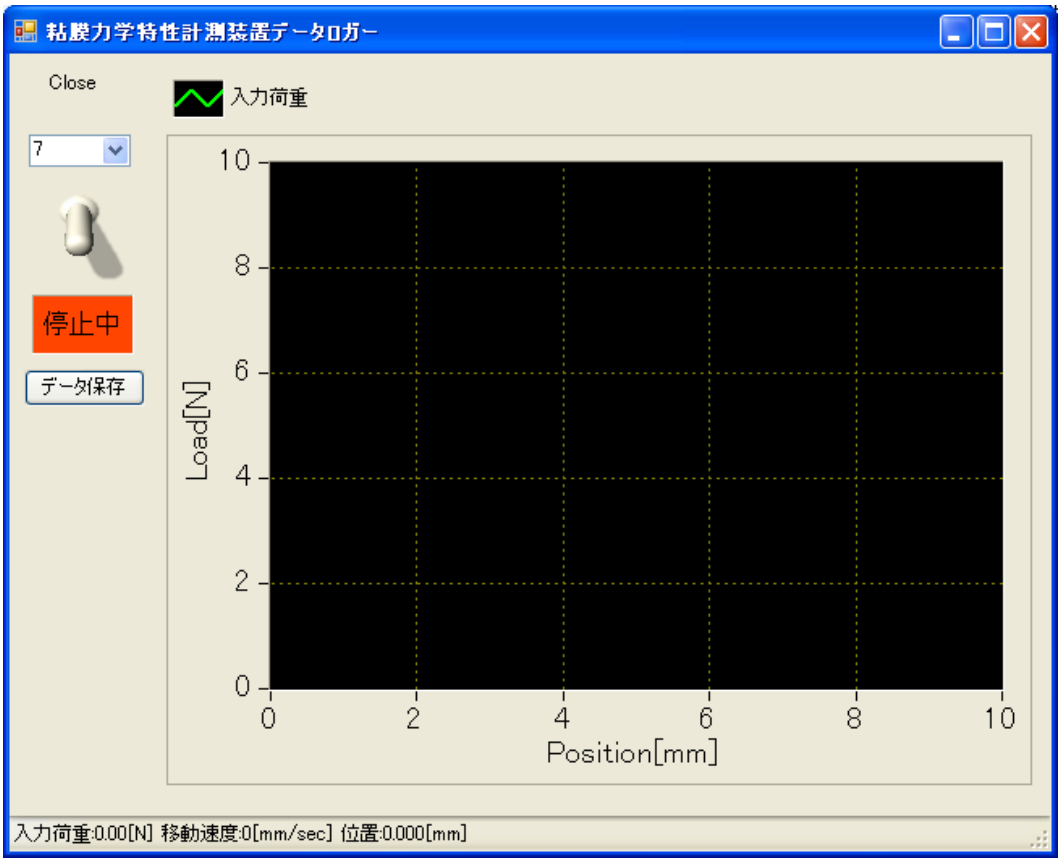

Figure 5.3 User interface of the mechanical testing apparatus in the data recording computer

The machine was also designed with portability in mind. This is because of the integration of engineering and dentistry discipline; it has to be portable for the machine to be easily brought to a clinician that have experienced in handling a fresh cadaver for the experiment. Fresh cadaver is the main focus of this study since to the properties of a cadaver could change if it is mummified with a liquid formalin and the results of the experiment could change drastically and not be applicable in a real surgery. Due to that,

the machine was designed with handles at both side and be made as small as possible without excluding any important characteristic.

5.1.2 Membrane holder

The membrane holder is the main part of the machine as it is the part which closely imitates the sinus lift process during the implant surgery. This part of the machine consists of a cassette holder, a cassette and also the steel bar that was roughly pointed out in the previous section. Figure 5.4 shows each part's computer-aided design (CAD) file. The design of each part mainly based on the characteristic of the membrane as the target of the machine and to imitate the sinus lift procedure.

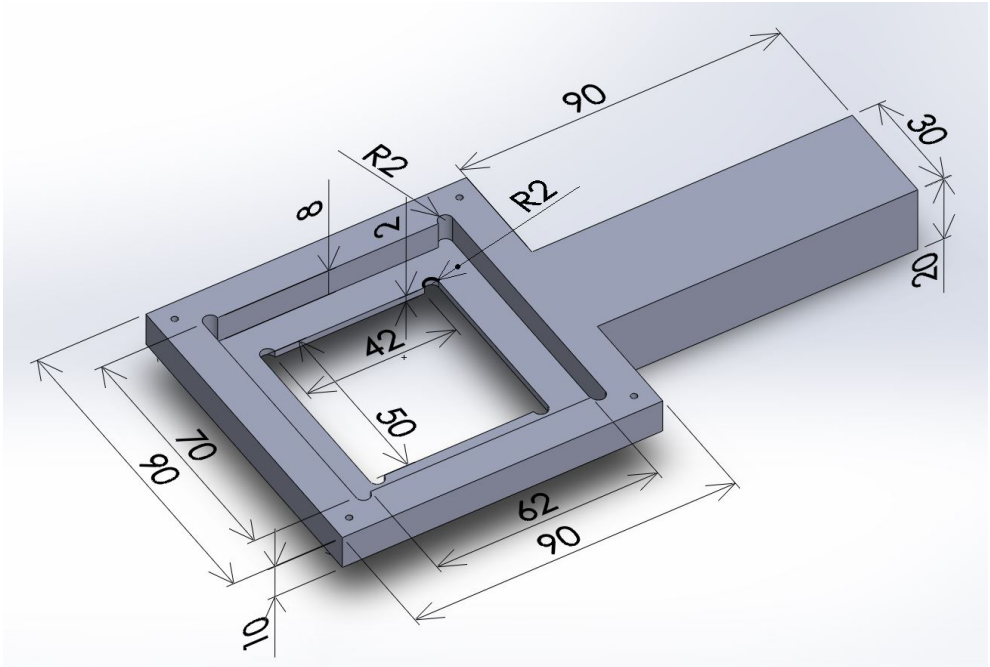

(a) Cassette holder (unit: mm)

Figure 5.4 CAD file of the main part consist in the membrane holder

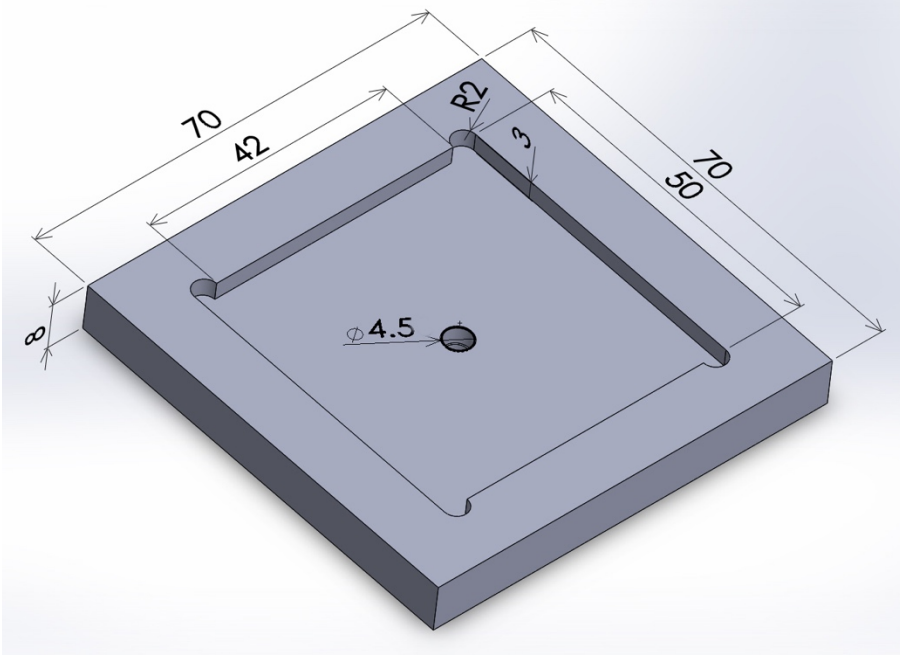

(b) Cassette (unit: mm)

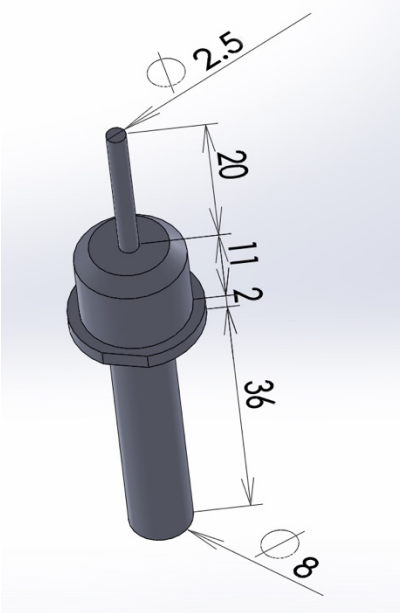

(c) Bar (unit: mm)

Figure 5.4 CAD file of the main part consist in the membrane holder (continued)

The design strategy for the cassette of the machine which holds the membrane

contains a rubber layer, a transparent layer, and a spring holder as shown in Figure 5.6. All the parts have a designated hole in the middle for the act of pushing the steel bar upwards. The rubber layer is made to constraint the movement of the membrane because of its wetness and eliminates uncertainty factor due to the sideways movement of the membrane. This can also be seen in Figure 2.4 where the membrane is attached to the sinus floor and it is constraint at the edge.

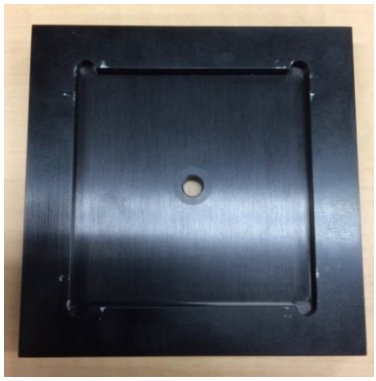

(a) The surface of the cassette

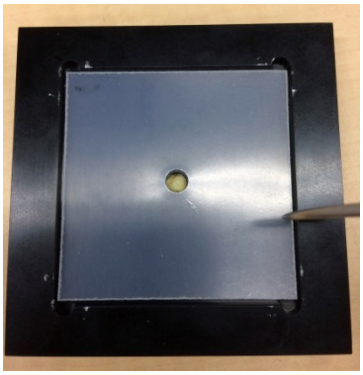

(b) A rubber layer or stopper inside the cassette

Figure 5.5 Component of the cassette

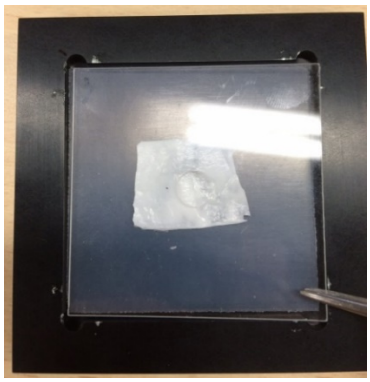

(c) The plastic layer with a hole in the middle

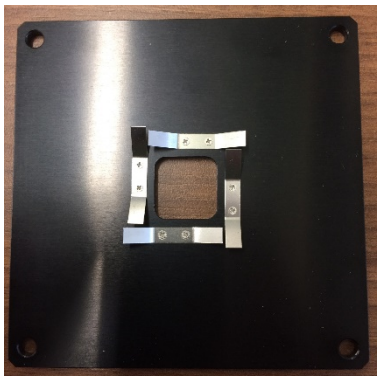

(d) The back of the spring holder

Figure 5.5 Component of the cassette (continued)

By taking the fact of the delamination of the area exposed after the fracture of the sinus lift, a transparent plastic layer is design to be put on top of the membrane with different diameter of hole available in the case of experimenting with different area of delamination as one of the uncertainty factor. There are three kinds of diameter designed at this point, a 5, 7, and 8 mm of diameter. Figure 5.6 shows the comparison of the delamination in case of the machine design and the real surgery. Note that only the delamination area of 5 mm and 8 mm of diameter are shown in the figure.

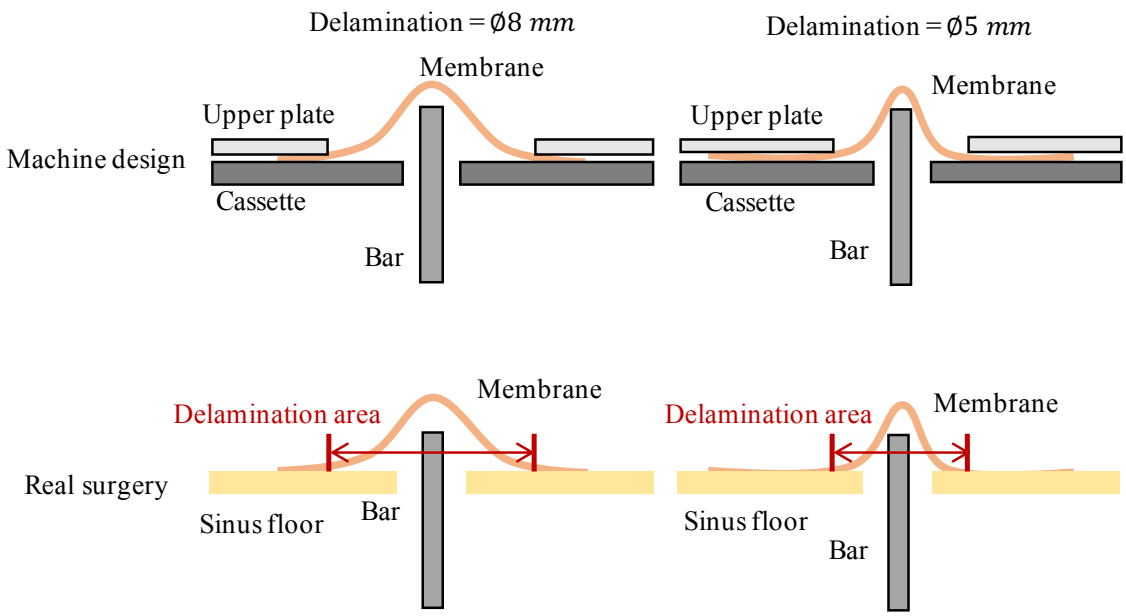

Figure 5.6 The delamination area considered in the apparatus compared to real surgery

In order to constraint the movement of the membrane horizontally, a spring holder was designed to lock the membrane on the cassette. Together with the transparent layer, the force from the spring holder with the transparent layer thickness can be adjusted to accommodate a thin layer of membrane. The design of the machine at this point even considers the membrane thickness as small as 0.01 mm. With all the parts of the cassette, the requirements to hold the membrane in place and also considering a few parameters such as the delamination, was fulfilled by these designs.

The bar part of the membrane holder was design to imitate the equipment used by dentist during the sinus lift up process. This is the part that considered to be in contact with the sinus membrane during the surgery. Although, usage of diamonds especially at the top end part of the bar was mostly reported (Franceschetti et al., 2012), this machine's

bar uses a steel as its material due to its cost compared to diamonds. The cylindrical bar was used because for many clinicians, it is much more informative than the usage of a semi-spherical bar. The steel bar part was actually designed to be exchangeable with any types of diameter but at this point, a 2.5 mm diameter steel bar was used.

The diameter of the bar is considered based on the tool used by clinician during the sinus lift up process. The smallest of the diameter is about 2.5 mm which is the same as used in this study. In addition, a smaller diameter bar will cause a much higher pressure leading to a very high strain concentration and faster breakage. The length was set at 20 mm considering the required height of the sinus lift in the crestal approach.

5.1.3 Actuator control system and usage of the apparatus

The control system of the apparatus is basically the same as the oral implant surgery training simulator. An actuator (DRS42SA2G-04MK, Oriental Motor Co. Ltd., Tokyo, Japan) is used to move the bar for the lift up process. Rather than using a center pole and a receiver plate, this apparatus uses a bar as shown in Figure 5.4(c). The bar is place on top of a load cell (LMB-A-50N) to measure the reaction force when lifting up the membrane. Different from the simulator, the location, Z, for this apparatus is defined as the lift up distance.

Similar to the actuator movement of the oral implant surgery, the distance is calculated based on the command signal sent from the control box. The calculated distance is verified using sensors that act as the limiter. The movement of the actuator is checked starting from the location of initialization sensor to the location of the upper

limiter. The movement according to that control signal was checked visually and verified.

In this apparatus, the user can input the movement speed of the bar and the lift up distance. The system will calculate the input value and move the bar accordingly. As the bar touches a membrane, if there is any reaction force detected, it will record the value at a predefined sampling time. The load identified by the load cell is recorded every 0.2 second until the user stops the machine or the determined height set, Z_{set}, is reached.

Conclusively, in order to use the machine, the bar is moved to the initial location through the initialization process. Then, the cassette is set on the membrane holder. Next, the user can input the determined height and speed on the machine. By starting the machine, the bar will move to the determined height with the set-up speed. The reaction force measured by the load cell will be recorded for each sampling time until the determine height.

5.2 Preliminary test of the machine

As a preliminary test to confirm the method of using the apparatus as describe in the previous section, a rubber membrane with a dimension of 15 x 15 mm and a thickness of 1 mm was used in this experiment. The rubber is a natural rubber that could be easily found in a home center. Firstly, the cassette is prepared by cleaning the surface. Next, the rubber layer is put inside the cassette. The specimen is then put in the middle of the cassette. It has to be made sure that the specimen covers the hole in the middle. Finally, a transparent plastic layer with a hole in the middle is put on top of the specimen.

The prepared cassette with the specimen is then put in the cassette holder on the machine. Right before the cassette is set up on the machine, the steel bar is put in place on the load cell. The cassette is then tightened with the spring holder. After the cassette is loaded, the movement of the steel bar is set at the control box with a speed of 0.3 mm/s and destination height of 2.0 mm. The bar then moved automatically by the set speed and lift up height. The result is recorded using the data recording computer attached to the apparatus.

In the case of this preliminary test, four samples of the same material were experimented on and the results is as shown in Figure 5.7. Based on the experiment, the load-deflection curve of each sample is almost the same as they can be seen to be almost parallel with one another.

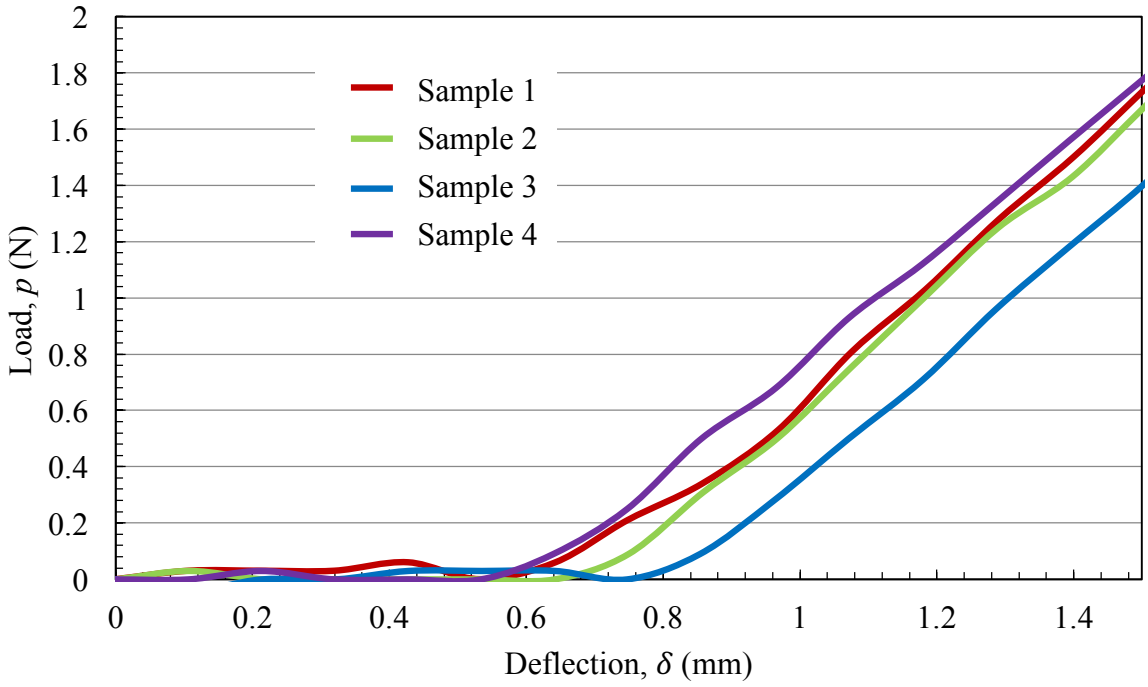

Figure 5.7 Results of the lift up experiment on rubber

5.3 Discussion and summary

With regard to the experimental results, there was a wrinkled condition considered to have happen when the membrane is set on the cassette. This may be due to the fact of the condition of a thin layer of membrane that does not have pretension on its edge and the membrane geometry is not flat as it seems to be. Consequently, the results of the experiment obtained from the recorded data is adjusted based on the schematic figure shown in Figure 5.8. The starting point which was set up at Z = 5.0 mm as mention earlier was set at about Z = 10.0 mm apart below the membrane. Thus, the starting point of deflection is the zero-point at the first recorded force during the experiment. This value is different with the setup of the lift up distance, Z on the machine.

This method was also considered in the test using sinus membrane which will be explained in the next chapter. Due to the uncertainty factor of the deflection the curve in a much higher deflection point is best taken for consideration. The parallel points between each sample as shown in Figure 5.7 proves that this is the best area to compare each sample. In order to compare the sample, it is best to thought of an error estimation calculation to find out the range and also for its validity. As of the author's knowledge, this is an initial method proposed so it is hard to make a comparison. The best way of validation and verification could be to increase the number of samples the test is done on and also doing an increase number of condition such as using the delamination condition or a different diameter of the bar to increase the confidence of the experimental method and values obtained.

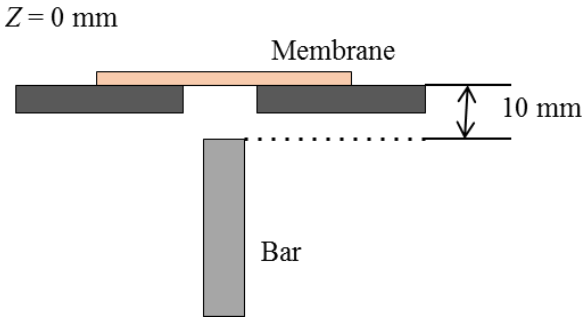

(a) The bar is set at 10 mm below the membrane

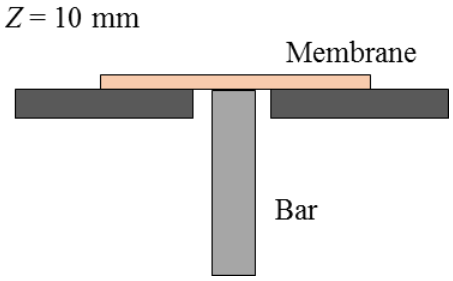

(b) The location of the bar when the recorded data is $Z = 10$ mm

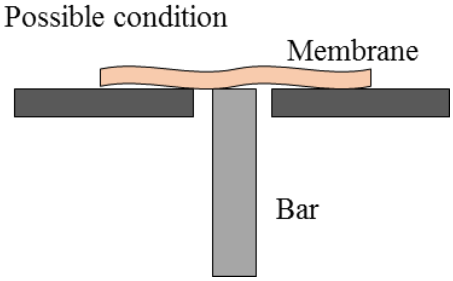

(c) The realistic possible condition of the membrane when $Z = 10$ mm

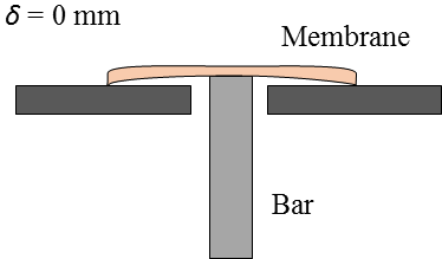

(d) The point when the reaction force is recorded is considered the zero-point deflection, $\delta = 0$

Figure 5.8 Schematic figures of the results adjustment

Chapter 6

Strain distribution in lifted sinus membrane

6.1 Outline of finding the strain distribution during sinus lift up process

Crestal sinus floor elevation is one of the sinus lift up process that could increase the residual bone height especially in the posterior maxillary to suitably accommodate a dental implant. This technique is based on the fracture or perforation of the sinus floor using osteotomes or burs (Summers, 1994). The exposed area of the membrane may also be augmented by condensing a graft material under the elevated sinus membrane (Fanuscu, Vu, & Poncelet, 2004; Fugazzotto & Vlassis, 2000; Pjetursson et al., 2009; Yan et al., 2014). This indirect method is much preferred because of its less invasive property thus leading to a much shorter recovery time. However, this method has a higher risk due to the sinus membrane being invisible. So, the process is mainly done based on the

experience or intuition of the dentist and there is fewer to no measurement done which put this method at risk (Reiser, Rabinovitz, Bruno, Damoulis, & Griffin, 1994).

A perforated sinus membrane increased the risk of sinusitis or infection and could lead to a much more complicated case (Peleg, Chaushu, Mazor, Ardekian, & Bakoon, 1999). Thus, in order to give the dentist, especially fresh graduate of the dentist college a much more quantifiable method, this study is done in order to observe the strain distribution on the sinus membrane which can later be transformed to a more appropriate method of quantifying the sinus lift process.

Figure 6.1 shows an overview of this study. Focusing on the crestal sinus floor elevation method, an experiment was done on a fresh cadaver using the method and apparatus described and designed in the previous chapter. Then, the load-deflection curve obtained from the experiment was calibrated with a numerical procedure which will be described later.

The membrane is assumed to be an elastic material in this study due to the limitation of number of samples for the experiment. To decide the viscoelastic properties, many specimens are needed. Even if the relaxation due to viscosity is neglected, the strain at the critical point can still be estimated. Thus, this study is established with an assumption of elastic material model. A constitutive equation of Ramberg-Osgood and material parameter was proposed to be used in the simulation for the calibration process. The results obtained were then used to calculate the strain on the membrane during the sinus lift up process.

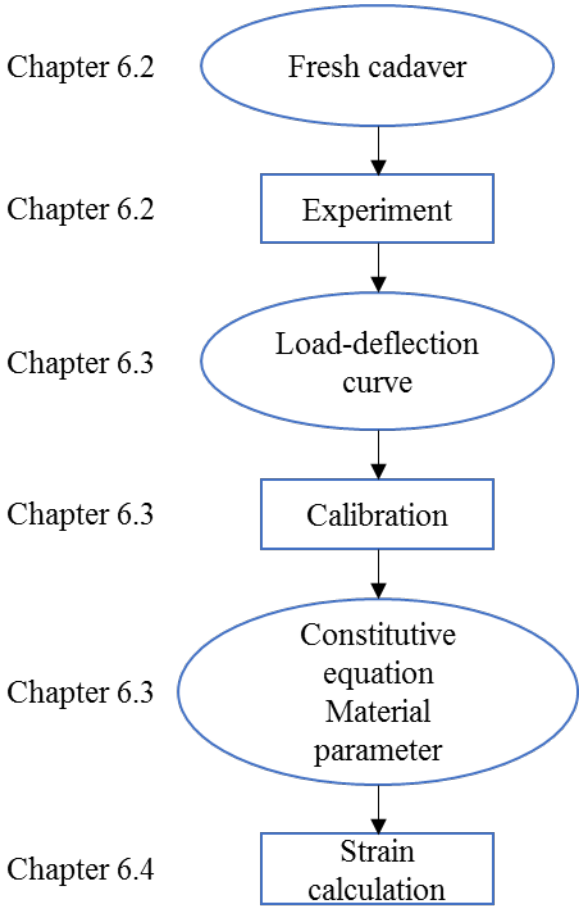

Figure 6.1 Outline of the study

6.2 Experiment using fresh cadaver

Roughly, the experiment done is based on the procedure described in the previous chapter. Under the supervision of a clinician from Tokyo Dental College, the sinus membrane was taken from the left part of a fresh cadaver which belongs to a 77-year-old male with a dimension of about 15 mm x 19 mm. Figure 6.2 shows the picture of the membrane after it was taken from the cadaver. Measurements of thickness were taken at different points of the membrane and the value is as shown in Table 6.1. This shows that the membrane

does not have a uniform thickness and the average value is employed in the numerical procedure. This is done in order to provide a much simple and faster computational calculation with assumption of constant thickness of 0.5 mm.

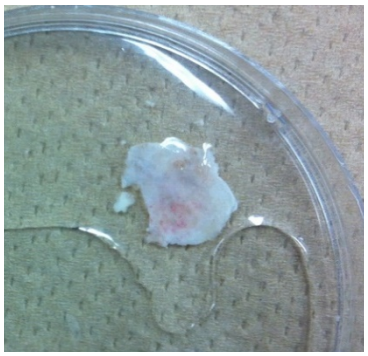

(a) Membrane (Specimen) taken from the fresh cadaver

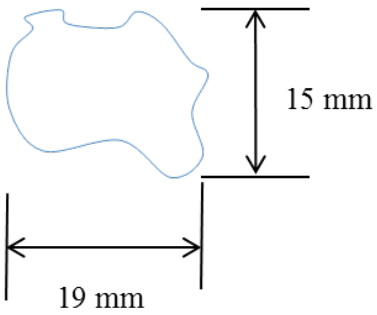

(b) Dimension of the membrane (Specimen)

Figure 6.2 View of the membrane right after it has been taken from the cadaver and its dimension

Table 6.1 Thickness of the membrane

	Thickness (mm)	Average (mm)	SD (mm)
Specimen	0.27	0.49	± 0.18
	0.51		
	0.42		
	0.77		

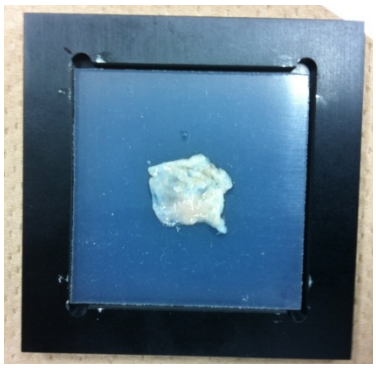

Figure 6.3 The membrane put on top of the test plate

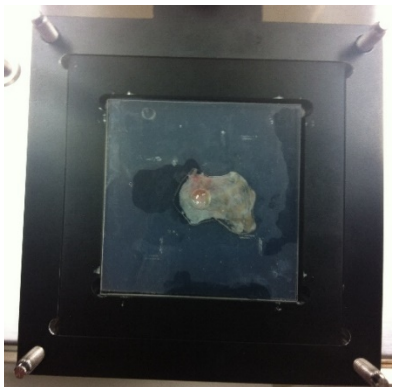

Figure 6.4 A transparent plate with a hole in middle (5 mm diameter) is put on top of the membrane

Firstly, the specimen is put on top of the test plate as shown in Figure 6.3. It is then covered with a transparent plate with a 5 mm hole in the middle and tighten with a spring holder. The plate assumed that the delamination area of the membrane is about 5 mm of diameter during the sinus lift up process. Next, the membrane is push upward with a speed of 0.5 mm/s using a steel bar with a diameter of 2.5 mm. The bar is attached to a load cell to measure and record the reaction force of the lift up process.

The data is recorded and exported in Microsoft Excel format. Result of the experiment is as shown in Figure 6.5. The result was adjusted from the raw data based on Figure 5.8. A total of 10 points were taken at each sampling time of 0.2 seconds and interpolated based on the 6^{th} order polynomial trendline of the graph to obtained a smooth curve of the experimental result for easier comparison with the numerical results. The lift up process is only able to record the deflection, δ, until about 0.9 mm. The graph however, was set until 0.9 mm. As shown in Figure 6.5, the value fluctuates during the lower part of the deflection, δ, due to the wrinkles and loss of muscle pretension on the membrane.

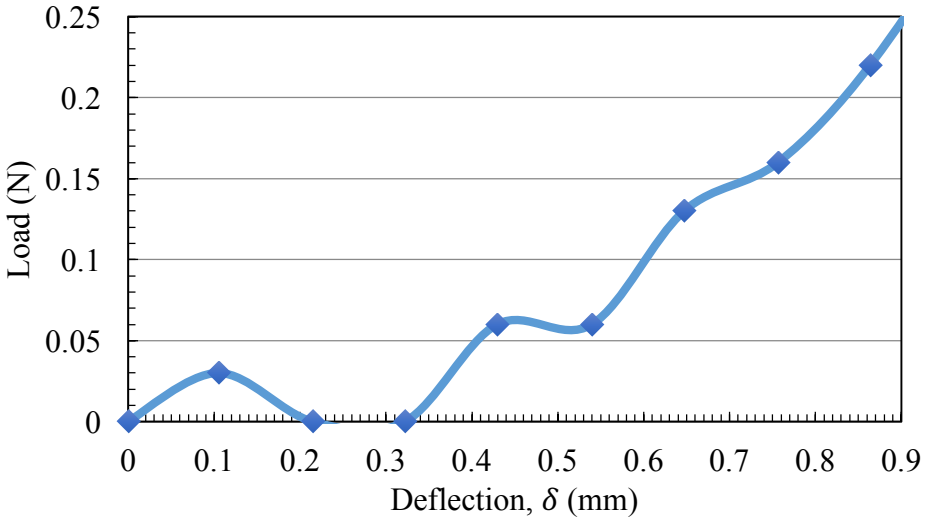

Figure 6.5 The load-deflection curve of the experiment on the membrane

The setup of the membrane is dominant but the oscillation is supposed to be caused by wrinkles in the membrane during the setup of the experiment. This is because it was very hard to stretch enough the thin and easy-to-break membrane. In the test, the force dropped once to zero value, but the measurement started the first time the force was recorded based on the definition of deflection as describe in Chapter 5. It was supposed that the zero-force happened by a locally wrinkled portion.

The temperature is also not considered in this study. The membrane is constraining the movement at the circumference and restricted it from moving in any direction. So, the wrinkle or slight deformation could only occur in the delamination area with a diameter of 5 mm. The experiment was done in a room temperature in January 2016.

6.3 Calibration of the constitutive model

The material model for the sinus membrane is unknown so a constitutive model is assumed in this study. The simulation assumed a nonlinear material model of Ramberg-Osgood. This power-law type constitutive model is applicable to large deformation. For uniaxial tension, the stress-strain curve is defined by the expression

$$\varepsilon = \frac{\sigma}{E} + \varepsilon_{ref}\left(\frac{\sigma}{\sigma_{ref}}\right)^{n} \tag{6.1}$$

where ε is the strain and σ is the stress. Here, E means the initial Young's modulus of the material and ε_{ref} is the strain reference at a reference stress, σ_{ref}. The parameter n

is the stress exponent. It is common to use $\varepsilon_{ref} = 0.002$ so σ_{ref} is the stress at 0.2% strain.

The Young's modulus measured by Pommer et al. (2009) which is $E = 70$ MPa was used with reference strain, $\varepsilon_{ref} = 0.002$. These leaves a set of undefined parameter of σ_{ref} and n to be checked and calibrated. Based on this equation,

$$\sigma_{ref} = E\varepsilon_{ref} \tag{6.2}$$

giving the value of reference stress, σ_{ref} of about 0.14 MPa. So, the range of σ_{ref} starts at 0.1 MPa. Table 6.2 shows the complete parameters used in this study.

Table 6.2 The parameter used in this study ($E = 70$ MPa)

E (MPa)	70														
ε_{ref}	0.002														
σ_{ref} (MPa)	0.1	0.2	0.3	0.4	0.5	1.0	2.0	3.0	4.0	5.0	6.0	7.0	8.0	9.0	10
n	1				2			3			4			5	

The parameters are then checked for its validity and sensitivity by calculating the strain-stress curve on a uniaxial tension test. As a result, Figure 6.6 shows the sensitivity of the all sets of parameters used in this study. As it can be seen the sensitivity moves toward the direction of lower value of reference stress, σ_{ref} and stress exponent, n. The sensitivity is much lower and less affecting the tension test with sets of high

reference stress, σ_{ref}. Whereas, lower value of reference stress, σ_{ref} and different stress exponent, n largely affects the tension test, All the parameters was then used in the finite element analysis (FEA) which will be described later.

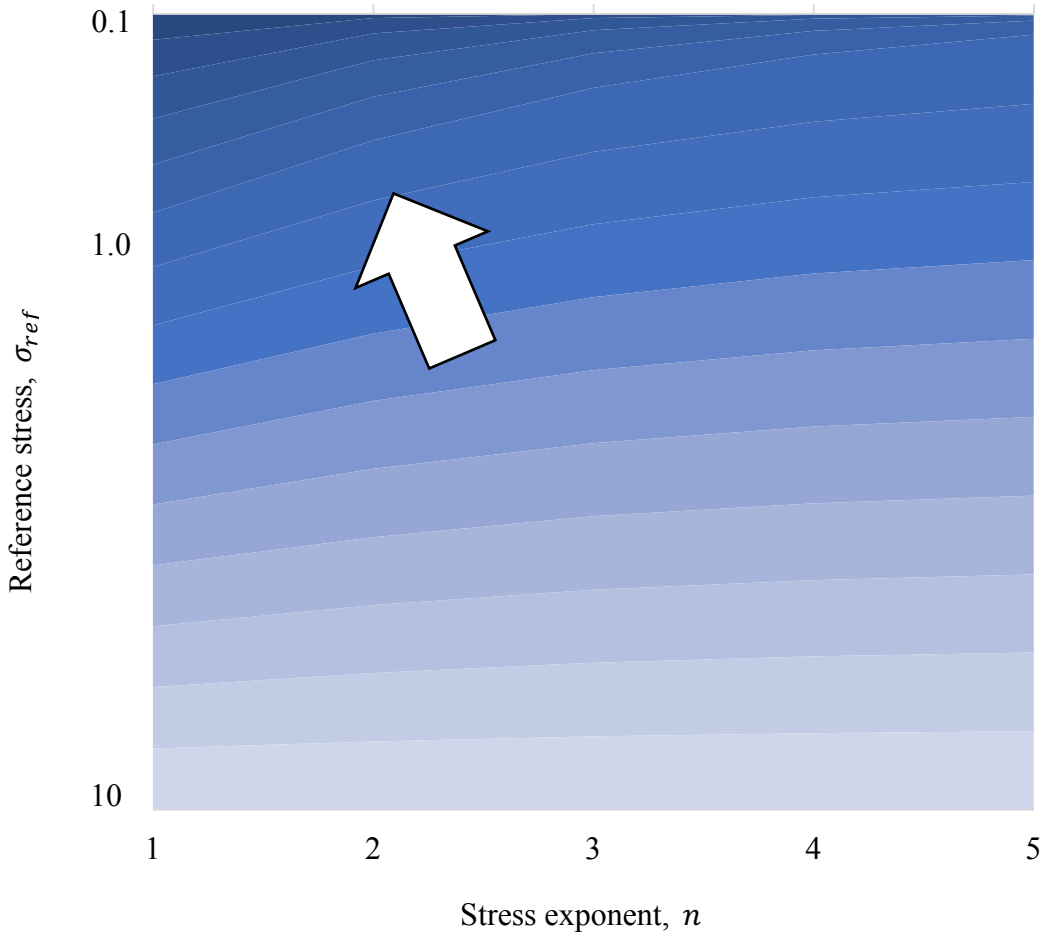

Figure 6.6 Sensitivity of the parameter for calibration ($E = 70$ MPa)

In order to reduce the number of variable parameter, the Young's modulus was firstly setup to be at a determined value. However, a larger Young's modulus than those measured by Pommer et al. is also considered for uncertainty. For the case of larger Young's modulus, the setup of the parameter and the sensitivity checked are as follows:

Table 6.3 The parameter used in this study ($E = 100$ MPa)

E (MPa)	100					
ε_{ref}	0.002					
σ_{ref} (MPa)	5.0	6.0	7.0	8.0	9.0	10
n	1	2	3	4	5	

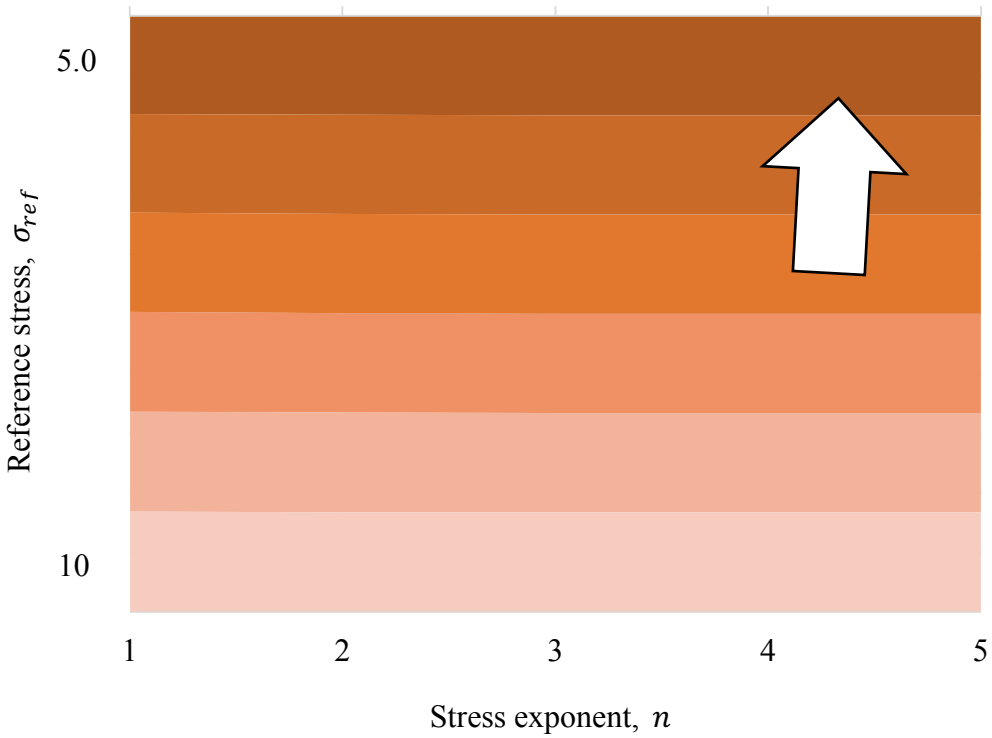

Figure 6.7 Sensitivity of the parameter for calibration ($E = 100$ MPa)

In order to calibrate the set of parameter and check the strain distribution on the membrane, a numerical simulation was proposed and done in this study. The simulation is designed to be as similar as possible with the experimental procedure as explained in the previous chapter. Figure 6.8 shows the design of the numerical procedure. The average

thickness of the membrane which is the value of 0.5 mm with uniform thickness is assumed for simpler and faster numerical procedure. The length of the bar is set at 10.0 mm and a fillet of 0.5 mm was assumed. This features of the bar is designed because for many clinicians, the strain in this case is much more informative rather than a semi-spherical head bar.

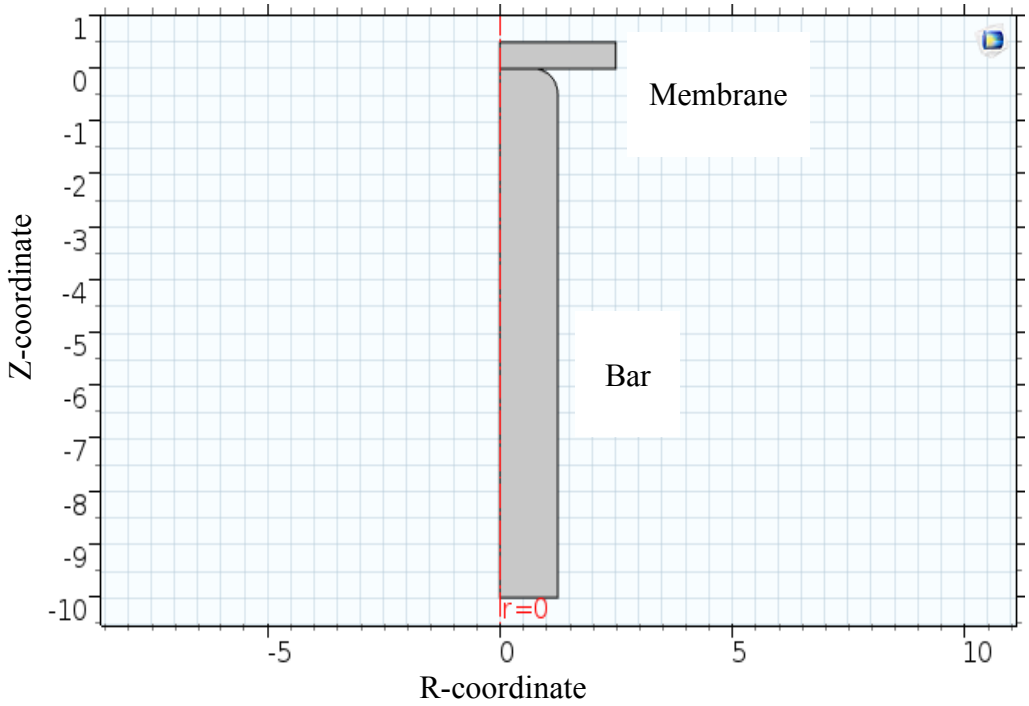

Figure 6.8 Design of the numerical procedure

Contact condition with no friction is assumed in this initial study due to the wet membrane and is set at (r, z) = (0<r<2.5, 0) which is the contact point between the bar and the membrane. Constraint condition was set up at every axis at the edge of the membrane (r, z) = (2.5, 0<z<0.5). By assuming an axisymmetric problem, the simulation was run inside COMSOL Multiphysics Version 5.2 with the bar pushing the membrane upwards with increment of 0.01 mm of prescribed displacement until the target height of

0.9 mm, the same value with the measured deflection.

The length of the bar is not a matter of concern as it is a rigid body. The results are not affected by the length of the bar but only the computational time was cut short. However, if the diameter is changed, it will change the results. For a thinner diameter of the bar, a higher strain value will be recorded. But, a constant geometry was considered in this initial study to check and compare between the experiment and numerical procedure for identification purposes.

Meshing was done by using a fine mesh for the membrane and a much coarser mesh for the bar as shown in Figure 6.9. A total of 1793 6-noded triangular axisymmetric element was generated in the software. The parameter range described previously was used in determining the best set for further analysis.

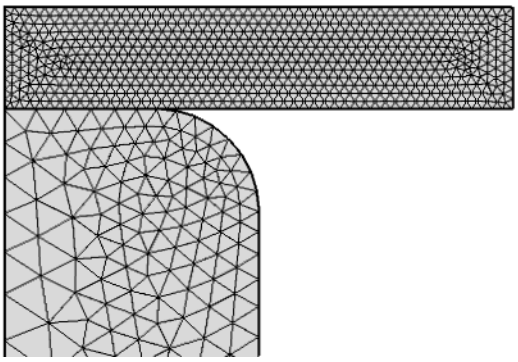

Figure 6.9 Meshing of the numerical procedure

The geometry of the experiment was simplified in the modeling because there is no way to measure the thickness distribution. It was impossible to put the membrane without wrinkling as mentioned previously so even a 3-dimensional shape is not perfect. For an initial study on the strain distribution on the sinus membrane, a uniform thickness is considered. Concerning the shape of the of the membrane, the apparatus was designed to avoid its influence by using a cover plate with a hole for constraint. Thus, the simulation is done only on the delaminated area of the membrane from the bone.

Based on the results of the simulation, the curves significantly agree with the experimental result in Figure 6.5 so it is then compared and analyzed further to check the difference based on error estimation. Due to the oscillation of the experimental results, the smooth curve between 0.7 mm and 0.9 mm is taken for comparison.

There are two types of error defined to analyze between the experimental and the simulation results, which is describe as follows:

i. The load derivative difference error

$$\Delta p^{err} = \frac{1}{N}\sum_{i=1}^{N}\frac{\left|\Delta p_i^{exp} - \Delta p_i^{sim}\right|}{\langle \Delta p^{exp} \rangle} \times 100 \qquad (6.3)$$

where Δp_i^{exp} is the load derivative of the experiment, Δp_i^{sim} is the load derivative of the numerical simulation, and $\langle \Delta p^{exp} \rangle$ is the average of load derivative at the taken point, which is in this case between 0.7 and 0.9 mm

ii. The load difference error

$$p^{err} = \frac{1}{N}\sum_{i=1}^{N}\frac{\left|p_i^{exp} - p_i^{sim}\right|}{\langle p^{exp}\rangle}\times 100 \tag{6.4}$$

where p_i^{exp} is the load result of the experiment at point *i*, p_i^{sim} is the load result of the numerical simulation at point *i*, and $\langle p^{exp}\rangle$ is the average of the experimental load result at the taken point, which is in this case between 0.7 and 0.9 mm. Figure 6.10 shows the definition of error based on the graph obtained.

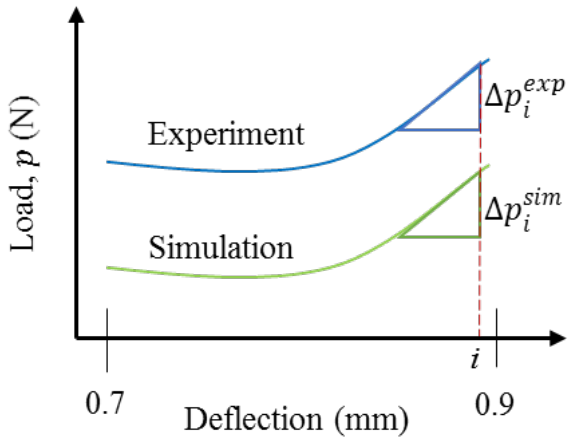

Figure 6.10 Definition of error

Table 6.4 and Table 6.5 shows the results based on each parameter defined in Table 6.2. Then, based on these result, a threshold error of below 0.15 percent is taken for the load derivative error in Table 6.4 and a threshold error of below 36 percent on the load difference error in Table 6.5. The threshold defined showed a set of available parameter

that is taken for further analysis. Based on further analysis of the parameter taken from the threshold, the curve shown not much difference for all the parameter sets considered. So, two sets of parameter from $E = 70$ MPa was chosen to be considered for comparison explained in the next step. Both sets of parameter showed significance in representing the parameter sets from the $E = 70$ MPa considered earlier. Next, considering the uncertainty factor of the value of Young's modulus, a higher value of Young's modulus of 100 MPa was set and the calculated error is shown in Table 6.6 and Table 6.7 for the load derivative error and load difference error respectively. The best combination of parameter sets of low load derivative error with low load difference error was taken for comparison with the parameter sets $E = 70$ MPa choosen earlier.

Table 6.4 The load derivative difference error, Δp^{err} (%) of E = 70 MPa

n / σ_{ref}	**1**	**2**	**3**	**4**	**5**
0.1	0.62	0.94	0.97	0.98	0.98
0.2	0.47	0.88	0.94	0.96	0.97
0.3	0.39	0.83	0.91	0.94	0.95
0.4	0.34	0.78	0.89	0.92	0.94
0.5	0.31	0.73	0.86	0.90	0.92
1	0.23	0.55	N.A.	0.81	0.85
2	0.18	0.35	N.A.	N.A.	N.A.
3	0.16	0.25	N.A.	N.A.	N.A.
4	0.15	0.21	0.30	0.40	0.47
5	0.15	0.18	0.24	0.31	0.38
6	0.14	0.16	0.20	0.25	0.30
7	0.14	0.15	0.18	0.21	0.25
8	0.14	0.15	N.A.	0.18	0.21
9	0.14	0.14	0.15	0.16	0.18
10	0.13	0.14	0.14	N.A.	0.16

Table 6.5 The load difference error, $\boldsymbol{p^{err}}$ (%) of E = 70 MPa

σ_{ref} \ n	**1**	**2**	**3**	**4**	**5**
0.1	69.5	90.8	93.5	94.3	94.7
0.2	59.0	85.8	90.8	92.3	93.0
0.3	53.4	81.4	88.1	90.4	91.5
0.4	49.9	77.7	85.6	88.5	89.9
0.5	47.5	73.7	83.2	86.7	88.4
1	41.9	60.2	N.A.	78.2	81.1
2	38.6	47.0	N.A.	N.A.	N.A.
3	37.4	41.6	N.A.	N.A.	N.A.
4	36.7	39.0	42.8	47.1	50.7
5	36.4	37.6	39.8	42.6	45.3
6	36.1	36.8	38.1	39.8	41.6
7	35.9	36.3	37.0	38.0	39.2
8	35.8	36.0	N.A.	36.9	37.6
9	35.7	35.8	35.9	36.2	36.6
10	35.6	35.6	35.6	N.A.	36.0

Table 6.6 The load derivative difference error, Δp^{err} (%) of E = 100 MPa

σ_{ref} \ n	**1**	**2**	**3**	**4**	**5**
5	0.21	0.11	0.10	0.26	0.45
6	0.21	0.15	0.09	0.13	0.22
7	0.22	0.17	0.10	0.10	0.24
8	0.23	0.19	0.13	0.09	0.17
9	0.23	0.20	0.15	0.11	0.10
10	0.23	0.21	0.18	0.13	0.11

Table 6.7 The load difference error, p^{err} (%) of E = 100 MPa

σ_{ref} \ n	**1**	**2**	**3**	**4**	**5**
5	11.6	16.0	23.2	30.6	36.9
6	11.1	14.0	18.9	24.5	29.4
7	10.7	12.7	16.0	20.1	24.5
8	10.5	11.8	14.0	16.9	20.2
9	10.2	11.1	13.0	14.7	17.0
10	10.1	10.6	11.6	13.0	14.7

Figure 6.11 shows the results of the set parameter based on defined earlier compared with the experimental results. The curve of the set parameter almost coincides with the experimental parameter showing agreeable results.

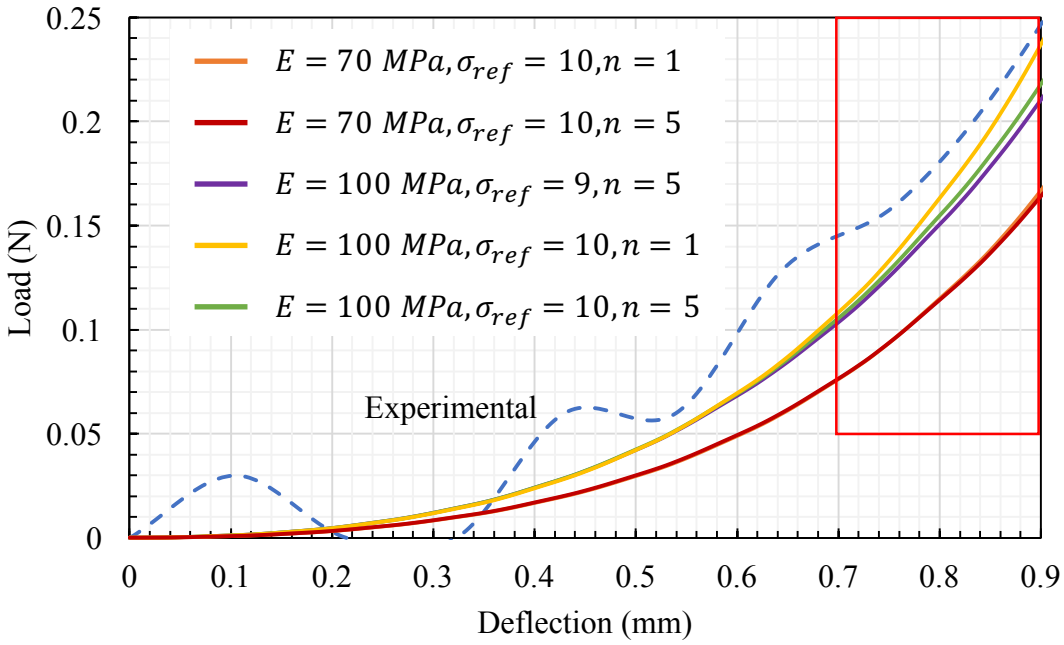

(a) Results of the comparison with the experimental value

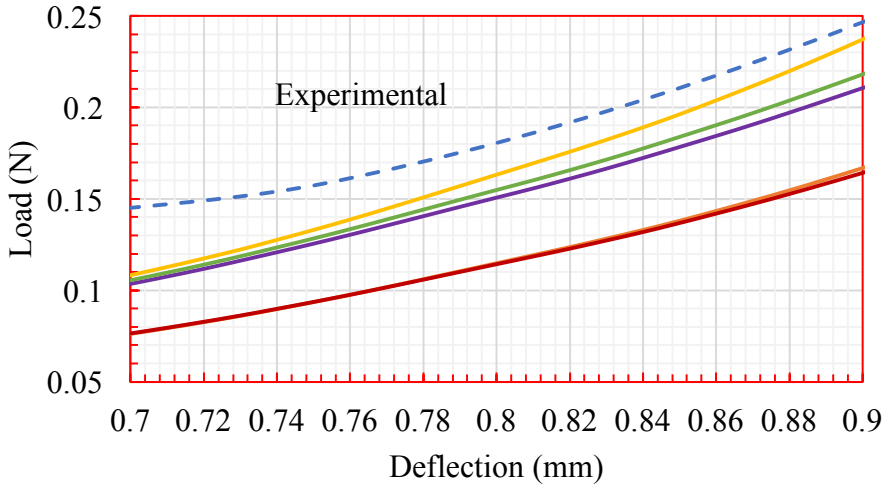

(b) Magnified view of the area defined for error

Figure 6.11 Results of the comparison of the set parameter based on the threshold defined earlier.

Based on Table 6.6 and 6.7, by appending the value of Young's modulus with a higher one, the error drops for most of the parameter sets. The value drops drastically around 20 percent for the load difference error but only a few percent for the load derivative error. This shows that there are actually many parameter sets that can be identified in order to calibrate the constitutive model by using the Ramberg-Osgood model. Takano et al. (2011) describe a calibration process for two different sets of parameter based on an equation regarding the etching process. The same algorithm can be used in order to identify the best sets of parameter concerning the Ramberg-Osgood model. The calibration was also verified by experiment and simulation procedure as what had been done in this study.

6.4 Calculation of strain distribution in the lifted sinus membrane

The analysis was expanded further by observing the strain distribution in the membrane. Using the calibrated parameter defined earlier, Figure 6.12 to Figure 6.19 shows the Green-Lagrange strain on each main direction of the analysis during the sinus lift up process using the parameter of $\sigma_{ref} = 10$, $n = 1$ for both cases of Young's modulus. The screenshot of the lift up process is taken at every 0.1 mm of deflection, δ. The other parameters showed similar distribution and characteristics during the lift up process but with different value seen.

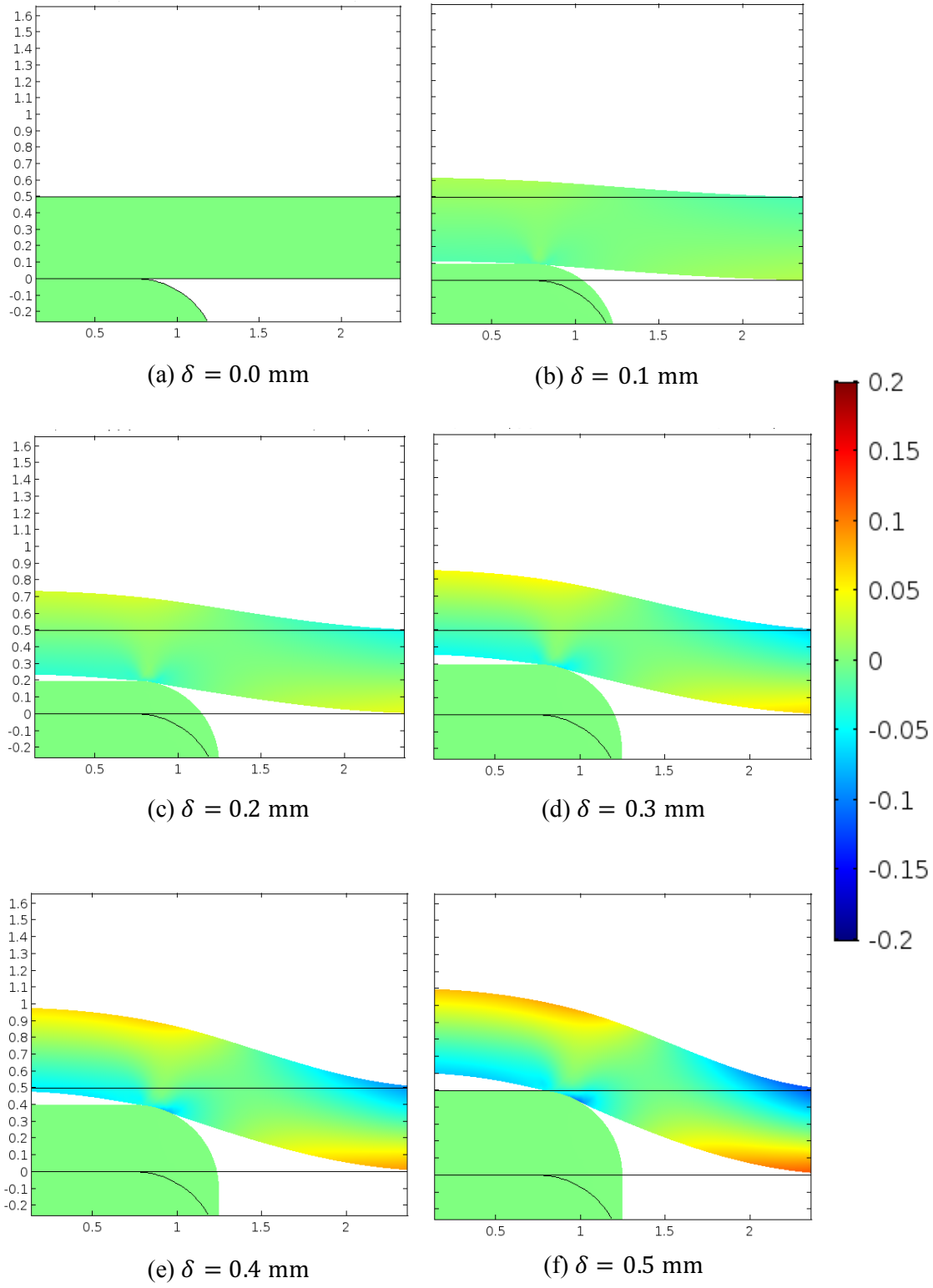

Figure 6.12 Screenshot of the *RR* strain on the membrane during sinus lift for $E = 70$ MPa

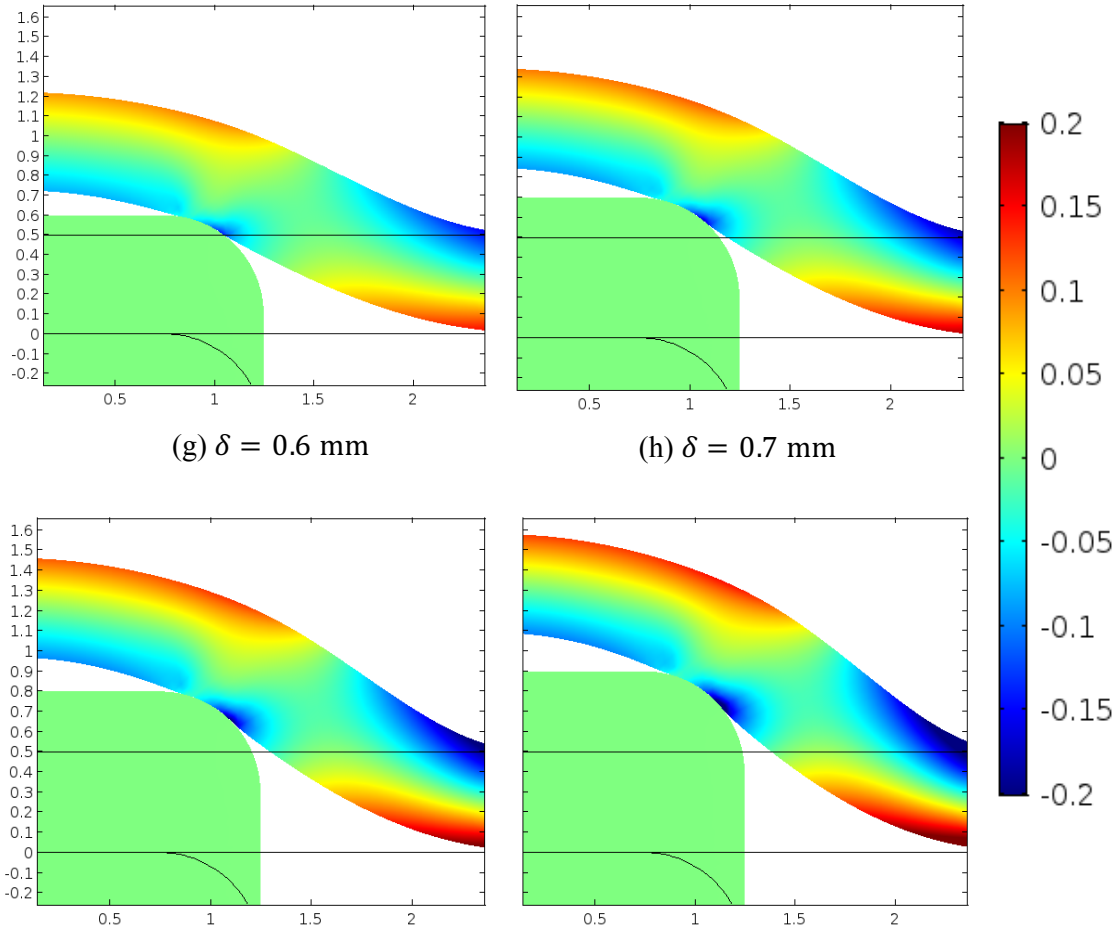

(g) $\delta = 0.6$ mm (h) $\delta = 0.7$ mm

(i) $\delta = 0.8$ mm (j) $\delta = 0.9$ mm

Figure 6.12 Screenshot of the *RR* strain on the membrane during sinus lift up for $E = 70$ MPa (continued)

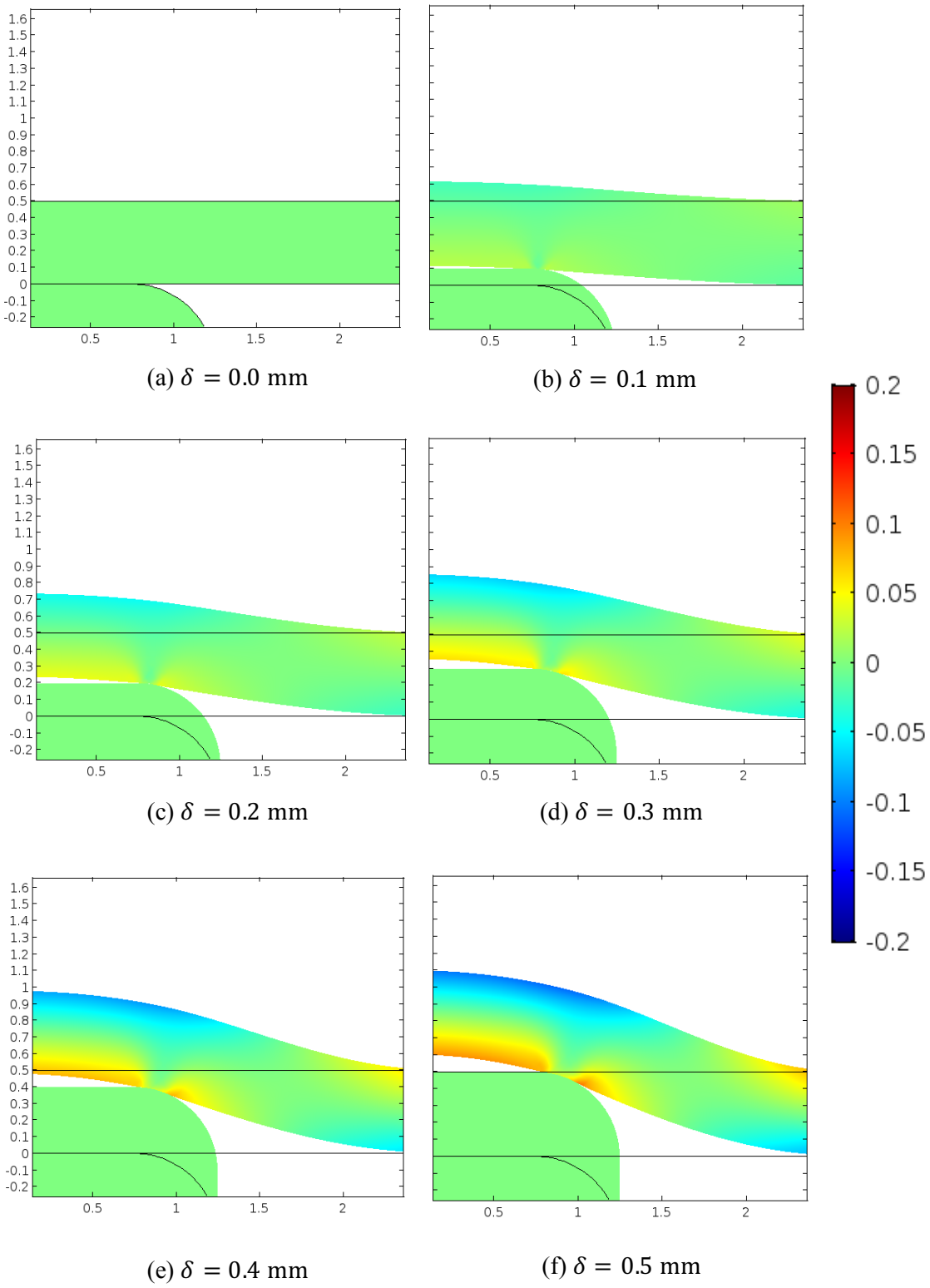

Figure 6.13 Screenshot of the *ZZ* strain on the membrane during sinus lift up for E = 70 MPa

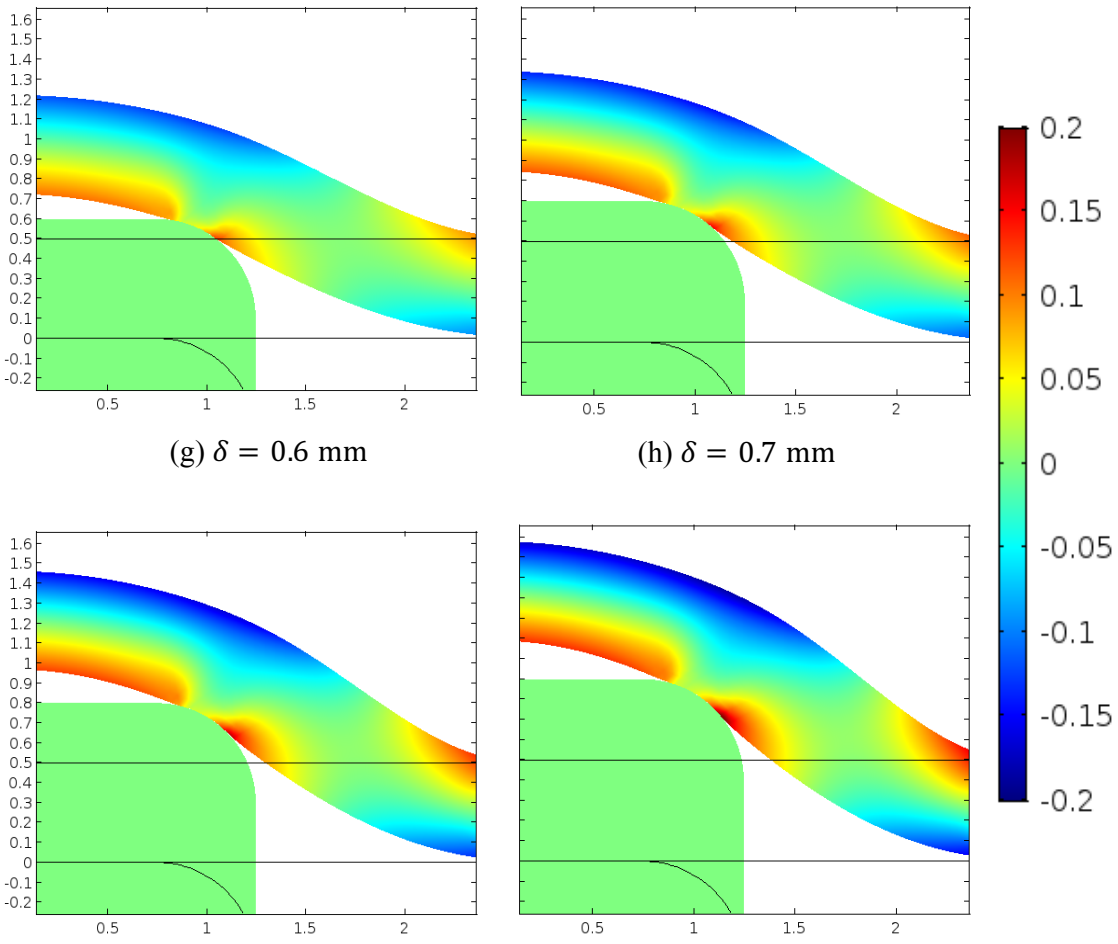

(g) $\delta = 0.6$ mm (h) $\delta = 0.7$ mm

(i) $\delta = 0.8$ mm (j) $\delta = 0.9$ mm

Figure 6.13 Screenshot of the *ZZ* strain on the membrane during sinus lift up for $E = 70$ MPa (continued)

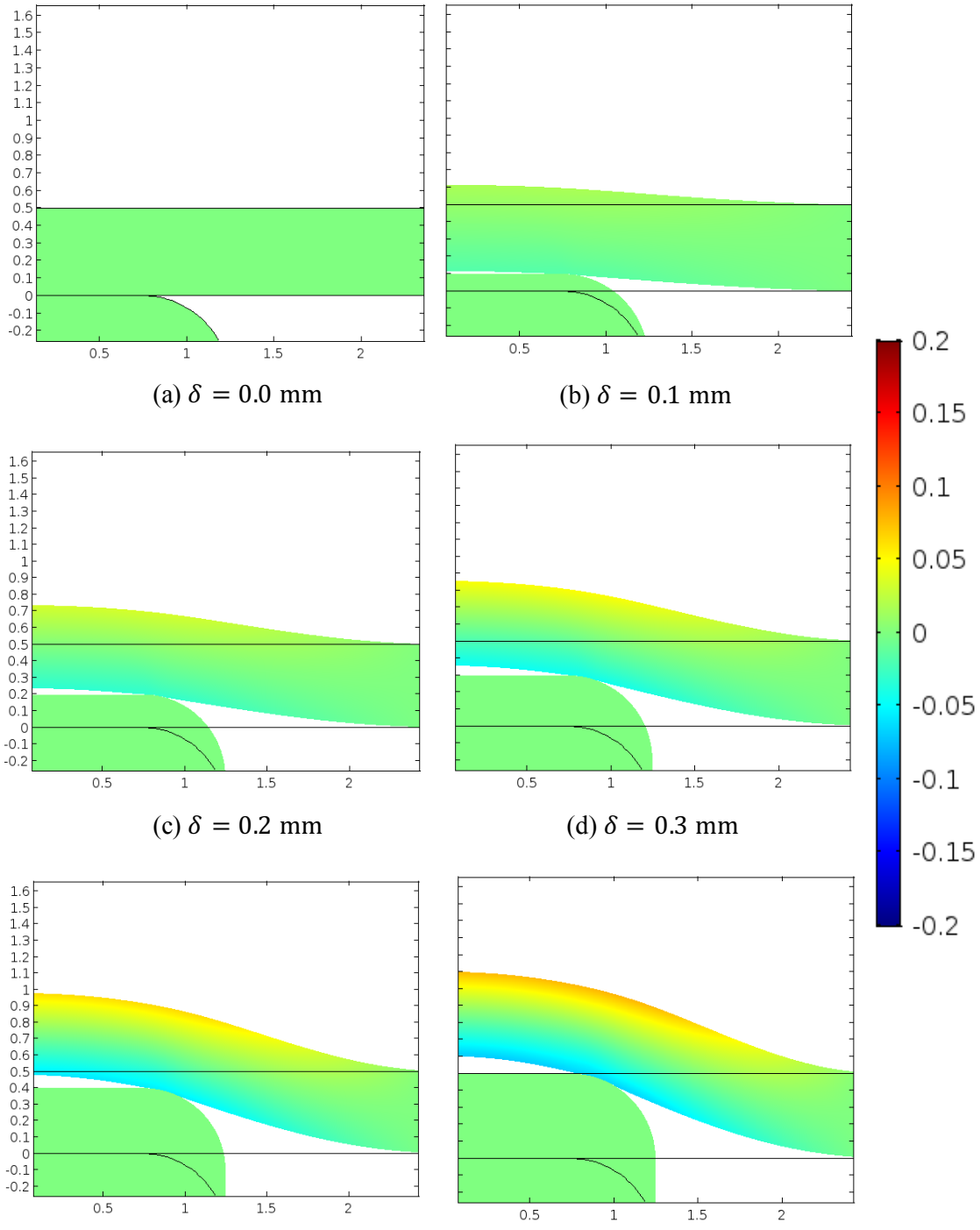

(a) $\delta = 0.0$ mm (b) $\delta = 0.1$ mm

(c) $\delta = 0.2$ mm (d) $\delta = 0.3$ mm

(e) $\delta = 0.4$ mm (f) $\delta = 0.5$ mm

Figure 6.14 Screenshot of the $\theta\theta$ strain on the membrane during sinus lift up for E = 70 MPa

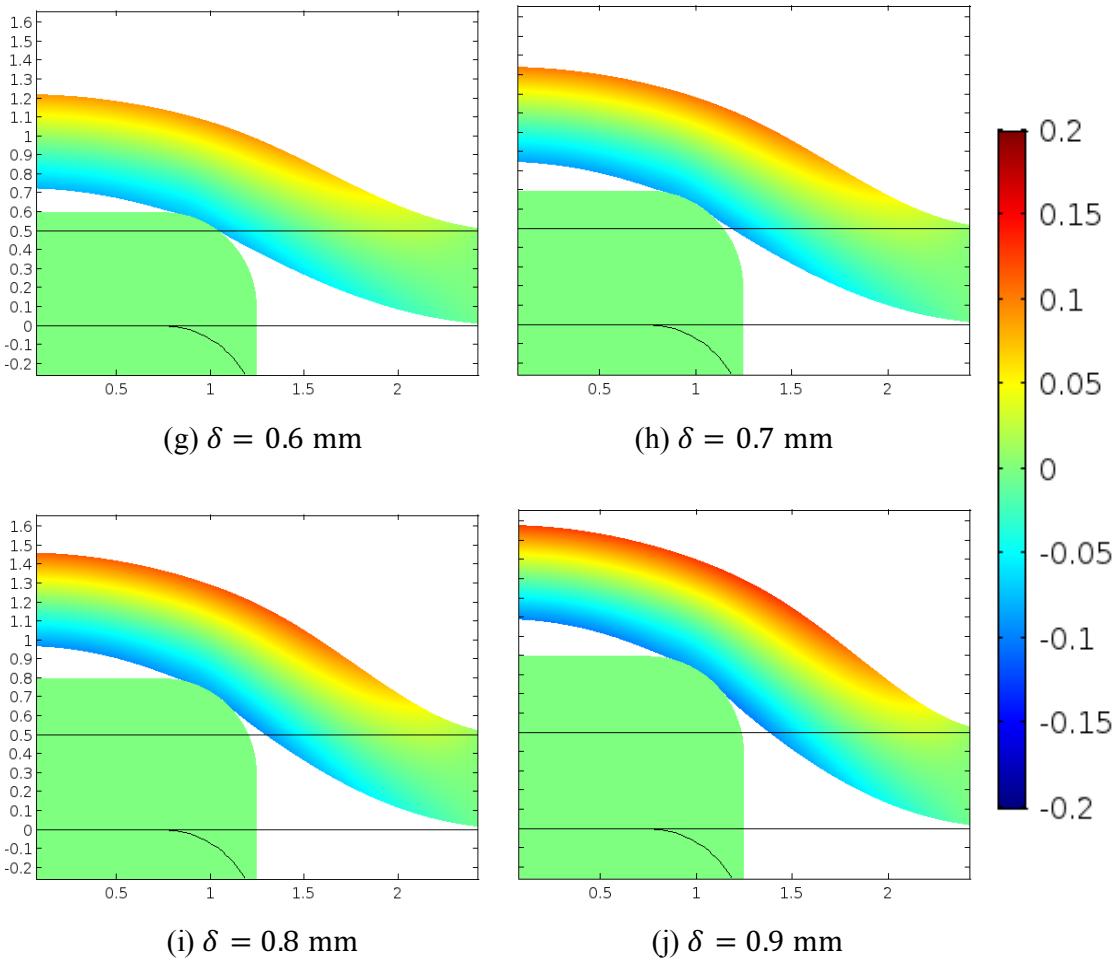

(g) $\delta = 0.6$ mm (h) $\delta = 0.7$ mm

(i) $\delta = 0.8$ mm (j) $\delta = 0.9$ mm

Figure 6.14 Screenshot of the $\theta\theta$ strain on the membrane during sinus lift up for E = 70 MPa (continued)

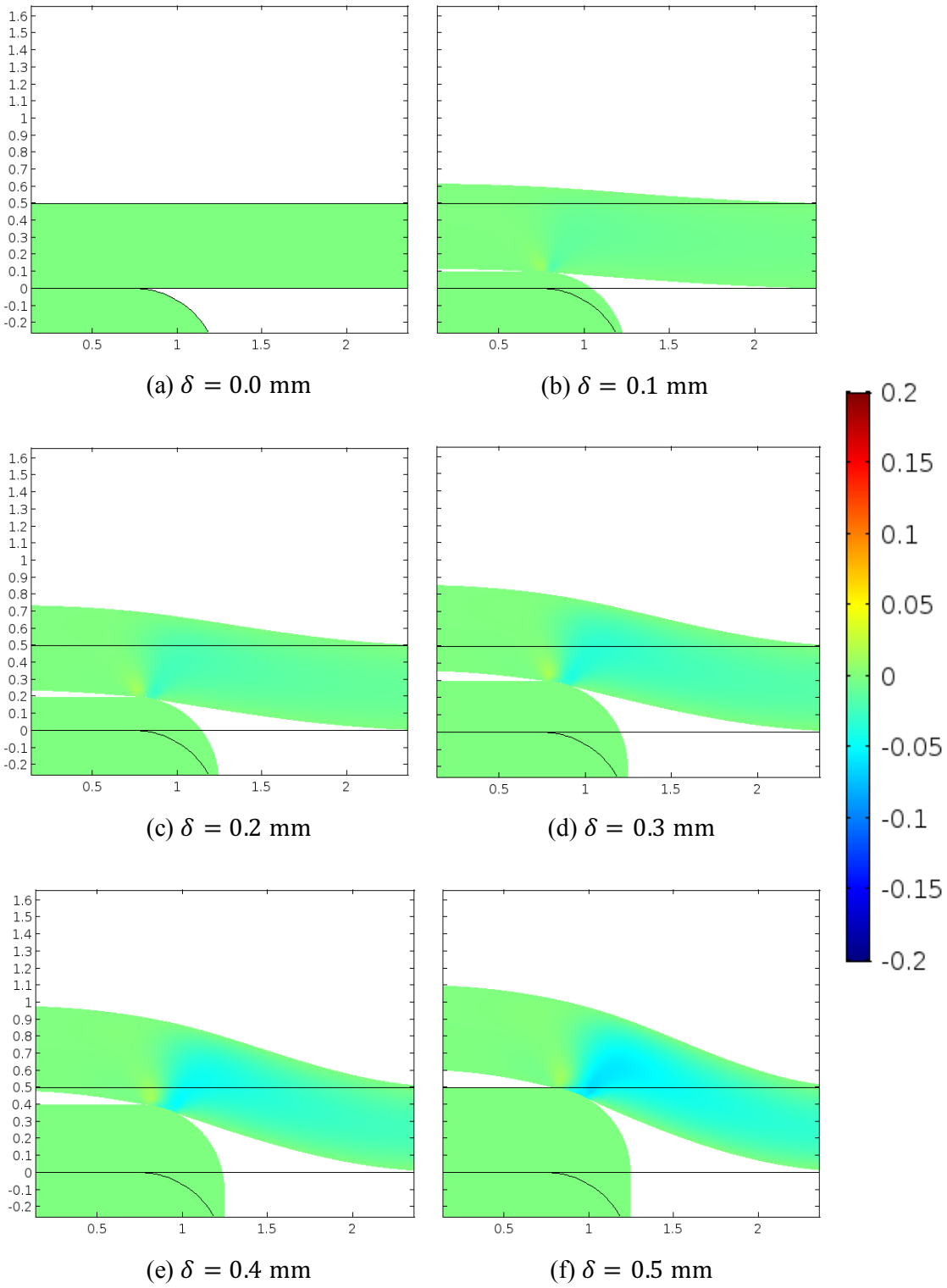

Figure 6.15 Screenshot of the *RZ* strain on the membrane during sinus lift up for $E = 70$ MPa

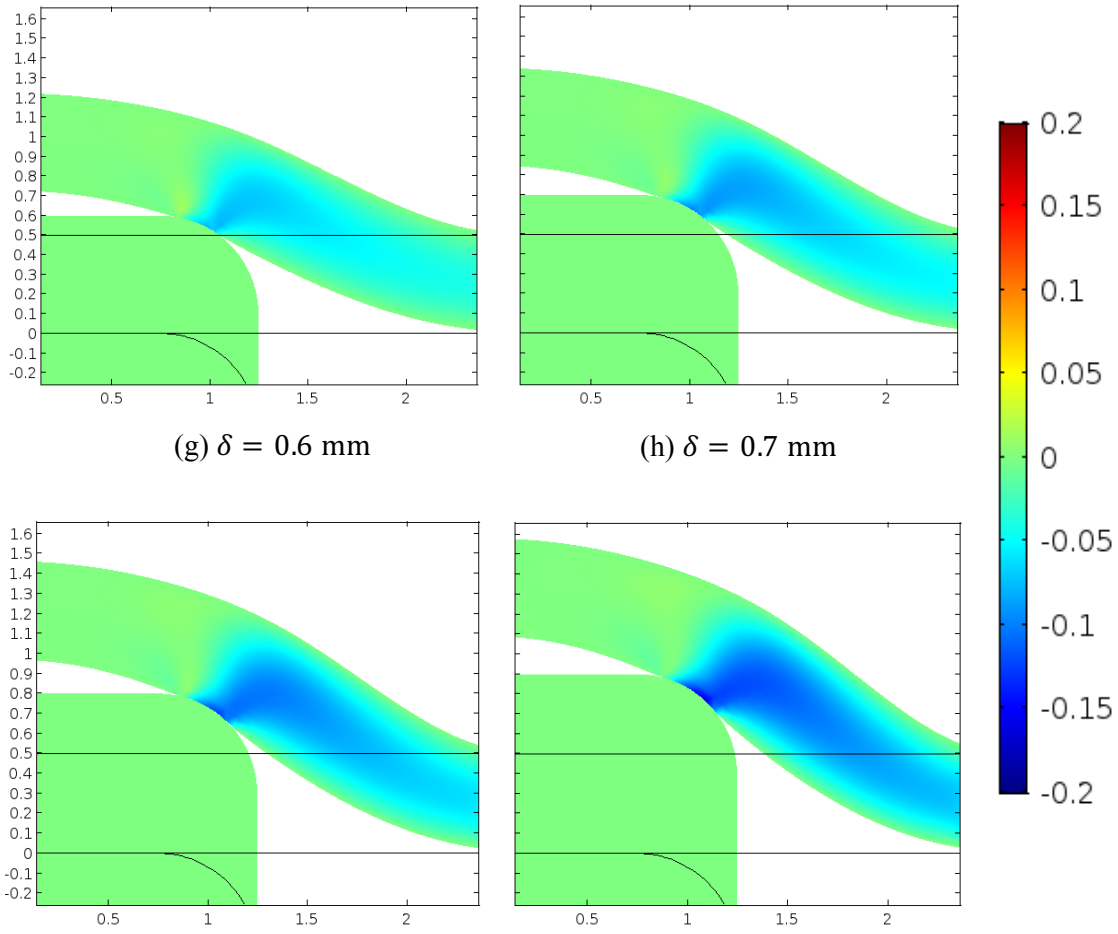

(g) $\delta = 0.6$ mm (h) $\delta = 0.7$ mm

(i) $\delta = 0.8$ mm (j) $\delta = 0.9$ mm

Figure 6.15 Screenshot of the *RZ* strain on the membrane during sinus lift up for $E = 70$ MPa (continued)

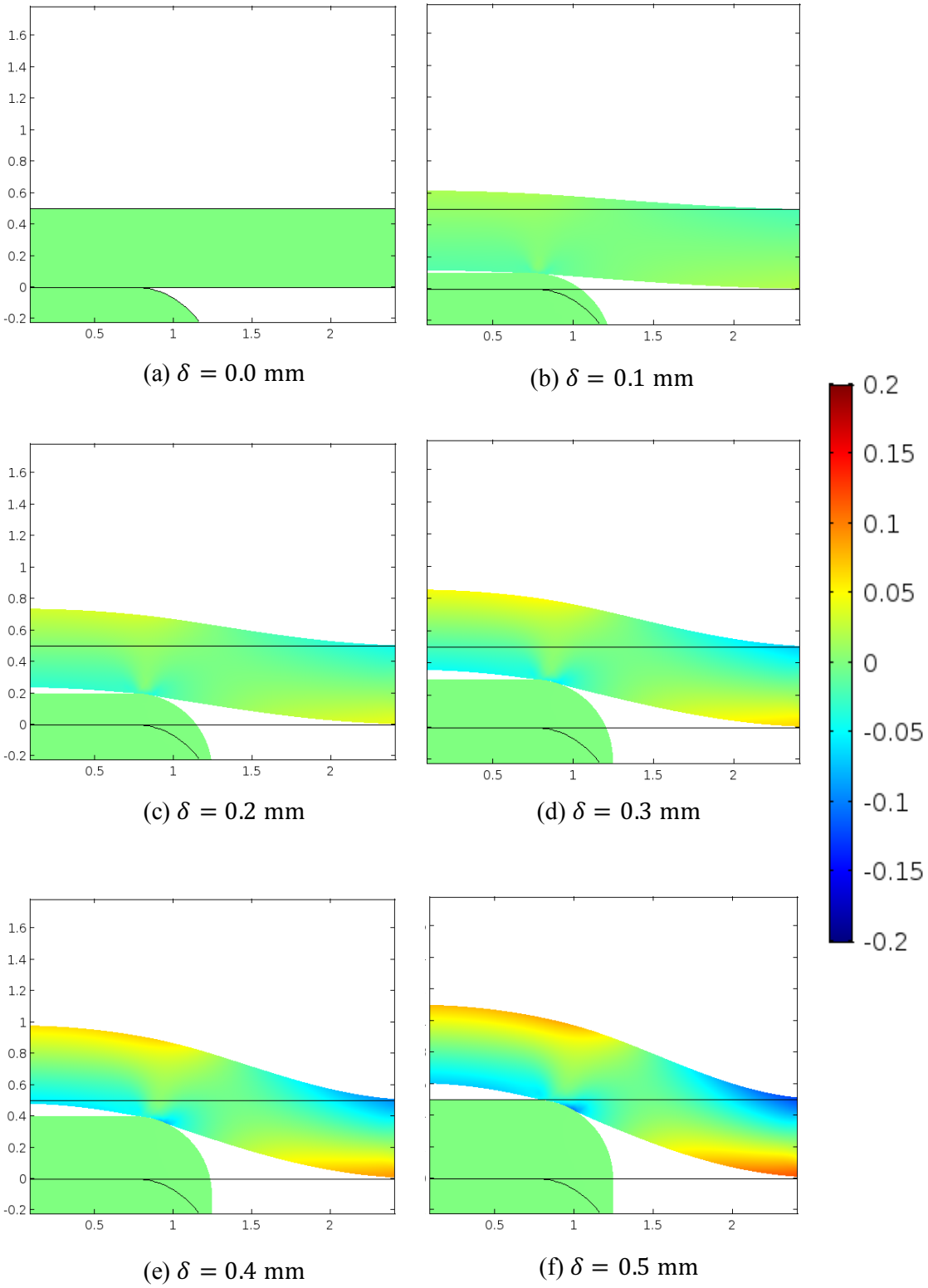

Figure 6.16 Screenshot of the *RR* strain on the membrane during sinus lift up for E = 100 MPa

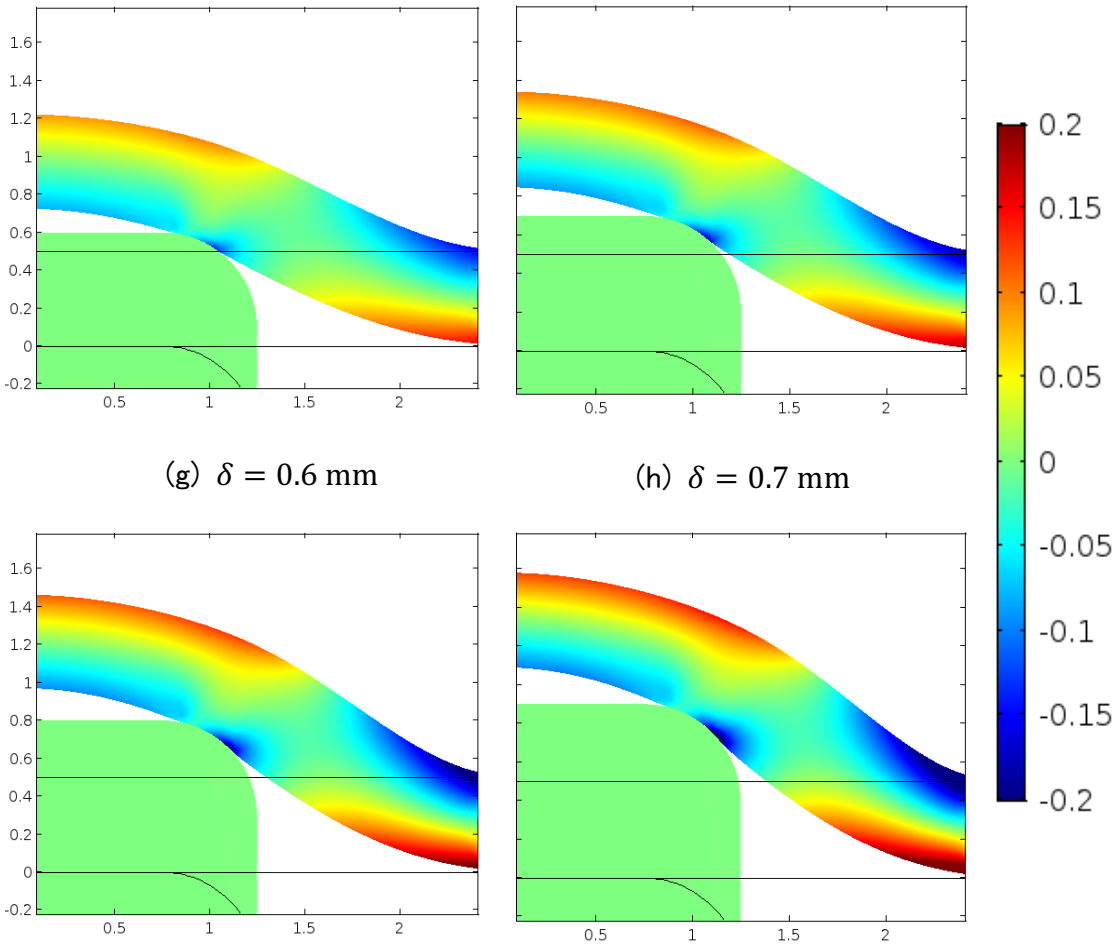

(g) $\delta = 0.6$ mm (h) $\delta = 0.7$ mm

(i) $\delta = 0.8$ mm (j) $\delta = 0.9$ mm

Figure 6.16 Screenshot of the *RR* strain on the membrane during sinus lift up for E = 100 MPa (continued)

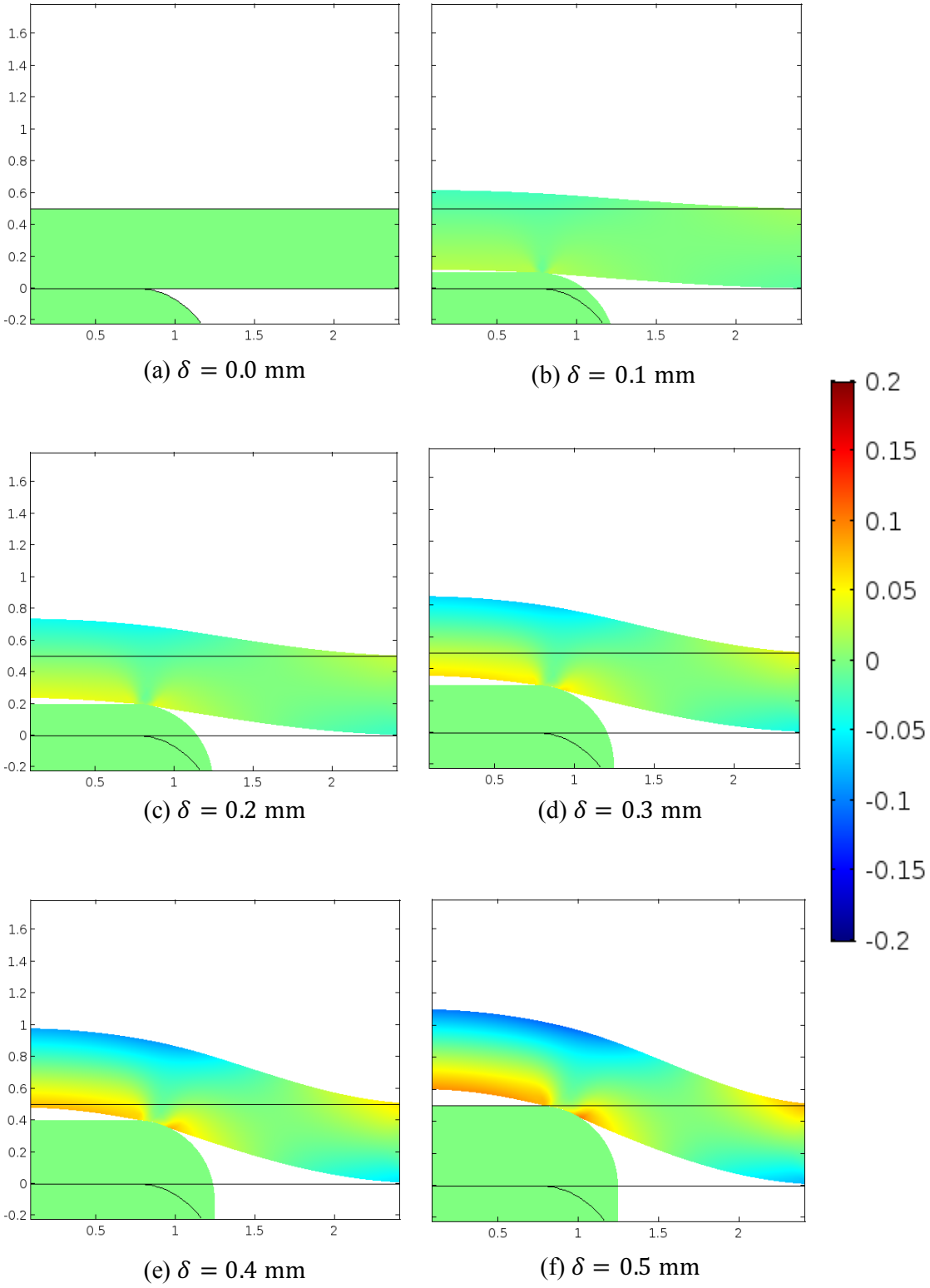

Figure 6.17 Screenshot of the *ZZ* strain on the membrane during sinus lift up for E = 100 MPa

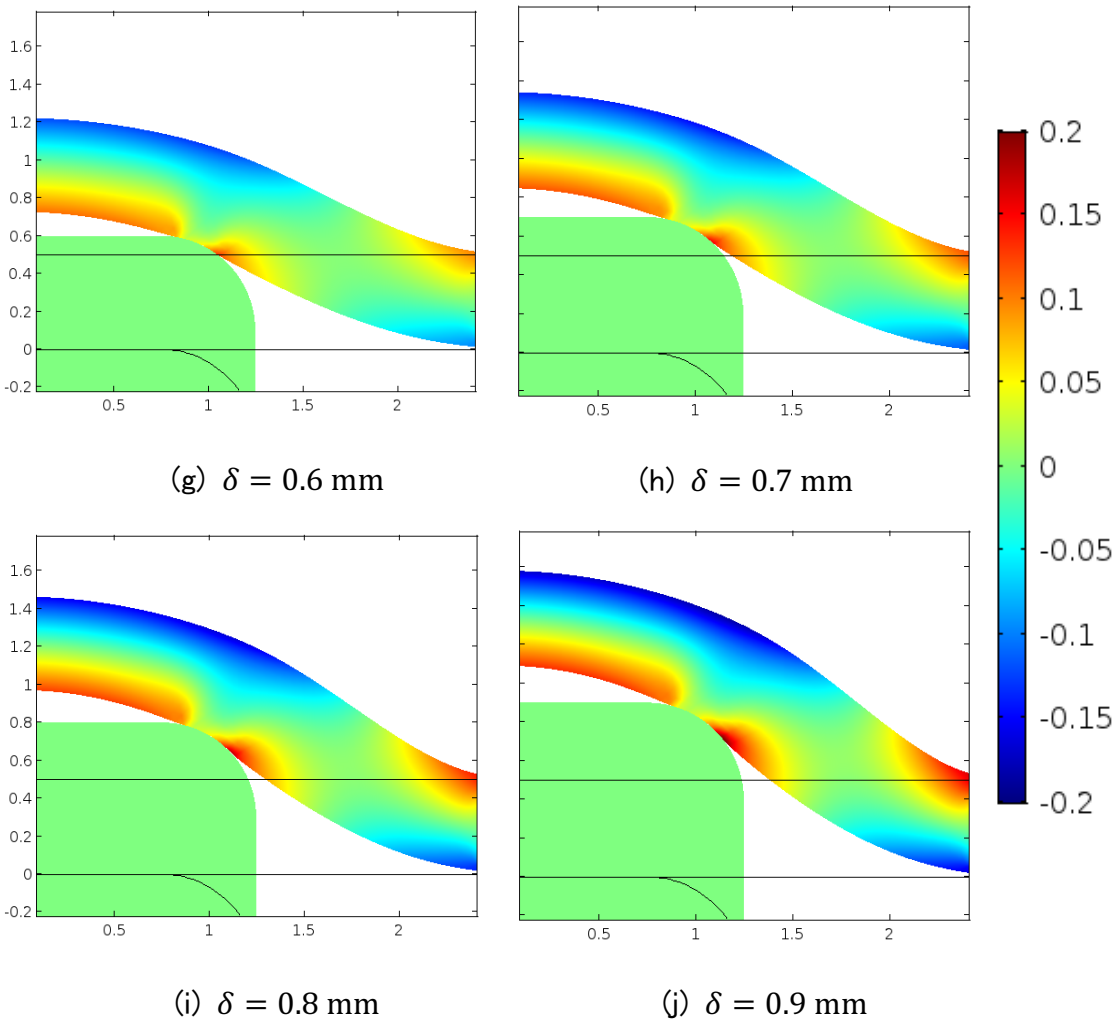

(g) $\delta = 0.6$ mm (h) $\delta = 0.7$ mm

(i) $\delta = 0.8$ mm (j) $\delta = 0.9$ mm

Figure 6.17 Screenshot of the *ZZ* strain on the membrane during sinus lift up for E = 100 MPa (continued)

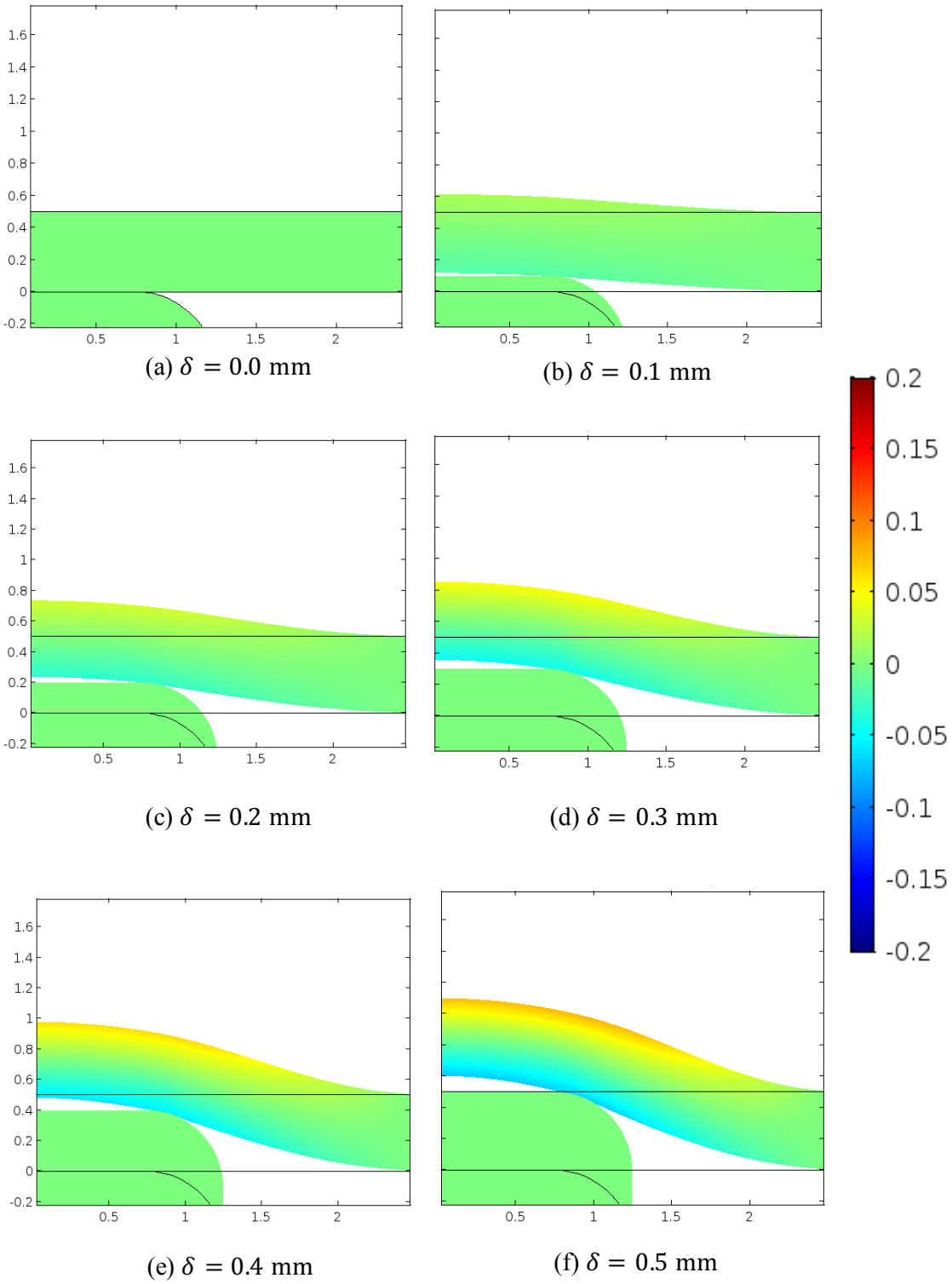

Figure 6.18 Screenshot of the $\theta\theta$ strain on the membrane during sinus lift up for E = 100 MPa

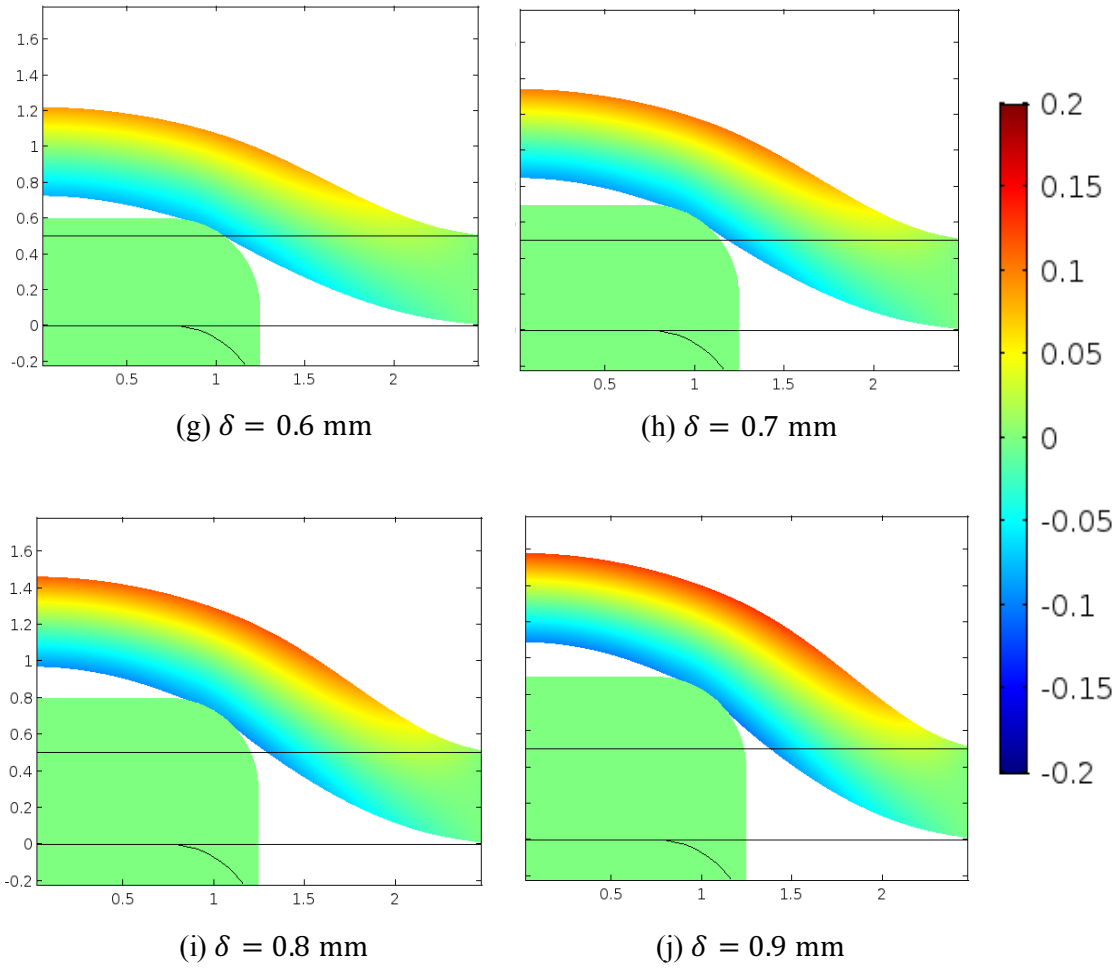

(g) $\delta = 0.6$ mm (h) $\delta = 0.7$ mm

(i) $\delta = 0.8$ mm (j) $\delta = 0.9$ mm

Figure 6.18 Screenshot of the $\theta\theta$ strain on the membrane during sinus lift up for E = 100 MPa (continued)

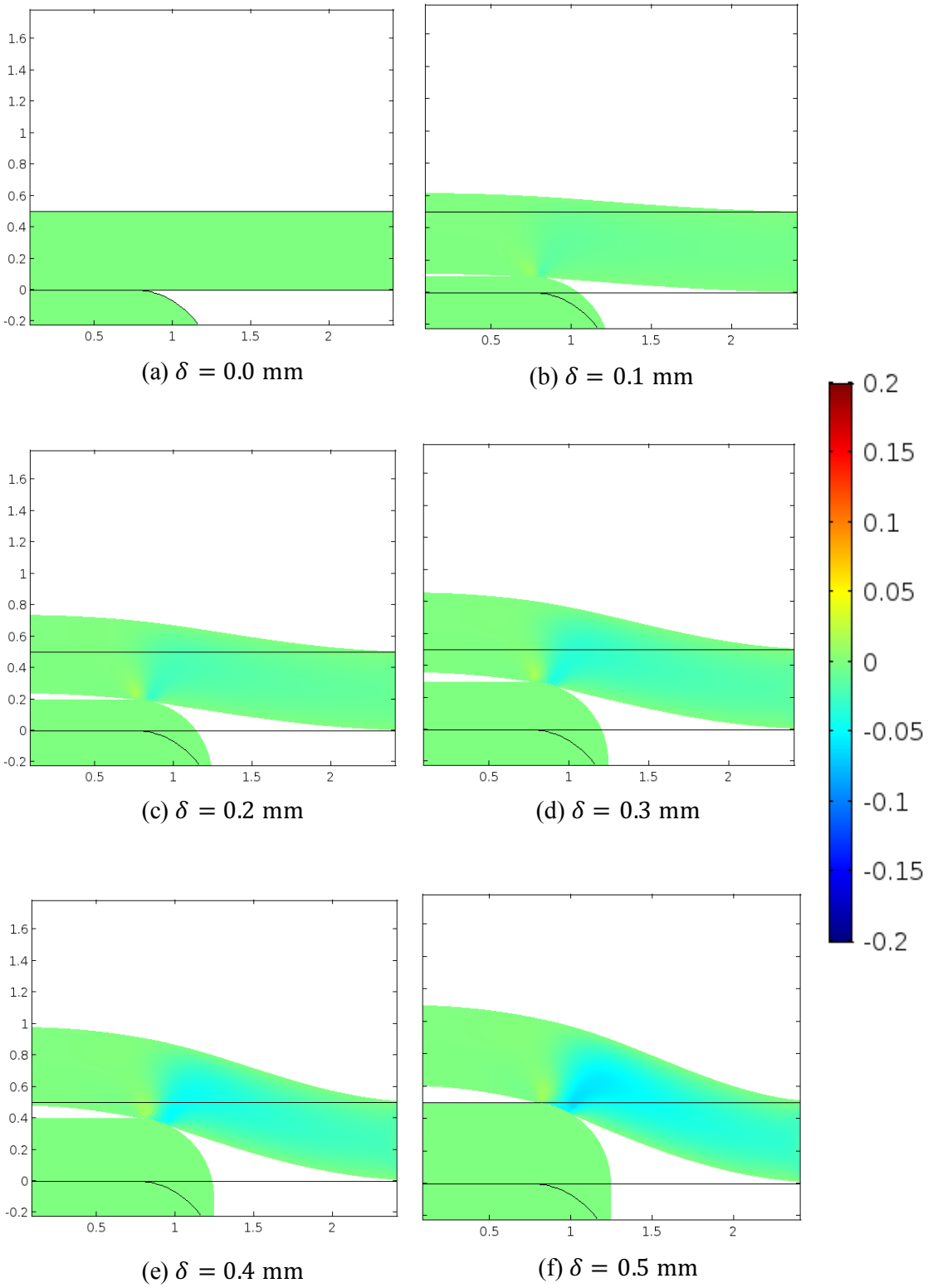

Figure 6.19 Screenshot of the *RZ* strain on the membrane during sinus lift up for E = 100 MPa

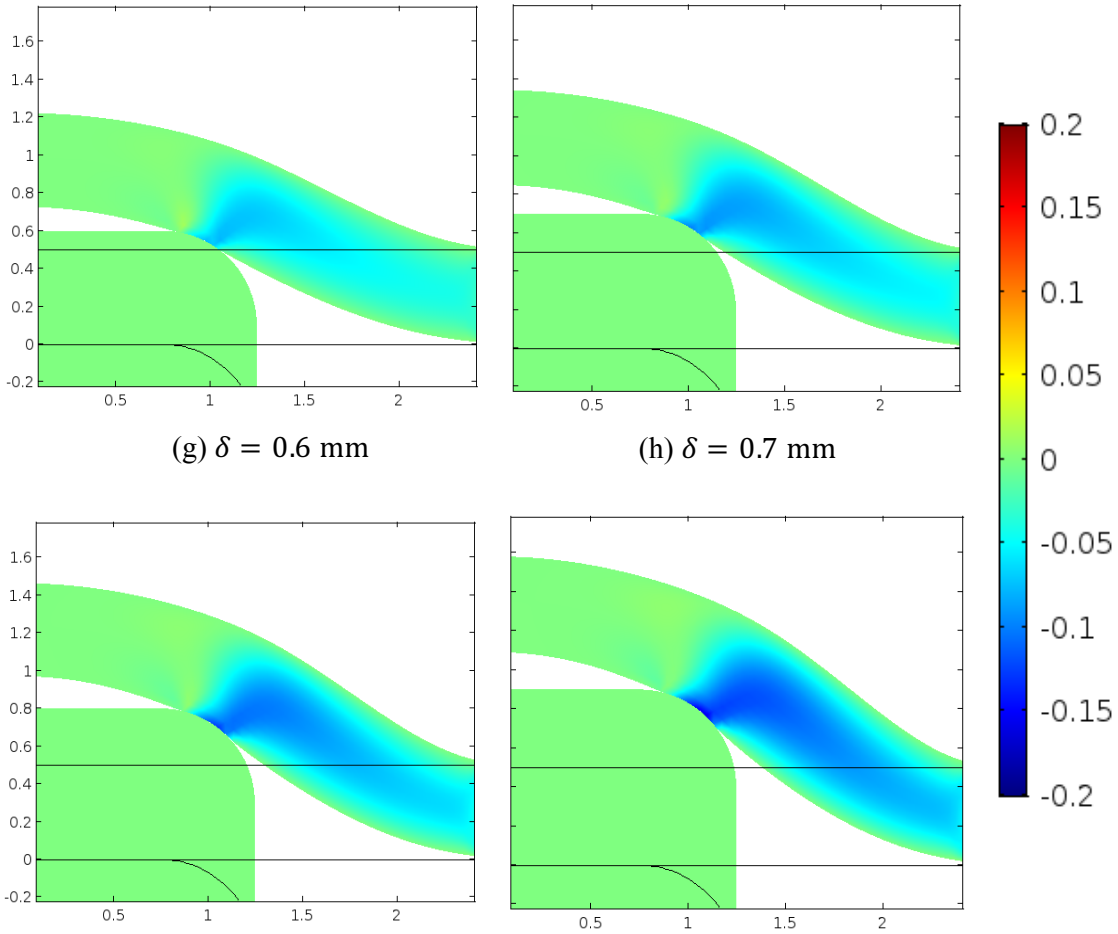

(g) $\delta = 0.6$ mm (h) $\delta = 0.7$ mm

(i) $\delta = 0.8$ mm (j) $\delta = 0.9$ mm

Figure 6.19 Screenshot of the *RZ* strain on the membrane during sinus lift up for E = 100 MPa (continued)

Based on each strain component, detailed analysis was further done comparing each parameter's results. The comparison of each strain component is shown in Figure 6.20.

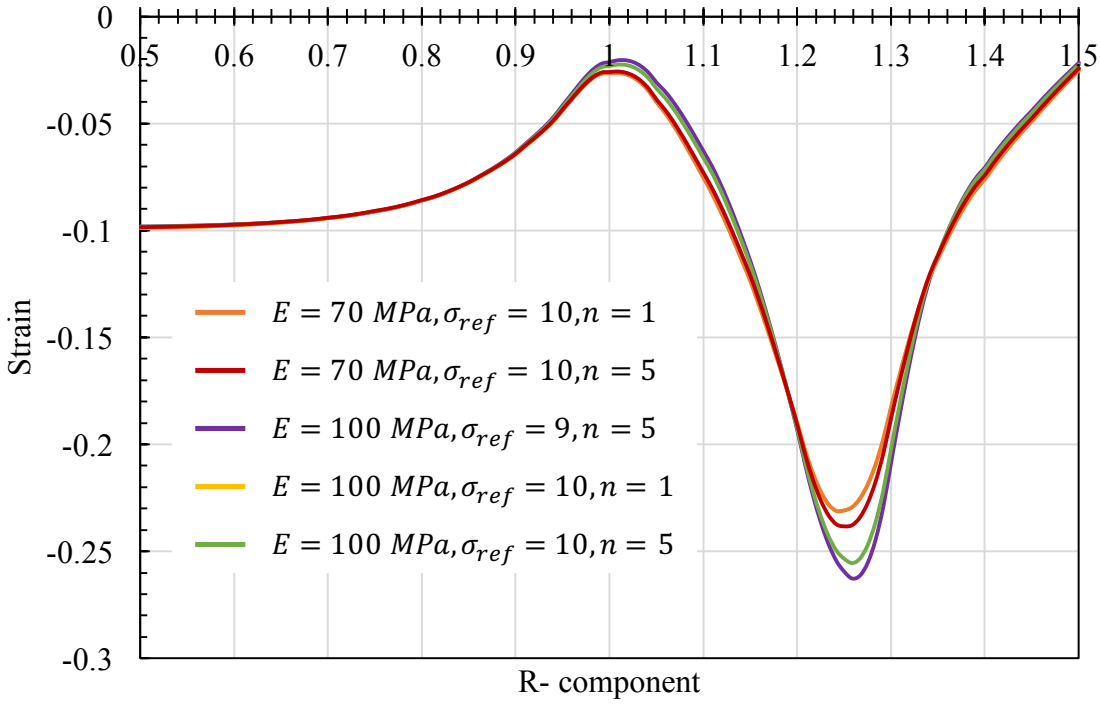

(a) Strain of the *RR* component

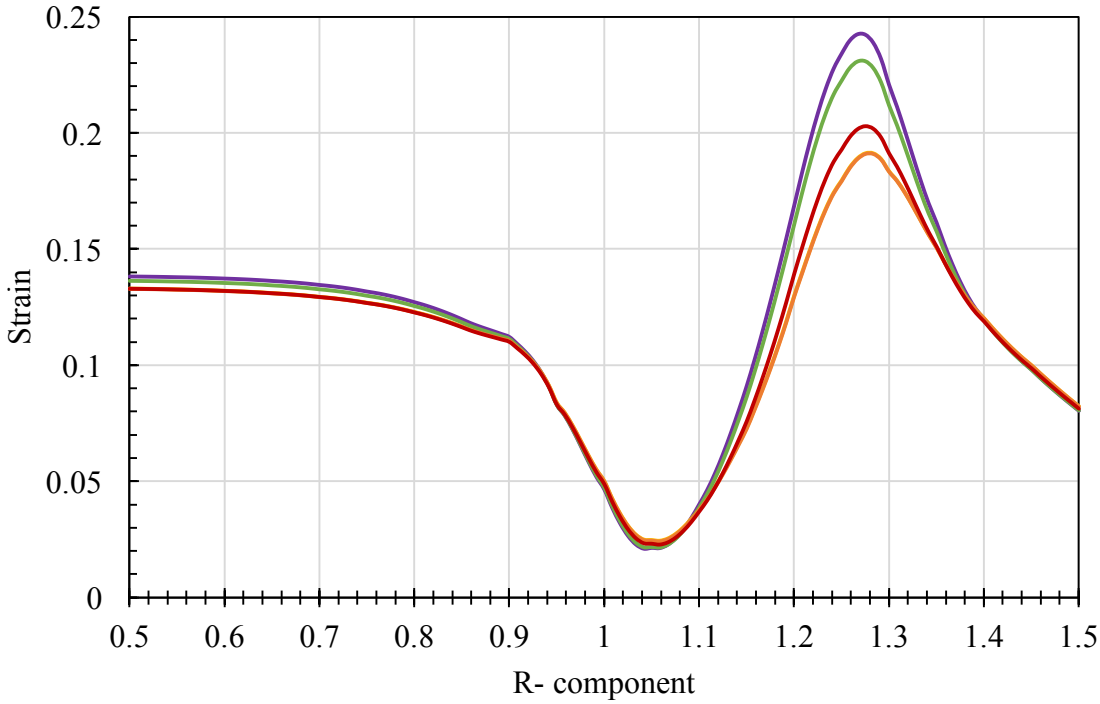

(b) Strain of the *ZZ* component

Figure 6.20 Comparison of each parameter strain component

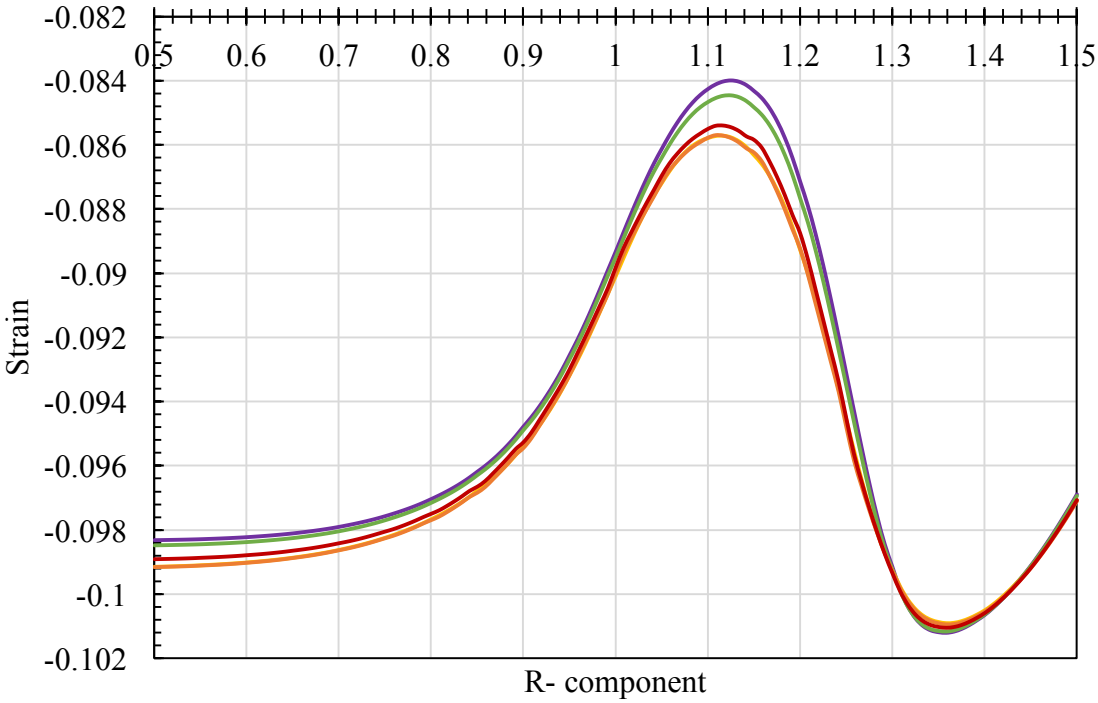

(c) Strain of the $\theta\theta$ component

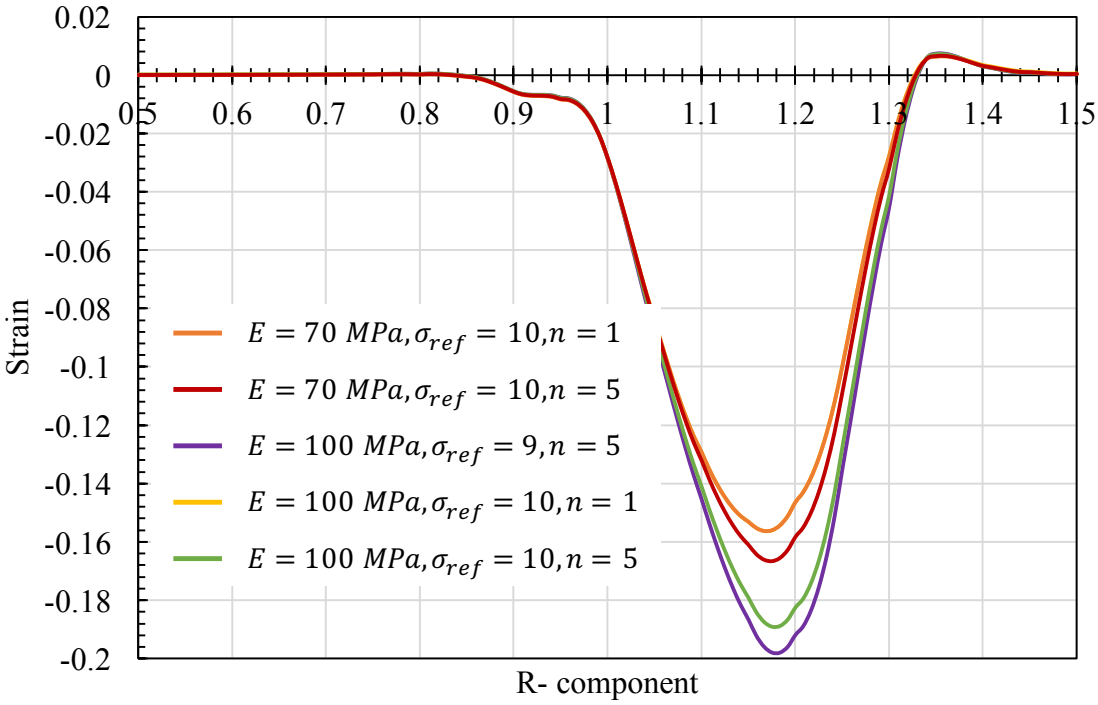

(d) Strain of the *RZ* component

Figure 6.20 Comparison of each parameter strain component (continued)

Looking at the screenshot of the deformation and strain distribution and considering the value of Young's modulus, the numerical simulation looks correct. When the constrained part is close to the bar, the high strain appears at the edge of the constrained part but when the constrained part is a bit far, the high strain occurred at the edge of the bar that finally lead to breakage. Similar results were obtained for the cultured human skin (Takano et al., 2009)

Based on each strain component, there is little to no difference of strain value for each set of parameter when E = 70 MPa. However, with different value of Young's modulus, difference could be seen. The qualitative characteristic of the curve for different sets of Young's modulus showed similarities. This means that the same strain value seems to be correlated to the cutting of the blood flow with the value of Young's modulus did not affect the strain component.

The significance of the strain is actually dependent on the direction of the blood capillary. However, in this study, considering the axisymmetric problem, the capillary is thought to be flowing in the RR direction. Based on this consideration, the tension of the membrane could lead to the compression of the blood flow but the tension is actually dependent on the direction of the strain. With consideration of the blood flow, the positive strain value of the RR direction with the negative value of the ZZ direction is dangerous as it can cause the compression of the blood capillary. Nevertheless, the negative value of the RZ direction seems also to be significant in the compression of the capillary thus, the small value of positive RR and negative ZZ in comparison with the shear strain showed that the shear strain is highly significant in this study. The characteristic showed that the RZ component of the strain value is significant in the cutting of the blood flow.

6.5 Discussion and summary

The result of the experiment in Figure 6.5 shows the load oscillate and not forming a smooth curve. The oscillation is supposed to be caused by many wrinkles in the membrane during the setup of the experiment. It was supposed that the force drop again to zero because of a locally wrinkled portion. The comparison between the experimental and the numerical simulation (Figure 6.11) shows an offset of results in higher value of deflection, δ. This shows an uncertainty factor of an initial strain value that could be due to the pretension of the muscle on the membrane and also the membrane attachment to the sinus floor. Another uncertainty factor could be due to the delamination area of the membrane.

The strain component of the membrane for 70 MPa of Young's modulus shows little difference in comparison even with a set of different parameter. By seeing the uniaxial tension test sensitivity in Figure 6.6, there is also not much difference and it can be concluded that the value is verified in this study. Based on the comparison done on the experiment and numerical value, the almost parallel line seems to be a nice feature. This shows quite a valid and agreeable method in the numerical procedure and could be further used to test more uncertainty factor in the sinus lift process using the procedure proposed.

The strain distribution obtained could not be compared with a real strain from the experiment as it shows the strain distribution in the membrane which is quite impossible to be compared. However, a comparison can be done to the surface of the membrane as the experiment could obtained the surface on the membrane but due to the limitation of the apparatus, it had not been done yet. The strain distribution on the surface of the membrane can also be output from the numerical procedure and both the

experiment and numerical results can be compared to improve its reliability. Anyhow, the point of interest is at the contact point between the membrane and the bar as high strain value seems to be happening at that point as shown in the Figure 6.15 and Figure 6.19.

Based on the strain value, there two sets of parameter that coincides with each other even for a different value of Young's modulus. This shows that there are many sets of parameter that can be used for the numerical procedure for different value of Young's modulus. Takano et al. (2011) describe a calibration process for two different sets of parameter based on an equation regarding the etching process. The same algorithm can be used in order to identify the best sets of parameter concerning the Ramberg-Osgood model. The calibration was also verified by experiment and simulation procedure. The same calibration process can be done in order to identify the sets of parameter best suited for the maxillary sinus membrane when using Ramberg-Osgood model.

Since this is an initial study as mentioned in the previous chapter, it is hard to make a truly confidence results due to many limitations and uncertainty factor considered. The best way that could be done is to increase the number of test on the sinus membrane and also doing a much more case and condition such as changing the delamination area in order to increase the confidence and reliability of the whole procedure.

The best condition is to do the experiment with consideration of different diameter of the bar. The first test is done in order to do an identification of the material properties. As there should be no influenced by the geometry of the membrane to the material properties, another test could be done to verify the entire process experimentally and also numerically. This will increase the confidence level of the whole process.

However, based on the calculated strain shown in Figure 6.12 to Figure 6.19 and

the comparison done in Figure 6.20, the results seem to be quite agreeable as the movement of the strain concentration is the same as hypothesized. Similar conditions were also seen in a previous work done on cultured human skin (Takano et al., 2009). The comparison also shown a fair result based on the sensitivity of the stress exponent and the reference stress as shown in Figure 6.6. The little difference shows that the results agree with the sensitivity of the calibrated material model's parameter.

In addition, based on the comparison of the calculated strain, the RZ component or the shear strain of the sinus membrane showed significance in the effect of the bar during the sinus lift up process. The shear strain showed that the blood flow could be cut due to the high strain value. Nonetheless, the value of the strain that showed the limitation of the membrane is still unknown. Conclusively, the significance of the shear strain in cutting the blood flow is highly reliable and could be expanded further in order to find out more about the relation of the blood flow in the sinus membrane with the strain value obtained. In regards to a real surgery, it is hard to set where the breaking point of the membrane might occur due to many uncertainties. However, it could be highly likely at the edge of the bar due to the high strain value compared to others

Chapter 7

Conclusion

7.1 New findings

The detailed knowledge of the cortical bone and trabecular bone from an engineer's point of view is very important in order to find out about the quantitative value of the bone rather than only the qualitative value. Both value seems to be essential to understand more about the bone thus making a surgery less risky with little to no complication occurs whether it is pre-surgery, during the surgery, or even post-surgery. In order to reduce the number of complications occurred, many methods had been researched and evaluated among the clinicians. Expert clinicians mainly plays an important role to make sure that their knowledge could be passed on to newer clinicians especially fresh graduates since they had the experience in knowing the qualitative value of a patient's body. By extracting the quantitative value from their experience, the knowledge could be passed on easily for the younger generation in order to reduce the number of complications occurred in a

surgery. With surgical repetition being one of the key point in the development of the oral implant surgery training simulator, the experience obtained from a clinician was able to be replicated and made it repeatable for everyone to learn and experience it themselves. The mastery through surgical repetition can be an important aspect in doing a surgery as the mastery can become a ‘second nature’ to them. This way the complications can be reduced through repeated usage and learning from a more experience person while avoiding any risk in difficult procedures.

The oral implant surgery training simulator was first developed with these in mind in order to educate students of dental colleges and universities. The development of the simulator was made by programming the movement of the actuator to work as what was input by the database software. The software was made from analyses done by calculating the drilling force on different types of cadaver. Taking the individual differences factor, the database implemented the stochastic homogenization theory to produce the database by assuming a probability factor of the human. Based on the database, it was found out that the theory works well in the application of the database for the simulator. However, inexperienced clinician may not be able to distinguish it well due to the low differences of the drilling force.

By implementing the database into the simulator, the quantification of the drilling force in the oral implant surgery was found out to be achievable and it even receive positive comments and reviews from a panel of expert clinicians. Most of the clinicians could recognize the different feeling of drilling different bone and one of them could even feel the difference force of about 1 N. The evaluation done shows that the repetition of surgical procedures works well to embed the feeling of doing the surgery itself into fresh

graduates. This is shown in the scale comparing other clinician's evaluation. Based on an average feeling of stiffness of drilling the jawbone, the feeling moves proportionally with their own experience. More experienced clinician felt the drilled bone as stiffer but a newly graduated clinician felt the same bone as soft. This shows that even with the same drilling force the feeling of stiffness could be different based on the person preferences.

The drilling of the same bone but caused different feeling of stiffness was checked by doing a comparison on drilling the educational polymeric model. It was found that the pattern drilling the polymeric model and using the simulator is partially similar. However, the polymeric model is considered to be softer due to its characteristic and target user which is the students of dental colleges. This is done to make sure that the students drill carefully especially when nearing the mandibular canal. Plus, the review from the panel of clinicians were very positive thus considering the simulator as a valid tool. This shows that the polymeric model could cause misunderstanding if used to teach the drilling force-sensed.

Based on the evaluation on the clinicians and also the experiment on the polymeric model, one interesting aspect was noticed. Even the drilling speed of the clinicians was not as high as drilling the polymeric model but the realistic feeling told was the key factor to classify not only the drilling force but also the drilling speed and the combination of both. Bearing this in mind, the evaluation continued to be implemented on students who had zero experience of the oral implant surgery. Interestingly, almost all the students gave similar results with the clinicians' evaluation results. One of them is recognizing the difference of two types of bone which is the cortical and trabecular bone. The students could also differentiate the feeling of stiffness accordingly based on the graph obtained.

Hence, the results of the clinicians' evaluation were looked into once more and it can be concluded that not only the drilling force but the combination of both the drilling force and speed is what defined the feeling of stiffness felt during the drilling process. This value was acquainted as the drilling force-sensed and this marked as the initial study to quantify the drilling force-sensed.

In conclusion, an oral implant surgery training simulator was developed in order to teach the force-sensed during the drilling process. This was done in order to reduce the number of complication that may arise from the serious medical problem in oral implant surgery. The clinicians then compared the force sense in real surgery and that using the simulator. Based on the comparison, all clinicians gave positive comments and reviews which considered the simulator as a valid tool. They even said that the simulator was very realistic. The comparison done with the experiment on the polymeric model showed that using the polymeric model could cause misunderstanding in teaching the force-sensed. Lastly, the device was used for around 24 students per year in the year 2014 and 2015. In 2016, more than 100 students used the simulator. It is helpful for students at dental college to learn about the biomechanics, bone quality, inter- and intra-individual differences, and force-sensed in various cases including serious accidental cases.

In the case of the sinus lift or popularly known as sinus augmentation, it is an advance technique which is mostly elective and not many experienced clinicians are able to do it. Besides, the high risk of doing this surgery is known to many. To reduce the risk and teach students of dental colleges the practical work of doing a sinus lift, a simulator with almost the same background as the oral implant surgery training simulator was proposed whether to be a newly built machine or added as a new feature of the said

simulator. As an initial study, the experiment on the sinus membrane needed to be done and a machine to evaluate the membrane while imitating the sinus lift process was made and presented in this study. The hurdles of handling a membrane was partially overcome with the initial study done on the membrane. By limiting the unknown factor through the set-up process such as the delamination area and the lift up length, the experiment was found to be achievable. Moreover, the comparison with the numerical procedure using COMSOL was highly likely validated the experiment procedure. In designing the numerical procedure, one of the difficulty was the setting of the material model as it is unknown as of the author's knowledge but it was managed to be calibrated by doing a range of model. The outcome of the initial procedure was acceptable based on the results of the strain concentration of the sinus membrane. It is believed that the procedure proposed in this study could be expanded even further with a more realistic condition and approach.

Based on the comparison of the component of the strain value, the shear strain component of the sinus membrane showed significance in finding out about the blood flow that could lead to the breakage of the membrane. The strain component is impossible to be found out based on experiment alone and it seems to be significant in cutting the blood flow based on the value and observation done on the strain distribution during the sinus lift up process. However, the value that seems to be the limitation of the membrane is not yet known. So, the observation of the shear strain distribution during the sinus lift up process could be done in the future in order to find out the effects of the strain on the blood flow through the sinus membrane.

In regards to the future plan of developing the force-sensing device explained in

Chapter 1, this study proves to be important and significant in the initial development of the device. Training simulator for the sinus lift up process is the final goal in the future since it is very much impossible to train and teach the process using a fresh cadaver.

Similar to the oral implant surgery training simulator explained in this study, the final product is in the form of the training simulator with the force-sensing capability to indicate the reaction force during the lifting process so that the user can understand the force-sensed when the maxillary sinus is broken and also understand the fundamental biomechanics including the strain concentration that leads to the breakage.

7.2 Assumptions and limitations

Some assumptions which were made in the present study should be highlighted because they might not be appropriate for other applications. Below is the list of key assumptions in this study.

1. Setup of the actuator to follow a linear movement based on a calculated method.
2. The thickness of the cortical bone in the upper part of the drilling force database.
3. Setup of the sinus membrane on the machine limiting the movement of the membrane in any direction.
4. Design of numerical procedure for the sinus lift up process with the considered contact and constrain conditions.
5. Calibrated parameter of Young's modulus limited to the value by previous study on maxillary sinus membrane.

Details of the assumption is included in the respective chapter that described their procedure. In addition, there is also a number of limitations associated with this study. First, the oral implant surgery training simulator is only limited to one movement thus making it harder to be as realistic as possible. However, the added feature of the decentering jig could add the feeling of the side vibration during drilling. Regardless, the feeling of mistake could only be done by changing the database to that of the perforation case.

Second, in order to obtain a more reliable result of the sinus membrane, a number of specimen is needed. However, only one specimen of fresh cadaver was available during this study. The wet surface of the membrane and the thickness made the membrane fragile thus making it harder to do a number of experiment on a single specimen. Moreover, in order to check the one specimen reliability, at the very least another specimen is needed. Although, a specimen managed to be obtained, due to the fact of being very careful, the data on the membrane until it burst was not able to be obtained. This data is also one of an important piece of data that is needed since the concentration of strain that could make the membrane break can be known based on the comparison with the numerical procedure.

Third is the consideration of graft material. The limitation of the testing machine could not afford to test the graft material as the hole to do the sinus lift process is kind of big for the graft material to be put inside. So, during the experiment, the material seems to overflow and some of them fall from the hole. This could break the actuator movement and made the experiment unreliable. The consideration of the graft material in the sinus lift up process is very important in order to provide a much more realistic data especially in the numerical procedure. The comparison of both procedures to calibrate the material

model could only be done if both procedure is almost the same.

Lastly, in relation to the numerical procedure, the high nonlinearity of the numerical study limited the option to make it as realistic as possible. Based on the assumptions that were made, some of the options was neglected thus making the result debatable. This is due to the limited time and cost in preparation of the numerical design. The limited knowledge of the sinus membrane in a realistic condition restrict the numerical procedure to the assumption that can only be known such as the contact and constraint condition of the sinus membrane.

7.3 Future works

7.3.1 Commercial version of oral implant surgery training simulator

The application of the oral implant surgery training simulator could open up to a lot of possibilities. The testing and evaluation done especially by the expert clinicians is what worth to be introduced to the public. The commercialization of the simulator could not only involve the students of dental colleges and universities but also dentist and other clinicians in a town clinic. With this initiative, the numbers of accidents could be reduced not only among fresh graduates but also in a veteran practitioner of the oral implant surgery. Moreover, Tokyo Dental College had already implemented the simulator in their PBL classes as of this year. The usage of the simulator in the class can be promoted to the public especially to other colleges and universities to take on the same syllabus including the usage of the simulator in their classes.

However, in order to reach this goal a commercial version of the oral implant surgery training simulator needed to be develop. The basic of the simulator need not be changed as described in this study but the outer design could be change in order to meet a lot of people's expectation and demand. The review and comments from the students and also more clinicians if possible could make the goal possible to commercialize the simulator.

7.3.2 Appended database of calculated drilling force

A total of 4 types of cadaver was included in the database. It was appended with two cases each making it a total of 8 databases available. By implementing the stochastic homogenization method, the results included the 50% probability and 90% probability for each condition, thus a total of 24 databases are currently available to be chosen. The increase number of database could make it more pleasant to the public as it could consider almost all the cases available in the world. The expansion of the database could be done by using a micro-CT images of the mandibular bone in particular. However, the images characteristic should be different than the current available database in order to cover yet undocumented cases.

During this study, a new method was found to be highly possible to increase the number of database. Based on the students' evaluation, an interesting result was obtained that some of the students could produce a quite similar graph with the samples evaluated. If the same procedure was done on clinician, this could very well produce a more accurate graph thus making it possible for the graph to be used directly as the database of the

simulator. This could cut the cost of simulation to calculate the drilling force using micro-CT. Moreover, a fresh feeling of the drilling force-sense could be obtained if the procedure was used during an oral implant surgery.

7.3.3 Material model of the maxillary sinus membrane

Being one of the unknown factor in the evaluation on the sinus membrane, the setting of the material model can be tedious. In this study, the Ramberg-Osgood's material model was proposed and calibrated to check the distribution of the sinus membrane. However, concerning the nonlinear material model, there are many types of material model available nowadays. The setting of other material model is timely and could increase the computational cost. Regardless, being an unknown factor, it could be useful for future study on the maxillary sinus membrane.

One of the material model that caught interest is the Mooney-Rivlin and Ogden material model since the sinus membrane kind of resemble a rubber, which is usually the Mooney-Rivlin and Ogden material model used on. The power law or the Ramberg-Osgood model is the non-linear material model commonly used to model the elastoplastic behavior of metals. The Mooney-Rivlin model is a hyperelastic material model commonly used in rubber and the Ogden model is used to model the hyperelastic deformation at a much higher strain than the Mooney-Rivlin. A significance difference can be seen when unloaded. That is, a hysteresis can be expressed by Mooney-Rivlin or Ogden models.

Future study could use the Mooney-Rivlin as the material model in exchange of

the Ramberg-Osgood in the numerical procedure. The condition could remain the same in order to check and evaluate the results for calibration. The comparison between both models could also be done in order to identify the material model of the sinus membrane. Nonetheless, the best way to identify the material model of the sinus membrane considering the Mooney-Rivlin material model is to do an experiment to calibrate the constant value needed in identifying the model.

Another consideration of the material model is the viscoelastic material model. In order to test on this type of material model, these two kind of test can be considered:

1. Small vibration to the membrane

   This test can be done to one or a few number of samples. Giving a small vibration of about 20 to 50 Hz to the membrane could be done to check the damping based on the delay movement of the membrane caused by its viscosity.

2. Changing movement speed of the lifting up

   Another test is to consider the speed of the lift up. Different lift up speed can be used in order to obtain the strain rate of the membrane. This way the viscosity of the membrane could be known based on the curve obtained using different speed of the lift up.

Both of the test could get us the relaxation time to characterize the relaxation due to the viscosity of the membrane. This parameter can be used to identify the viscoelastic material model of the membrane. However, a number of fresh cadaver will be needed but it seems to be one of the limitation during this study.

7.3.4 Consideration of graft material

In the sinus augmentation process, sometimes there is a need to include graft material in order to promote the osseointegration process faster to reduce the time for the implantation. In this case, the bone is grafted from a different part of the bone such as the femur or the usage of material that highly resembles the bone. This is usually in the form of crystallized hydroxyapatite. The consideration of the graft material could make the experiment process nearly realistic in comparison with the sinus lift up since almost all the surgery needed the usage of the graft material. However, due to some limitations of the machine, the usage of the graft material cannot be done in this initial study.

So, the next step is to get the graft material properties and determine the critical strain value during the breakage of the membrane by curve-fitting the experiment with and without the graft material. The strain concentration obtained by direct contact of the steel bar could be different with the contact of the graft material since the difference of stiffness and importantly the condition of the material. The works could be done on a known material parameter rather than using the sinus membrane and the relation of the strain based on different volume or weight of the graft material could also be proposed. With the added graft material in the experiment, the calculated strain distribution will be highly reliable since it almost represents a real case of the sinus lift up surgery.

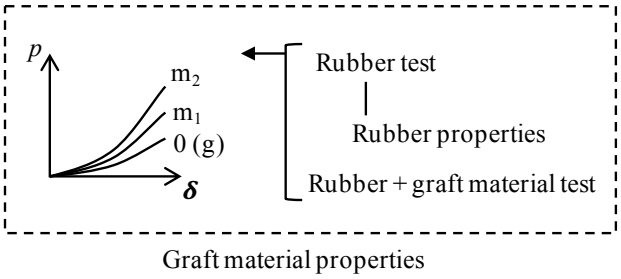

Figure 7.1 Determining the graft material properties

7.3.5 Consideration of condition of the bar during lifting up of the sinus membrane

From a mechanical viewpoint, the semi-spherical head bar is better in reducing the strain. However, for many clinicians, the strain in the case of cylindrical bar is much more informative. So, this study considers the cylindrical bar in order to provide more information for a clinician. A semi-spherical head bar can be appended in the numerical and experimental procedure in order to compare the strain value obtained by different type of tools used.

In the case of the diameter of the bar, a different diameter could also be considered as one of the parameter. This system was established based on the tool used by clinician during the sinus lift up process. The smallest of the diameter is about 2.5 mm which is the same as used in this study. The biggest consideration of the bar's diameter is 6.6 mm which is the same diameter of the drill used during the drilling process.

Usage of different diameter of the bar is also considered in order to do a verification process. Using the same delamination area, two different diameters can be used with one type of the bar is used in order to calibrate the material properties and the other is used to verify it. This is because the calibrated parameter is not to be affected by any geometrical parameter. With the verification process done, finally a prediction of strain distribution in the sinus membrane can be done with a very high reliability compared with this study.

Appendix A

List of publications and presentations

A.1 Articles on periodicals

1) **Mohammad Aimaduddin Atiq bin Kamisan**, Kenichiro Yokota, Takayuki Ueno, Hideaki Kinoshita, Shinya Homma, Yasutomo Yajima, Shinichi Abe, and Naoki Takano, Drilling force and speed for mandibular trabecular bone in oral implant surgery, *Biomaterials and Biomechanics in Bioengineering*, Vol. 3, No. 1 (2016), pp. 15-26

2) **Mohammad Aimaduddin Atiq bin Kamisan**, Hideaki Kinoshita, Fumiya Nakamura, Shinya Homma, Yasutomo Yajima, Satoru Matsunaga, Shinichi Abe, and Naoki Takano, Quantitative study of force sensing while drilling trabecular bone in oral implant surgery, *Journal of Biomechanical Science and Engineering*, Vol. 11, No. 3 (2016), pp. 1-9

A.2 Presentations at international conferences

1) **Mohammad Aimaduddin Atiq bin Kamisan**, Naoki Takano, Yasutomo Yajima, and Shinichi Abe, Development of oral implant surgery training simulator with drilling force sensing capability, *21st Congress of the European Society of Biomechanics (ESB 2015)*, 5-8 July 2015, Prague, Czech Republic
2) **Mohammad Aimaduddin Atiq bin Kamisan**, Naoki Takano, and Shinichi Abe, Experimental study on drilling force for jawbone in oral implant surgery using polymeric model, *The 8th Asian-Pacific Conference on Biomechanics (AP Biomech 2015)*, 16-19 September 2015, Sapporo, Japan
3) **Mohammad Aimaduddin Atiq bin Kamisan**, and Naoki Takano, Development of oral implant surgery training simulator with drilling force sensing capability and its use in PBL class at dental college, *KSME-JSME Joint Symposium on Computational Mechanics & CAE 2015 (KSME-JSME CM&CAE 2015)*, 26 October 2015, Tokyo, Japan; (Awarded the Silver Prize of Altair Award)

A.3 Presentations at domestic meetings

1) **Mohammad Aimaduddin Atiq bin Kamisan**, Kenichiro Yokota, Masahiro Nagahata, Naoki Takano, Hideaki Kinoshita, and Shinichi Abe, Experimental and numerical studies on drilling force for jawbone in oral implant surgery, *Japan Society of Mechanical Engineering 27th Conference on Bioengineering (JSME 27th Bioengineering)*, 9-10 January 2015, Niigata, Japan
2) **Mohammad Aimaduddin Atiq bin Kamisan**, Masahiro Nagahata, Naoki Takano, Daisuke Tawara, and Shinichi Abe, Study on drilling force influenced by mandibular trabecular microarchitecture in oral implant surgery, *Japan Society for Computational Engineering and Science 20th Conference on Computational Engineering and Science (JSCES 2015)*, 8-10 June 2015, Tsukuba, Japan

Bibliography

Abouzgia, M. B., & James, D. F. (1995). Measurements of shaft speed while drilling through bone. *Journal of Oral and Maxillofacial Surgery*, *53*(11), 1308–1315.

Adell, R., Lekholm, U., Rockler, B., & Brånemark, P. I. (1981). A 15-year study of osseointegrated implants in the treatment of the edentulous jaw. *International Journal of Oral Surgery*, *10*(6), 387–416.

Agamy, E. M. T. M., & Niedermeier, W. (2010). Indirect sinus floor elevation for osseointegrated prostheses. A 10-year prospective study. *The Journal of Oral Implantology*, *36*(2), 113–121.

Al-Dajani, M. (2014). Recent Trends in Sinus Lift Surgery and Their Clinical Implication. *Clinical Implant Dentistry and Related Research*, *18*(1), 204–212.

Albrektsson, T., Sennerby, L., & Wennerberg, A. (2008). State of the art of oral implants. *Periodontology 2000*, *47*(1), 15–26.

Aljohani, H. A., & AlGhamdi, A. S. T. (2009). Predoctoral dental implant education at King Abdulaziz University. *Saudi Dental Journal*, *21*(3), 135–138.

Augat, P., & Schorlemmer, S. (2006). The role of cortical bone and its microstructure in bone strength. In *Age and Ageing* (Vol. 35).

Augustin, G., Davila, S., Mihoci, K., Udiljak, T., Vedrina, D. S., & Antabak, A. (2008). Thermal osteonecrosis and bone drilling parameters revisited. *Archives of Orthopaedic and Trauma Surgery*, *128*(1), 71–77.

Bachus, K., Rondina, M., & Hutchinson, D. (2000). The effects of drilling force on cortical temperatures and their duration: an in vitro study. *Medical Engineering & Physics*, *22*(2000), 685–691.

Basaruddin, K. S., Takano, N., & Nakano, T. (2013). Stochastic multi-scale prediction on the apparent elastic moduli of trabecular bone considering uncertainties of biological apatite (BAp) crystallite orientation and image-based modelling. *Computer Methods in Biomechanics and Biomedical Engineering*, (June), 37–41.

Basler, S. E., Traxler, J., Müller, R., & van Lenthe, G. H. (2013). Peri-implant bone microstructure determines dynamic implant cut-out. *Medical Engineering and Physics*, *35*(10), 1442–1449.

Bonnet, A. S., Postaire, M., & Lipinski, P. (2009). Biomechanical study of mandible bone supporting a four-implant retained bridge. Finite element analysis of the influence of bone anisotropy and foodstuff position. *Medical Engineering and Physics*, *31*(7), 806–815.

Büchter, A., Kleinheinz, J., Wiesmann, H. P., Kersken, J., Nienkemper, M., Von Weyhrother, H., & Meyer, U. (2005). Biological and biomechanical evaluation of bone remodelling and implant stability after using an osteotome technique. *Clinical Oral Implants Research*, *16*(1), 1–8.

Călin, C., Petre, A., & Drafta, S. (2014). Osteotome-mediated sinus floor elevation: a systematic review and meta-analysis. *Int J Oral Maxillofac Implants*, *29*(3), 558–76.

Çehreli, M. C., Kökat, A. M., Comert, A., Akkocaoğlu, M., Tekdemir, I., & Akça, K. (2009). Implant stability and bone density: Assessment of correlation in fresh cadavers using conventional and osteotome implant sockets. *Clinical Oral Implants Research*, *20*(10), 1163–1169.

Ching-Chieh, H., Li-Wen, C., Dong-Feng, W., & Yung-Chuan, C. (2012). Finite Element Simulations of the Contact Stress between Rotary Sinus Lift Kit and Sinus Membrane during Lifting Process. *Life Science Journal*, *9*(2), 167–171.

Chrcanovic, B. R., Albrektsson, T., & Wennerberg, A. (2014). Reasons for failures of oral implants. *Journal of Oral Rehabilitation*, *41*(6), 443–476.

Clarke, B. (2008). Normal bone anatomy and physiology. *Clinical Journal of the American Society of Nephrology : CJASN*.

Coelho, P. G., Granjeiro, J. M., Romanos, G. E., Suzuki, M., Silva, N. R. F., Cardaropoli, G., & Lemons, J. E. (2009). Basic research methods and current trends of dental implant surfaces. *Journal of Biomedical Materials Research. Part B, Applied Biomaterials*, *88*(2), 579–96.

Cowin, S., & Telega, J. (2003). *Bone Mechanics Handbook, 2nd Edition. -. Applied Mechanics Reviews* (Vol. 56).

Curran, J. B. (2006). Regarding: Editorial 'Mastery Through Surgical Repetition'. *Oral Surgery, Oral Medicine, Oral Pathology, Oral Radiology and Endodontology*, *102*(2), 141–142.

da Silva, E. F., Pellizzer, E. P., Quinelli Mazaro, J. V., & Garcia Júnior, I. R. (2010). Influence of the connector and implant design on the implant-tooth-connected prostheses. *Clinical Implant Dentistry and Related Research*, *12*(3), 254–262.

De Bruyn, H., Koole, S., Mattheos, N., & Lang, N. P. (2009). A survey on undergraduate implant dentistry education in Europe. *European Journal of Dental Education*, *13*(SUPPL1.), 3–9.

Del Fabbro, M., Corbella, S., Weinstein, T., Ceresoli, V., & Taschieri, S. (2012). Implant Survival Rates after Osteotome-Mediated Maxillary Sinus Augmentation: A Systematic Review. *Clinical Implant Dentistry and Related Research*, *14*(SUPPL. 1).

Dempster, D. W. (2000). The contribution of trabecular architecture to cancellous bone quality. *Journal of Bone and Mineral Research : The Official Journal of the American Society for Bone and Mineral Research*, *15*(1), 20–23.

Derrick, D. D. (1986). Dentistry. An illustrated history. *Journal of Dentistry*.

Donnelly, E. (2011). Methods for assessing bone quality: A review. In *Clinical Orthopaedics and Related Research* (Vol. 469, pp. 2128–2138).

Donos, N., Mardas, N., & Buser, D. (2009). An outline of competencies and the appropriate postgraduate educational pathways in implant dentistry. *European Journal of Dental Education*, *13*(SUPPL1.), 44–54.

Esposito, M., Grusovin, M. G., Rees, J., Karasoulos, D., Felice, P., Alissa, R., Worthington, H., & Coulthard, P. (2010). Effectiveness of sinus lift procedures for dental implant rehabilitation: a Cochrane systematic review. *European Journal of Oral Implantology*, *3*(1), 7–26.

Fanuscu, M. I., Vu, H. V, & Poncelet, B. (2004). Implant biomechanics in grafted sinus: a finite element analysis. *The Journal of Oral Implantology*, *30*(2), 59–68.

Fincham, A. G., & Shuler, C. F. (2001). The changing face of dental education: the impact of PBL. *Journal of Dental Education*, *65*(5), 406–421.

Franceschetti, G., Minenna, P., Farina, R., & Trombelli, L. (2012). Smart Lift Technique for Minimally Invasive Transcrestal Sinus Floor Elevation, 24–27.

Friberg, B., Sennerby, L., Roos, J., & Lekholm, U. (1995). Identification of bone quality in conjunction with insertion of titanium implants. A pilot study in jaw autopsy specimens. *Clinical Oral Implants Research*, *6*(4), 213–9.

Fugazzotto, P. A, & Vlassis, J. (2000). Long-term success of sinus augmentation using various surgical approaches and grafting materials. *The International Journal of Oral & Maxillofacial Implants*, *13*(1), 52–8.

Gibson, L. J., & Ashby, M. F. (1997). *Cellular Solids: Structure and Properties*. *Bone*

(Vol. 7).

Goodyear, S. R., Gibson, I. R., Skakle, J. M. S., Wells, R. P. K., & Aspden, R. M. (2009). A comparison of cortical and trabecular bone from C57 Black 6 mice using Raman spectroscopy. *Bone*, *44*(5), 899–907.

Guedes, J., & Kikuchi, N. (1990). Preprocessing and postprocessing for materials based on the homogenization method with adaptive finite element methods. *Computer Methods in Applied Mechanics and Engineering*, *83*, 143–198.

Hadjidakis, D. J., & Androulakis, I. I. (2006). Bone remodeling. In *Annals of the New York Academy of Sciences* (Vol. 1092, pp. 385–396).

Hannam, A. G. (2005). The biomechanical–biological interface and its significance in oral disease. *International Congress Series*, *1284*, 3–10.

Holmgren, E., Seckinger, R., Kilgren, L., & Mante, F. (1998). Evaluating parameters of osseointegrated dental implants using finite element analysis—a two-dimensional comparative study examining the effects of implant diameter, implant. *Journal of Oral Implantology*, *26*(2), 80–88.

Inglam, S., Suebnukarn, S., Tharanon, W., Apatananon, T., & Sitthiseripratip, K. (2010). Influence of graft quality and marginal bone loss on implants placed in maxillary grafted sinus: A finite element study. *Medical and Biological Engineering and Computing*, *48*(7), 681–689.

Janner, S. F. M., Caversaccio, M. D., Dubach, P., Sendi, P., Buser, D., & Bornstein, M. M. (2011). Characteristics and dimensions of the Schneiderian membrane: A radiographic analysis using cone beam computed tomography in patients referred for dental implant surgery in the posterior maxilla. *Clinical Oral Implants Research*, *22*(12), 1446–1453.

Jianping, G., Weiqi, Y., & Wei, X. (2008). *Application of the Finite Element Method in Implant Dentistry*. *Application of the Finite Element Method in Implant Dentistry*.

Jurisic, M., Markovic, A., Radulovic, M., Brkovic, B. M. B., & Sándor, G. K. B. (2008). Maxillary sinus floor augmentation: comparing osteotome with lateral window immediate and delayed implant placements. An interim report. *Oral Surgery, Oral Medicine, Oral Pathology, Oral Radiology and Endodontology*, *106*(6), 820–827.

Karaca, F., & Aksakal, B. (2013). Effects of various drilling parameters on bone during implantology: An in vitro experimental study. *Acta of Bioengineering and Biomechanics*, *15*(4), 25–32.

Keaveny, T. M., Morgan, E. F., Niebur, G. L., & Yeh, O. C. (2001). Biomechanics of trabecular bone. *Annual Review of Biomedical Engineering*, *3*(1), 307–33.

Kim, S.-J., Yoo, J., Kim, Y.-S., & Shin, S.-W. (2010). Temperature change in pig rib bone during implant site preparation by low-speed drilling. *Journal of Applied Oral Science : Revista FOB*, *18*(5), 522–527.

Koole, S., Vandeweghe, S., Mattheos, N., & De Bruyn, H. (2014). Implant dentistry education in Europe: 5 years after the Association for Dental Education in Europe consensus report. *European Journal of Dental Education*, *18 Suppl 1*(5), 43–51.

Kusumoto, N., Sohmura, T., Yamada, S., Wakabayashi, K., Nakamura, T., & Yatani, H. (2006). Application of virtual reality force feedback haptic device for oral implant surgery. *Clinical Oral Implants Research*, *17*(6), 708–713.

Lekholm, U. (1985). Patient selection and preparation. *Tissue-Integrated Prosthesis: Osseointegration in Clinical Dentistry*, 199–209.

Lekholm, U., & Zarb, G. (1985). Patient selection and preparation. *Brånemark PI, Zarb GA, Albrektsson T (Eds.). Tissue Integrated Prostheses. Quintessance, Chicago*, 199–209.

Limbert, G., van Lierde, C., Muraru, O. L., Walboomers, X. F., Frank, M., Hansson, S., Middleton, J., & Jaecques, S. (2010). Trabecular bone strains around a dental implant and associated micromotions--a micro-CT-based three-dimensional finite element study. *Journal of Biomechanics*, *43*(7), 1251–61.

Martin, R. B., & Burr, D. B. (1989). Structure function, and adaptation of compact bone. *Raven Press, New York, NY*, 275–276.

Mathieu, V., Michel, A., Flouzat Lachaniette, C. H., Poignard, A., Hernigou, P., Allain, J., & Haïat, G. (2013). Variation of the impact duration during the in vitro insertion of acetabular cup implants. *Medical Engineering and Physics*, *35*(11), 1558–1563.

Mathieu, V., Vayron, R., Richard, G., Lambert, G., Naili, S., Meningaud, J. P., & Haiat, G. (2014). Biomechanical determinants of the stability of dental implants: Influence of the bone-implant interface properties. *Journal of Biomechanics*, *47*(1), 3–13.

Matsunaga, S., Shirakura, Y., Ohashi, T., Nakahara, K., Tamatsu, Y., Takano, N., & Ide, Y. (2010). Biomechanical role of peri-implant cancellous bone architecture. *The International Journal of Prosthodontics*, *23*(4), 333–338.

Matsunaga, S., Takano, N., Tamatsu, Y., Abe, S., & Ide, Y. (2011). Biomechanics of Jaw Bone Considering Structural Properties of Trabecular Bone. *Journal of Oral Biosciences*, *53*(2), 143–147.

Mattheos, N., Albrektsson, T., Buser, D., De Bruyn, H., Donos, N., Hjørting Hansen, E., Lang, N. P., Sanz, M., & Nattestad, A. (2009). Teaching and assessment of implant dentistry in undergraduate and postgraduate education: A European consensus. *European Journal of Dental Education*, *13*(SUPPL1.), 10–17.

Mattheos, N., Wismeijer, D., & Shapira, L. (2014). Implant dentistry in postgraduate university education. Present conditions, potential, limitations and future trends. *European Journal of Dental Education*, *18 Suppl 1*(S1), 24–32.

Melo, M. D., Shafie, H., & Obeid, G. (2006). Implant Survival Rates for Oral and Maxillofacial Surgery Residents: A Retrospective Clinical Review With Analysis of Resident Level of Training on Implant Survival. *Journal of Oral and Maxillofacial Surgery*, *64*(8), 1185–1189.

Misch C. E., Bone character: second vital implant criterion. *Dent Today 39-40*, June/July 1988.

Misch, C. E., Perel, M. L., Wang, H.-L., Sammartino, G., Galindo-Moreno, P., Trisi, P., Steigmann, M., Rebaudi, A., Palti, A., Pikos, M. A., Schwartz-Arad, D., Choukroun, J., Gutierrez-Perez, J. L., Marenzi, G., & Valavanis, D. K. (2008). Implant success, survival, and failure: the International Congress of Oral Implantologists (ICOI) Pisa Consensus Conference. *Implant Dentistry*, *17*(1), 5–15.

Misch, C. E., Qu, Z., & Bidez, M. (1999). Mechanical properties of trabecular bone in the human mandible: implications for dental implant treatment planning and surgical placement. *Journal of Oral and Maxillofacial Surgery*, *57*, 700–706.

Miyabe, S., Nakano, T., Ishimoto, T., Takano, N., Adachi, T., Iwaki, H., Kobayashi, A., Takaoka, K., & Umakoshi, Y. (2007). Two-Dimensional Quantitative Analysis of Preferential Alignment of BAp c-axis for Isolated Human Trabecular Bone Using Microbeam X-ray Diffractometer with a Transmission Optical System. *Materials Transactions*, *48*(3), 343–347.

Neufeld, V., & Barrows, H. S. (1974). The 'McMaster philosophy': an approach to medical education. *Journal of Medical Education*, *49*(11), 1040–1050.

Nolan, P. J., Freeman, K., & Kraut, R. A. (2014). Correlation between schneiderian membrane perforation and sinus lift graft outcome: A retrospective evaluation of 359 augmented sinus. *Journal of Oral and Maxillofacial Surgery*, *72*(1), 47–52.

Oftadeh, R., Perez-Viloria, M., Villa-Camacho, J. C., Vaziri, A., & Nazarian, A. (2015). Biomechanics and Mechanobiology of Trabecular Bone: A Review. *Journal of Biomechanical Engineering*, *137*(1), 1–15.

Ohashi, T., Matsunaga, S., Nakahara, K., Abe, S., Ide, Y., Tamatsu, Y., & Takano, N. (2010). Biomechanical role of peri-implant trabecular structures during vertical loading. *Clinical Oral Investigations*, *14*(5), 507–513.

Paquette, D. W., Brodala, N., & Williams, R. C. (2006). Risk Factors for Endosseous Dental Implant Failure. *Dental Clinics of North America*.

Peleg, M., Chaushu, G., Mazor, Z., Ardekian, L., & Bakoon, M. (1999). Case Series

Radiological Findings of the Post-Sinus Lift Maxillary Case Series. *Journal Of Periodontology*, *70*, 1567.

Pjetursson, B. E., Rast, C., Brägger, U., Schmidlin, K., Zwahlen, M., & Lang, N. P. (2009). Maxillary sinus floor elevation using the (transalveolar) osteotome technique with or without grafting material. Part I: Implant survival and patients' perception. *Clinical Oral Implants Research*, *20*(7), 667–676.

Pommer, B., Unger, E., Sütö, D., Hack, N., & Watzek, G. (2009). Mechanical properties of the Schneiderian membrane in vitro. *Clinical Oral Implants Research*, *20*(6), 633–637.

Pothuaud, L., Van Rietbergen, B., Mosekilde, L., Beuf, O., Levitz, P., Benhamou, C. L., & Majumdar, S. (2002). Combination of topological parameters and bone volume fraction better predicts the mechanical properties of trabecular bone. *Journal of Biomechanics*, *35*(8), 1091–1099.

Razavi, M., Talebi, H. A., Zareinejad, M., & Dehghan, M. R. (2015). A GPU-implemented physics-based haptic simulator of tooth drilling. *International Journal of Medical Robotics and Computer Assisted Surgery*, *11*(4), 476–485.

Reingewirtz, Y., Szmukler-Moncler, S., & Senger, B. (1997). Influence of different parameters on bone heating and drilling time in implantology. *Clinical Oral Implants Research*.

Reiser, G. M., Rabinovitz, Z., Bruno, J., Damoulis, P. D., & Griffin, T. J. (1994). Evaluation of maxillary sinus membrane response following elevation with the crestal osteotome technique in human cadavers. *The International Journal of Oral & Maxillofacial Implants*, *16*(6), 833–840.

Reporting of Emergency Survey on Serious Medical Trouble Related to Implant Surgery (Preliminary). (2011). *Japan Academy of Maxillofacial Implants*.

Rhienmora, P., Haddawy, P., Khanal, P., Suebnukarn, S., & Dailey, M. N. (2010). A virtual reality simulator for teaching and evaluating dental procedures. *Methods of*

Information in Medicine, *49*(4), 396–405.

Rho, J. Y., Kuhn-Spearing, L., & Zioupos, P. (1998). Mechanical properties and the hierarchical structure of bone. *Medical Engineering and Physics*, *20*(2), 92–102.

Rohlin, M., Peterson, K., & Svensater, G. (1998). The Malmo model: a problem-based learning curriculum in undergraduate dental education. *European Journal of Dental Education*, *2*(3), 103–114.

Sanchez-Palencia, E. (1980). *Non-Homogeneous Media And Vibration Theory*. *Non-homogeneous media and vibration theory* (Vol. 127).

Sansalone, V., Bousson, V., Naili, S., Bergot, C., Peyrin, F., Laredo, J. D., & Haïat, G. (2012). Anatomical distribution of the degree of mineralization of bone tissue in human femoral neck: Impact on biomechanical properties. *Bone*, *50*(4), 876–884.

Seeman, E., & Delmas, P. D. (2006). Bone quality--the material and structural basis of bone strength and fragility. *The New England Journal of Medicine*, *354*(21), 2250–2261.

Sohmura, T., Kusumoto, N., Otani, T., Yamada, S., Wakabayashi, K., & Yatani, H. (2009). CAD/CAM fabrication and clinical application of surgical template and bone model in oral implant surgery. *Clinical Oral Implants Research*, *20*(1), 87–93.

Sugaya, K. (1990). Study on method for examining bone quality for dental implant. Relationship between cutting force and bone mineral content. *Shika Gakuho. Dental Science Reports*, *90*(4), 607–33.

Sui, J., Sugita, N., Ishii, K., Harada, K., & Mitsuishi, M. (2014). Mechanistic modeling of bone-drilling process with experimental validation. *Journal of Materials Processing Technology*, *214*(4), 1018–1026.

Summers, R. B. (1994). A new concept in maxillary implant surgery: the osteotome technique. *Compendium (Newtown, Pa.)*, *15*(2), 152, 154–156, 158 passim; quiz 162.

Tachikawa, H., Takano, N., Nisiyabu, K., Miki, N., & Ami, Y., (2010). Effect of tension

and curvature of skin on insertion characteristics of microneedle array, *Journal of Solid Mechanics and Material Engineering, 4*(3),470-480

Takano, N., Sato, K., Toriyama, T., Yamasaki, T., & Uesugi, S. (2011). Calibration of wet etching parameters for sacrifice layer of MEMS. *Journal of Computational Science and Technology, 5*(3), 106-119.

Takano, N., Tachikawa, H., Miyano, T., & Nishiyabu, K. (2009). Insertion testing of polyethylene glycol microneedle array into cultured human skin with biaxial tension, *Journal of Solid Mechanics and Material Engineering, 3*(3) ,604-611

Takano, N., Zako, M., Kubo, F., & Kimura, K. (2003). Microstructure-based stress analysis and evaluation for porous ceramics by homogenization method with digital image-based modeling. *International Journal of Solids and Structures*, *40*(5), 1225–1242.

Tawara, D., Nagahata, M., Takano, N., Kinoshita, H., & Abe, S. (2015). Probabilistic analysis of mechanical behaviour of mandibular trabecular bone using a calibrated stochastic homogenization model. *Acta Mechanica*, *226*(10), 3275–3287.

Tilotta, F., Lazaroo, B., & Gaudy, J. F. (2008). Gradual and safe technique for sinus floor elevation using trephines and osteotomes with stops: a cadaveric anatomic study. *Oral Surgery, Oral Medicine, Oral Pathology, Oral Radiology and Endodontology*, *106*(2), 210–216.

Tiwana, P. S., Kushner, G. M., & Haug, R. H. (2006). Maxillary Sinus Augmentation. *Dental Clinics of North America*.

Ucer, T. C., Botticelli, D., Stavropoulos, A., & Mattheos, N. (2014). Current trends and status of continuing professional development in implant dentistry in Europe. *European Journal of Dental Education*, *18*(S1), 52–59.

Urbankova, A. (2010). Impact of computerized dental simulation training on preclinical operative dentistry examination scores. *Journal of Dental Education*, *74*(4), 402–409.

Van De Velde, T., Glor, F., & De Bruyn, H. (2008). A model study on flapless implant placement by clinicians with a different experience level in implant surgery. *Clinical Oral Implants Research*, *19*(1), 66–72.

van den Bergh, J. P., ten Bruggenkate, C. M., Disch, F. J., & Tuinzing, D. B. (2000). Anatomical Aspects of Sinus Floor Elevations. *Clinical Oral Implants Research*, *11*(3), 256–265.

Weiner, S., Traub, W., & Wagner, H. D. (1999). Lamellar bone: structure-function relations. *Journal of Structural Biology*, *126*(3), 241–255.

Wierinck, E. R., Puttemans, V., Swinnen, S. P., & van Steenberghe, D. (2007). Expert performance on a virtual reality simulation system. *Journal of Dental Education*, *71*(6), 759–766.

Woo, I., & Le, B. T. (2004). Maxillary sinus floor elevation: review of anatomy and two techniques. *Implant Dentistry*, *13*(1), 28–32.

Xiaojun, C., Yanping, L., Chengtao, W., Yiqun, W., Xudong, W., & Guofang, S. (2010). An integrated surgical planning and virtual training system using a force feedback haptic device for dental implant surgery. In *Audio Language and Image Processing (ICALIP), 2010 International Conference on* (pp. 1257–1261).

Yan, X., Zhang, X., Chi, W., Ai, H., & Wu, L. (2015). Association between implant apex and sinus floor in posterior maxilla dental implantation: A three-dimensional finite element analysis. *Experimental and Therapeutic Medicine*, 868–876.

Yan, X., Zhang, X., Gao, J., Matsushita, Y., Koyano, K., Jiang, X., & Ai, H. (2014). Maxillary Sinus Augmentation without Grafting Material with Simultaneous Implant Installation: A Three-Dimensional Finite Element Analysis. *Clinical Implant Dentistry and Related Research*, 1–10.

Yeniyol, S., Jimbo, R., Marin, C., Tovar, N., Janal, M. N., & Coelho, P. G. (2013). The effect of drilling speed on early bone healing to oral implants. *Oral Surgery, Oral Medicine, Oral Pathology and Oral Radiology*, *116*(5), 550–555.

Zheng, F., Lu, W. F., Wong, Y. S., & Foong, K. W. C. (2012). An analytical drilling force model and GPU-accelerated haptics-based simulation framework of the pilot drilling procedure for micro-implants surgery training. *Computer Methods and Programs in Biomedicine*, *108*(3), 1170–1184.